Numerical Modeling of Tracer Tests

By

© Lili Xin

A Thesis submitted to the School of Graduate Studies in partial fulfillment of the requirements for the degree of

Master of Engineering

Faculty of Engineering and Applied Science

Memorial University of Newfoundland

October 2016

St. John's

Newfoundland and Labrador

Abstract

Tracer tests are widely used in the oil and gas industry. The response curves from tracer tests can provide reservoir engineers with important reservoir information, such as flow direction, presence of faults, reservoir heterogeneities and fluid saturation. As tracer tests provide reservoir engineers representative results from the reservoir, they are very useful for enhanced oil recovery.

This research begins by numerical modeling of one-dimensional single-phase tracer flow and develops to a complete two-phase partitioning tracer flow that includes convection, Langmuir adsorption, partitioning between phases, hydrodynamic dispersion and radioactive decay. This model implemented in Matlab (2014b) is an improvement of previously-used models as it includes radioactive decay and uses Langmuir adsorption instead of linear adsorption. It is also fast and easy to use.

The different tracer models are discussed and compared. A case study reveals that the adsorption model chosen, the partitioning coefficients and the reservoir wetting conditions all have effects on the tracer profiles and breakthrough times. This can be applied to tracer test design and analysis.

Acknowledgements

I would like to take this opportunity to express my gratitude to my supervisors, Dr. Lesley James and Dr. Thormod Johansen. Thank you for your patience and guidance during my research. I am grateful for your support and your valuable suggestions.

I would also like to thank all the people in our research group for their help and suggestions. Special thanks go to Norah Hyndman for helping me with my writing.

Last but not least, I would like to thank my family and friends for their care and love, without which I could not finish my research in such a happy way.

Table of Contents

List of Tables

List of Figures

Nomenclature

a	Langmuir adsorption empirical constant
b	Langmuir adsorption empirical constant, m^3/kg
C	Tracer mass concentration, kg/m^3
C_{ij}	Mass concentration of component i in phase j, kg/m^3
C_L, C_R	Injected, initial tracer concentration, kg/m^3
C_S	Adsorbed tracer concentration, kg/m^3
C_w, C_o	Tracer concentration in water, oil phase, kg/m^3
C^*	Dimensionless tracer concentration
D	Hydrodynamic dispersion coefficient, m^2/s
D_{ij}	Overall dispersion coefficient of component i in phase j, m^2/s
F_{conv}	Mass flux caused by convection, $kg \cdot m^{-2} \cdot s^{-1}$
F_D	Mass flux caused by hydrodynamic dispersion, $kg \cdot m^{-2} \cdot s^{-1}$
I_{USBM}	USBM index
k	Absolute permeability
k_{ro}, k_{rw}	Relative permeabilities of oil, water phases
$k_{r,wet}$, $k_{r,non-wet}$	Relative permeability of wetting, non-wetting phases
K	Partitioning coefficient
L	Distance between injection well and production well
N	Number of atoms
N_0	Initial number of atoms
$N(t)$	Number of atoms after time t

$\vec{N}_{ij}$	Mass flux, $kg \cdot m^{-2} \cdot s^{-1}$
N_c	Number of components
N_p	Number of phases
N_{pe}	Peclet number
P_c	Capillary pressure, Pa
P_o, P_w	Pressures of oil, water phases, Pa
r_{ij}	Reaction rate of component i in phase j, $g \cdot m^{-3} \cdot s^{-1}$
R_{ij}	Source term, $kg \cdot m^{-3} \cdot s^{-1}$
S_w	Water saturation
S_{wc}	Connate water saturation
S_{or}	Residual oil saturation
$t_{1/2}$	Half-life of the radioactive tracer, year
t_l	Tracer travelling time of leading edge, s
t_t	Tracer travelling time of trailing edge, s
t^*	Dimensionless time
T_b	Tracer slug breakthrough time
u_j	Volumetric flux of phase j, m/s
u_o, u_w	Volumetric fluxes of oil, water phases, m/s
u_T	Total volumetric flux, m/s
W_{ij}	Accumulation term, kg/m^3
ε_j	Volume fraction occupied by phase j
λ	Decay constant, s^{-1}
λ_o, λ_w	Phase mobility of oil, water phases

μ_o, μ_w	Viscosity of oil, water phases, $Pa \cdot s$
ρ_j	Density of phase j, kg/m^3
ω_{ij}	Mass fraction of component i in phase j

Abbreviations

EOR	Enhanced Oil Recovery
SWTT	Single-Well Tracer Test
IWTT	Inter-Well Tracer Test
USBM	US Bureau of Mines

Chapter 1 Introduction

Tracer tests are field tests performed by injecting and producing a tracer in a reservoir to determine key reservoir properties, such as flow direction, knowledge of the existence of and communication across faults, reservoir heterogeneities, residual oil saturation and connate water saturation (BjØrnstad, 1992). Before any enhanced oil recovery method is applied in the field, a reservoir simulation is conducted to estimate additional information and provide guidance for the upcoming production. Trustworthy input parameters from tracer tests give confidence to reservoir simulation results.

Laboratory testing of reservoir rock provides important information about the reservoir but may not be representative of the entire field. Tracer tests can provide useful data at the field scale as additional information to lab tests. As tracer tests are conducted in the field and may occupy a large portion of the formation, they provide information from a different scale than laboratory testing, i.e. field scale as opposed to core scale.

This chapter presents a brief introduction to the different types of tracers and an introduction of tracer tests. This is followed by an introduction to the application of tracer tests to provide qualitative and quantitative reservoir information. Finally, the objectives of this research are outlined with my specific contributions highlighted.

1.1 Tracers

Tracers are chemicals or radioactive chemicals that can be mixed with fluids without changing the properties of the fluids. As tracers move with their carrying fluids, the tracer response curves (tracer concentration distributions) can reflect both the flowing conditions and the movements of the carrying fluids. Generally, tracers can be classified into three categories: radioactive tracer, chemical tracer and fluorescent tracer (Melo *et al.*, 2001).

Radioactive tracers contain isotopes that emit beta or gamma radiation, depending on the isotope. Alpha radiation radioactive tracers are seldom used because of their low penetration; they can easily be stopped by a few centimeters of air or a thin sheet of paper. Radioactive tracers are the most commonly used tracers and have low detection values. With higher sensitivities, radioactive tracers can be detected easily by liquid scintillation, solid scintillation or semiconductor detectors (Bj Ø rnstad, 1992). However, due to radioation effects, there are safety and environmental concerns associated with their use. The most frequently used radioactive tracers and their half-life are listed in Table 1.1 (Dugstad, 2006).

Applications of nonradioactive chemical tracers are also found in the literature. Chemical tracers are cheaper than radioactive tracers, but their lack of sensitivity results in relatively difficult detection (Melo *et al*, 2001). Chemical water tracers are categorized into dyes, ionic and organic tracers. Chemical gas tracers that have been

successfully used include inert gases such as nitrogen, argon and inorganic compounds such as sulfur hexafluoride (Lichtenberger, 1991).

Fluorescent tracers are safe and easy to detect. They are also inexpensive. However, the major disadvantage is their reaction with reservoir rocks. The excessive and unpredictable reactions make the test hard to control and analyze. Therefore, they are seldom used in tracer tests (Melo *et al*, 2001).

Table 1.1: Frequently used radioactive tracers, after (Dugstad, 2006)

Tracer	**Name**	**Half-life (year)**
HTO	Tritiated Water	12.32
CH_3TOH	Tritiated Methanol	12.32
$^{14}CO_2$	14C Labelled Carbon Dioxide	5730
$S^{14}CN^-$	14C Labelled Thiocyanate	5730
^{85}Kr	85 Labelled Krypton	10.76

Tracers can also be classified by their interactions with fluid phases and reservoir rocks, i.e. passive tracers and active tracers (Dugstad, 2006).

Passive tracers follow the fluid phase passively without chemical or physical reactions with the fluids and reservoir rocks. The tracer and the traced phase must not influence the behavior of each other. Because of their stable flow behavior in the flowing system, passive tracers are usually used to measure fluid directions, interwell communications, indication of stratifications, and the detection of heterogeneities and faults, which are the primary goals of tracer tests (BjØrnstad, 1992). Passive tracer

tests have been applied to the oil field for several decades and are proven and mature techniques.

Active tracers exhibit interactions with the system, either with the fluids or with the reservoir rock. The interactions can be phase partitioning or adsorption on the rock, both of which can be predicted quantitatively and used to measure properties of the system. The partitioning behavior of tracers makes it possible to measure residual oil saturation and connate water saturation based on their levels of chromatographic separation. The adsorption behavior of tracers has the potential to measure ion exchange capacity, which is important in polar or ionic surfactants injections (IAEA, 2012).

1.2 Types of Tracer Tests

Currently, two types of tracer tests are commonly used: single-well tracer tests (SWTT) and inter-well tracer tests (IWTT).

Single-well tracer test (SWTT)

In SWTTs, tracers are injected in one well and, after a period of time, produced from the same well. The operational steps of SWTT are shown in Figure 1.1 (Deans and Carlisle, 2006).

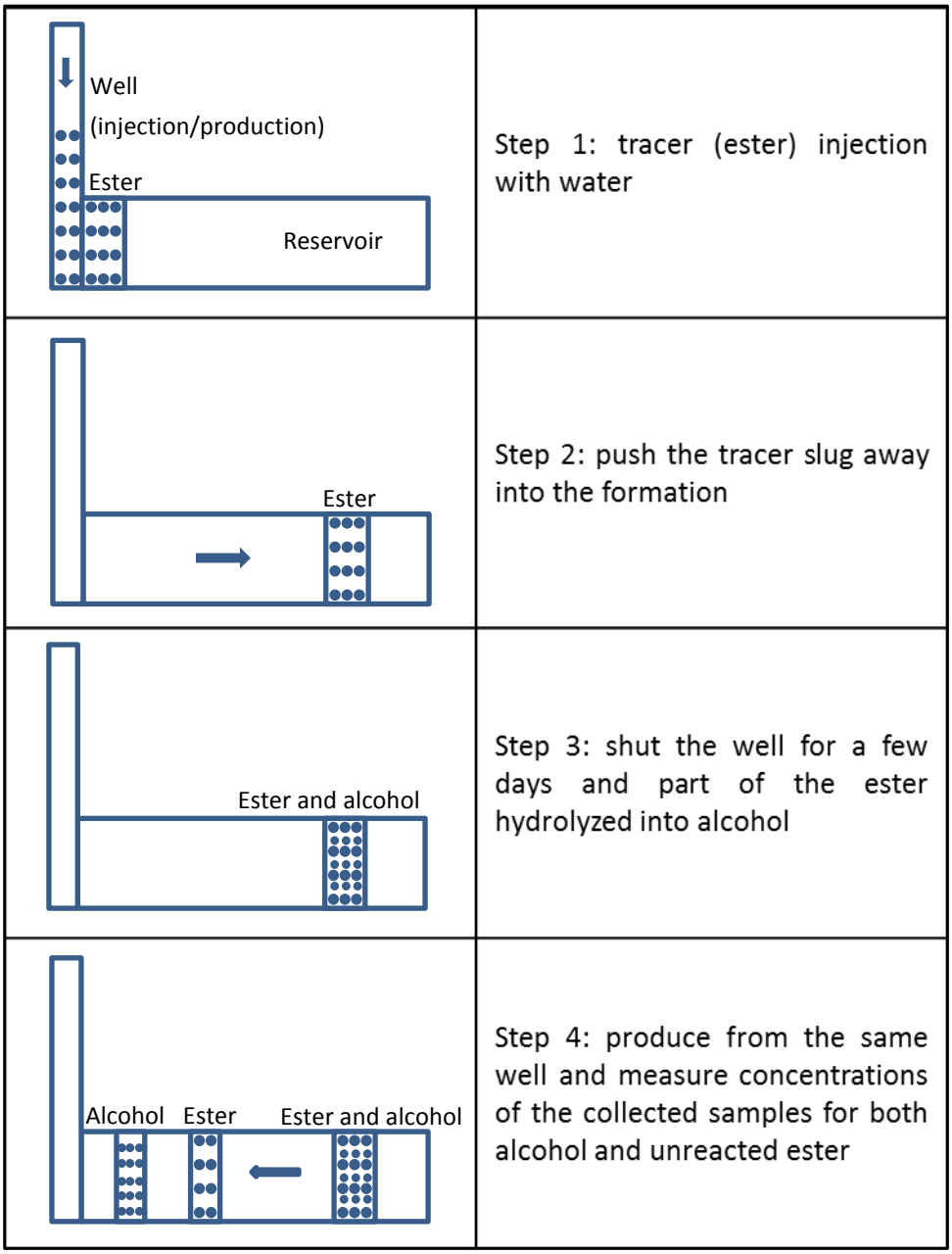

Figure 1.1: SWTT operational steps

For a SWTT, as illustrated above, instead of injecting two tracers (ester and alcohol) together into the reservoir, a primary tracer (ester) is injected to form a secondary tracer (alcohol).

When two phases are present, both the ester and alcohol would partition into the two phases at a certain concentration ratio. The partitioning coefficient is defined as the tracer concentration in the oil phase divided by the tracer concentration in the water phase. The partitioning coefficient of alcohol is very small, which means that the partitioning of alcohol into oil can be neglected so that the alcohol travels only with the water phase. Therefore, the velocity of water can be obtained by testing the alcohol velocity. However, the ester has a larger partitioning coefficient and partitions between the oil phase and the water phase, which results in a much slower velocity. If the two tracers were injected together, the alcohol would travel a longer distance than the ester, as shown in Figure 1.2 (Deans and Carlisle, 2006).

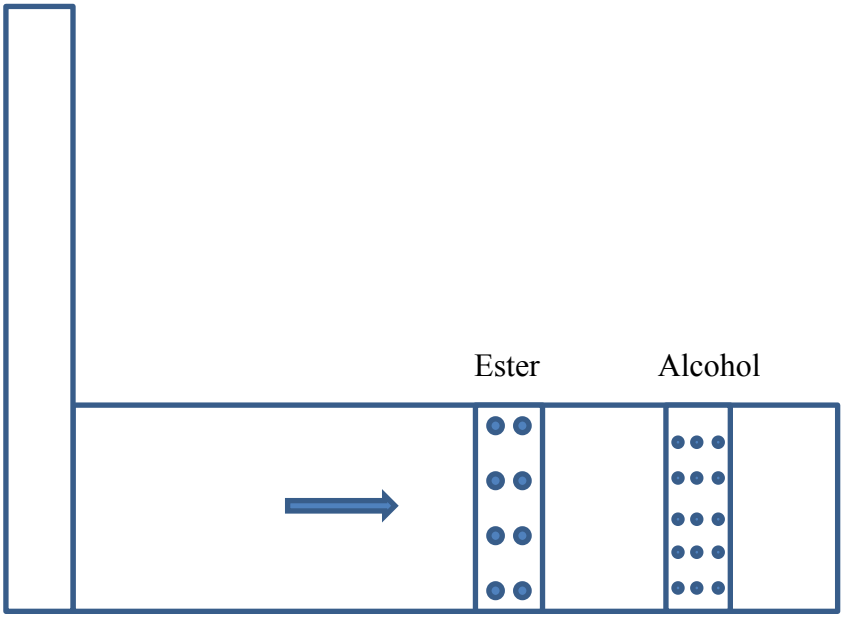

Figure 1.2: The separation of alcohol and ester if injected together

Then, during the production period, the alcohol travels faster and catches up with ester so that the two tracers arrive at the wellbore at the same time, as shown in Figure 1.3.

The difference in arrival time of the two tracers provides important information when analyzing the response curves; hence the method of injecting two tracers together does not work for a SWTT (Deans and Carlisle, 2006).

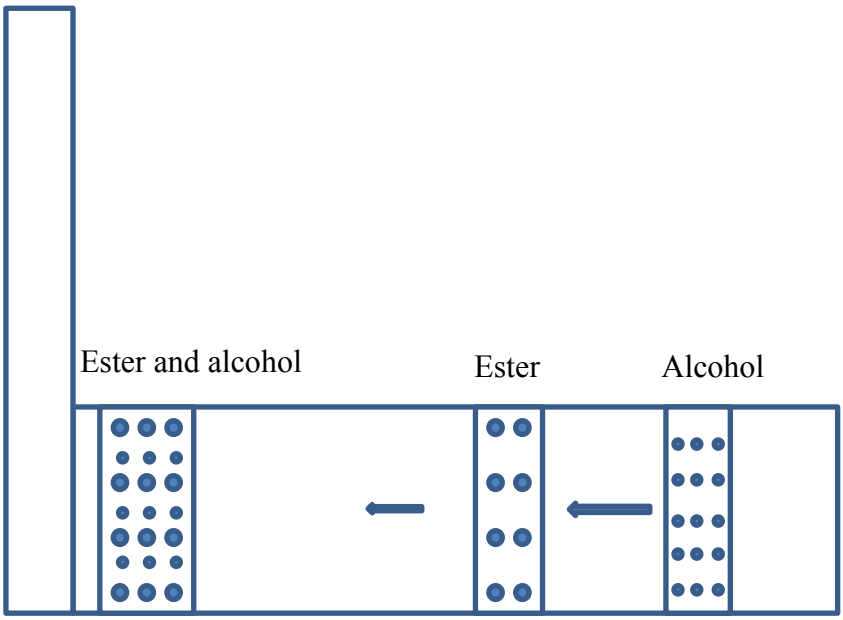

Figure 1.3: The production of alcohol and ester if injected together for a SWTT

Inter-well tracer test (IWTT)

The procedure for conducting an IWTT is similar to the SWTT. The difference is that IWTT uses one well for tracer injection and another well for tracer production (Figure 1.4). Therefore, instead of injecting a primary tracer to form a secondary tracer inside the reservoir, during an IWTT, two tracers with different partitioning coefficients are injected together. In addition, an IWTT usually occupies a larger portion of formation than SWTT; hence IWTTs are more often used to test fluid directions and well communication, it is also more time consuming (Dugstad, 2006).

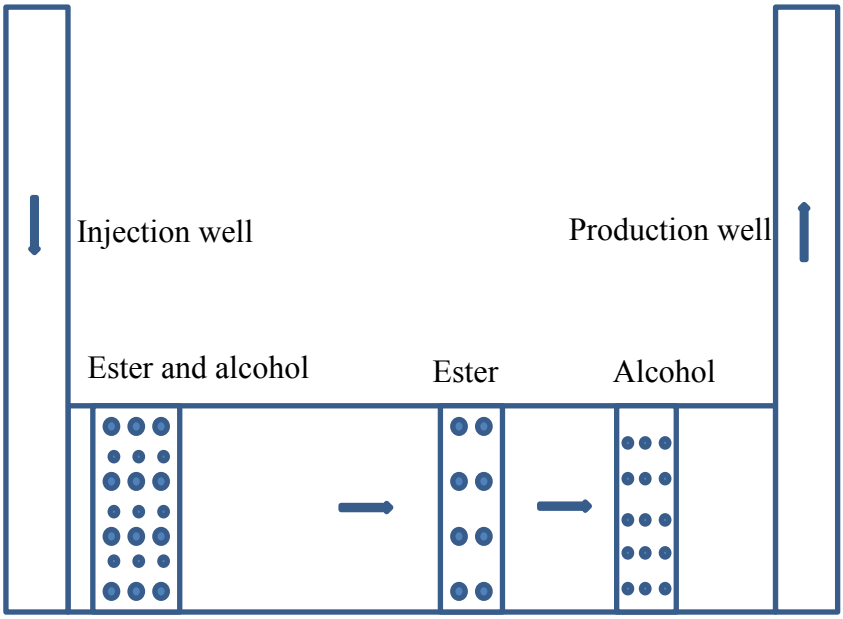

Figure 1.4: The production period of alcohol and ester if injected together

1.3 Application

The results from tracer tests can be used qualitatively, interpreted analytically or modeled numerically (Guan *et al*, 2005). Each of these three applications produces different information from tracer tests. The qualitative approach is the simplest and earliest method used in the petroleum industry. Analytical interpretation is more complicated than the qualitative approach and results in quantitative information based on simple assumptions. Numerical modeling is the most complex and accurate method, as it includes reservoir conditions and tracer behaviors.

1.3.1 Qualitative Approach

The qualitative application of tracer test in the petroleum industry started in the early 1950s when reservoir engineers first applied tracer tests. This method is primarily

used to measure well connectivities and flow directions based on the arrival and non-arrival of tracers at producing wells (Sturm and Johnson, 1951). It is easy to conduct and it is the most widely-used tracer test technique. However, this approach has a high potential for misinterpretation. The misinterpretation can be caused by inadequate measurement of tracer responses, tracer loss by adsorption or radioactive decay or concentration below the detection limit (Shook *et al*, 2004).

1.3.2 Analytical Interpretation

The analytical interpretation of tracer test started in 1965 with Brigham and Smith. Since then, analytical methods have been commonly applied to tracer tests. Analytical interpretation provides quantitative information, for example the residual oil saturation can be obtained through tracer test analysis based on the partitioning behavior of tracers. However, in order to interpret the results analytically, assumptions are made throughout the analysis, which makes it less accurate compared to numerical modeling (Brigham and Smith, 1965).

1.3.3 Numerical Modeling

Although numerical modeling is the most accurate procedure to analyze a tracer test, it is not widely used in the petroleum industry as it is complex and time-consuming. The numerical method involves tracer test simulation and history matching by modifying the reservoir properties (Hagoort, 1982). Powerful computer software has been developed for numerical modeling and simulation of tracer tests, but usually requires a

huge amount of reservoir information and the models are not integrated for all the scenarios.

1.4 Research Objectives

This research focuses on the numerical modeling of tracer flow. The purpose of this research is to build complete one-dimensional tracer models for both single-phase miscible displacement (convection, Langmuir adsorption, hydrodynamic dispersion and radioactive decay) and two-phase partitioning displacement (convection, Langmuir adsorption, partitioning between phases, hydrodynamic dispersion and radioactive decay), and then to implement them in Matlab® using explicit finite difference methods. This model is an improvement to existing literature as it includes radioactive decay and uses Langmuir adsorption instead of linear adsorption, which makes the model more accurate and closer to reality. It is also fast and easy to use. The motivation of this research is to develop a complete and accurate model of tracer test applying numerical method, and using this model to discuss the effect of adsorption type, partitioning coefficient and reservoir wetting condition on tracer profile and breakthrough time through case studies.

The numerical modeling results of the different models are compared with each other and also compared with analytical solutions to investigate the effect of each factor (adsorption, hydrodynamic dispersion, partitioning and radioactive decay). In the end, a case study is conducted using the most complete two-phase tracer model to

investigate the effect of adsorption type, partitioning coefficient and reservoir wetting condition on tracer profile and breakthrough time.

1.5 Outline of Thesis

Chapter 2 presents a review of current literature on tracer tests. The history of tracer tests and the behavior of tracer flow inside a porous media are presented and the concepts of different kinds of waves are introduced, which helps to better understand and later develop this research.

Chapter 3 provides useful mathematical concepts and theories related to this thesis. A brief introduction to mass conservation, fractional flow theory and relative permeability are presented, which are applied in the tracer models in Chapter 4.

In Chapter 4, both the analytical model and numerical model for single-phase tracer flow are presented. Subsequently, the analytical models using different conditions and the complete numerical model of two-phase tracer flow are introduced.

Chapter 5 presents a case study applying the complete tracer model to interpret the tracer concentration distributions with different input parameters and a discussion on the effects of partitioning coefficient, adsorption type, and wetting condition on tracer breakthrough time.

Chapter 6 gives the conclusions and suggestions for further research. Figure 1.5 shows the research map of this study.

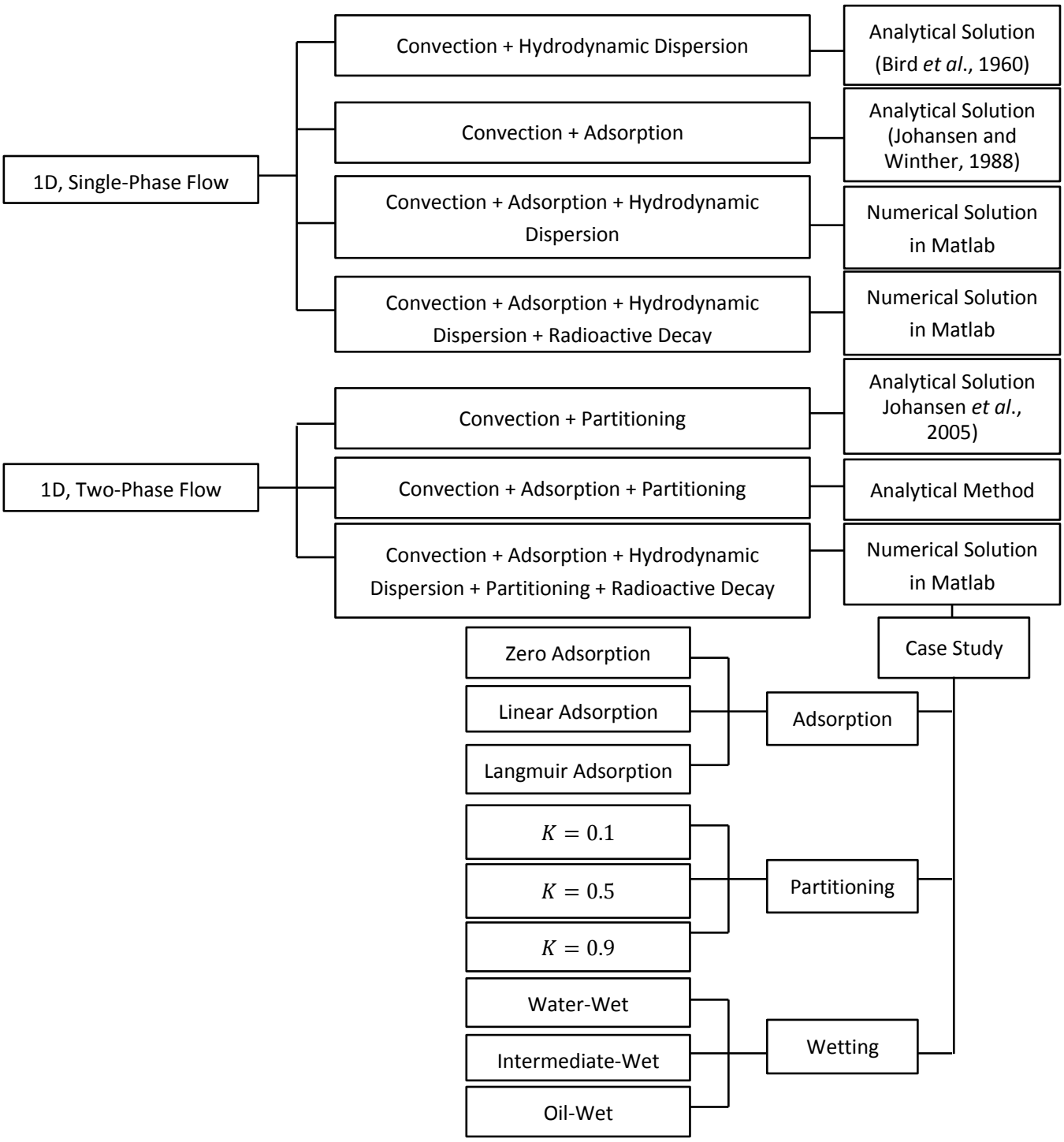

Figure 1.5: Research map

Chapter 2 Literature Review

2.1 History of Tracer Test Modeling

In the early 1950s, reservoir engineers started to apply tracer tests in the petroleum industry. At that time, they were used to obtain simple reservoir communication information qualitatively, such as the directional flow characteristics in the reservoir (Sturm and Johnson, 1951) and the presence of channels in the formation (Carpenter *et al*., 1952).

Brigham and Smith (1965) made attempts to analyze tracer tests quantitatively. They built a semi-analytical model to predict the breakthrough time and the peak concentration of tracers for a five-spot flow pattern. In their model, only convection and diffusion were considered.

Cooke (1971) proposed the first inter-well tracer test to predict residual oil saturation. Two tracers with different partitioning coefficients were injected together into the formation, which resulted in different levels of retardation relative to the carrying fluid, because the retardation is caused by partitioning between phases. The residual oil saturation was obtained based on the separation of the two tracers.

Tomich *et al*. (1973) presented a method to measure residual oil saturation from a single-well tracer test. This test was carried out in a watered-out formation. After the primary tracer was injected, the well was shut in to allow the primary tracer to react

with the water in the reservoir, which formed a secondary tracer. The two tracers had different partitioning coefficients and separated during the production period and arrived at the wellbore at different times. Based on the difference in arrival time, the residual oil saturation was estimated.

Deans and Shallenberger (1974) modified the residual oil saturation measurement model of Tomich *et al*. (1973) and reported the first single well tracer test to measure connate water saturation. This test was carried out in a formation that was producing water-free oil. The procedure and the theory are the same as the residual oil saturation measurement. The determination of connate water saturation is also based on the relative arrival time of the two tracers.

In the 1980s, numerical simulations were applied to interpret tracer tests. Hagoort (1982) developed a two-phase immiscible tracer model. The model has the following restrictions: straight-line relative permeabilities; oil and water have equal density and viscosity, and a special capillary pressure function.

Johansen *et al*. (1989) extended the model to a two-phase partitioning adsorption model with multiple tracers. An analytical solution with an arbitrary number of tracers was obtained and a simulator for tracers in one-dimensional, two-phase flow was introduced.

Datta Gupta *et al*. (1986) conducted a numerical simulation for a three-dimensional multiphase, multicomponent tracer model. The model is solved using the IMPES

(implicit pressure, explicit saturations) formulation with diffusion and adsorption included but no partitioning between phases or radioactive decay.

From the 1990s to present, most modeling of tracer tests has been conducted using commercial computer software. The most well-developed and widely-used software is UTCHEM, which is a chemical flooding simulator. The tracer model in UTCHEM can simulate a tracer test including diffusion, linear adsorption, partitioning between phases and radioactive decay. This study focuses on the development of a tracer model with diffusion, Langmuir adsorption, partitioning between phases and radioactive decay, which adds complexity of the previous models.

The most established classic laboratory tests for wettability determination in previous study is Amott-Harvey imbibition test (Amott, 1959) and the US Bureau of Mines test (Donaldson *et al*., 1969). The case study of this research shows that tracer tests could be a method to determine reservoir wettability.

2.2 Theory of Tracer Flow in Porous Media

Bear (1972) discussed the transport mechanisms of chemical species in porous media including the transport of tracers. In general, tracer transport is governed by convection, hydrodynamic dispersion, adsorption and partitioning. For radioactive tracers, radioactive decay also needs to be incorporated. In this section, all the important mechanisms for tracer flow are discussed. Previous models used the same methodology; however, not all the mechanisms discussed here are concluded in the

models.

2.2.1 Convection

Convection refers to the bulk flow of fluids governed by Darcy's Law (Darcy, 1856). The flow is caused by potential gradients in the system. In a reservoir, the gradients are caused by density differences between the flowing fluids and by pressure differences in production and injection wells.

The convection expression for one-dimensional flow of a species is given by:

$$F_{conv} = uC, \tag{2.1}$$

where F_{conv} is the mass flux caused by convection ($kg \cdot m^{-2} \cdot s^{-1}$), u is the volumetric flux (m/s) and C is the tracer mass concentration (kg/m^3).

2.2.2 Hydrodynamic Dispersion

Hydrodynamic dispersion consists of molecular diffusion and mechanical dispersion (Lake, 1989). The mechanisms of molecular diffusion and mechanical dispersion are different. Molecular diffusion is the process of mixing caused by molecular concentration gradients; however, mechanical dispersion is a result of the different flow paths that particles take through the porous media, which is strongly velocity dependent. Due to hydrodynamic dispersion, tracer flow spreads as it propagates and occupies an increasing portion of the flow domain.

Even though the mechanisms of molecular diffusion and mechanical dispersion are different, they can be expressed together and assumed to have a Fickian form (Fick, 1855):

$$F_D = -D\frac{\partial C}{\partial x}, \tag{2.2}$$

where F_D is the mass flux caused by hydrodynamic dispersion ($kg \cdot m^{-2} \cdot s^{-1}$), D is the hydrodynamic dispersion coefficient (m^2/s), C is the tracer mass concentration (kg/m^3) and x is the travel distance of tracer (m). Throughout this thesis, dispersion refers to hydrodynamic dispersion if not otherwise specified.

2.2.3 Adsorption

In this thesis, adsorption refers to the amount of tracer molecules that attach to the solid surface resulting in tracer concentration loss in the fluids. In this research, we build and solve the tracer model with Langmuir adsorption. The case study in Chapter 5 compares this model with zero adsorption model and linear adsorption model to investigate the effect of adsorption model on tracer breakthrough time.

The Langmuir adsorption isotherm represents the equilibrium distribution of ions between the fluid phase and the stationary phase and after equilibrium no further adsorption takes place. It assumes monolayer adsorbate attached to a finite number of sorption sites and there are no interactions between adsorbed molecules and neighboring sites (Langmuir, 1916).

The Langmuir adsorption is given by:

$$C_S = \frac{aC}{1 + bC}, \tag{2.3}$$

where C is the tracer mass concentration (kg/m^3), C_S is the adsorbed tracer concentration (kg/m^3), a and b are empirical constants. The unit of b is m^3/kg, which is the reciprocal of the unit of C and a is dimensionless. As shown from Eq. (2.3), the adsorbed concentration C_S (kg/m^3) depends only on the tracer concentration in single-phase flow.

Linear adsorption is a special case of Langmuir adsorption isotherm:

$$C_S = aC, \tag{2.4}$$

where $bC \ll 1$.

As linear adsorption is a simplification of Langmuir adsorption at a certain circumstance ($bC \ll 1$), Langmuir adsorption would be more accurate and can be applied to a wider range compared to linear adsorption. Figure 2.1 shows the general form of the Langmuir adsorption and linear adsorption isotherm.

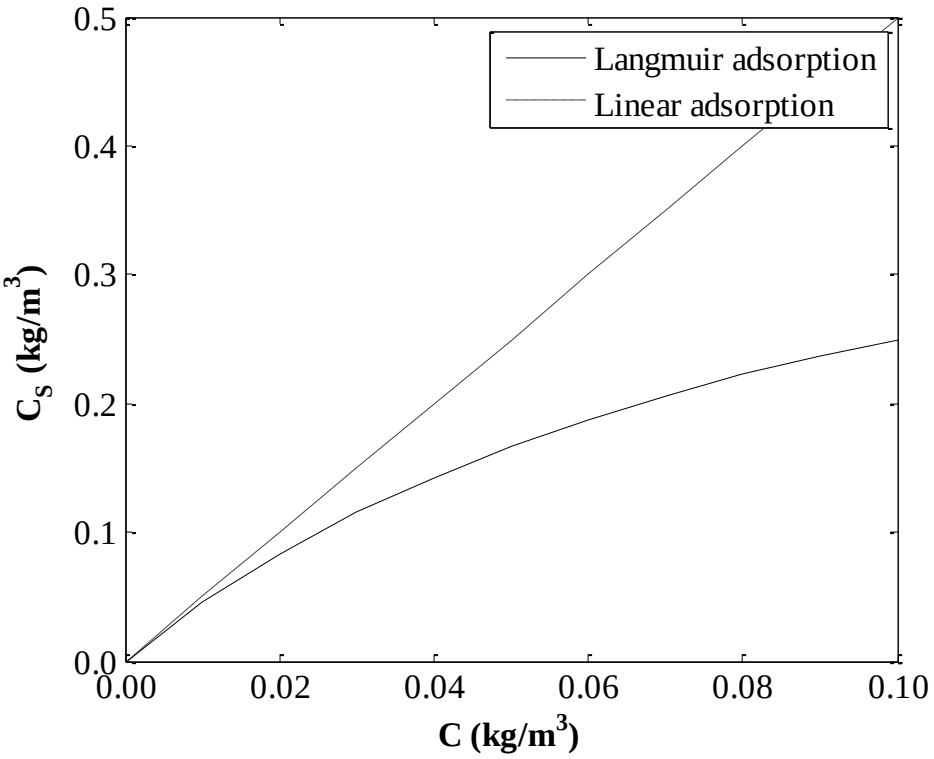

Figure 2.1: Langmuir adsorption and linear adsorption isotherm

2.2.4 Radioactive Decay

Radioactive decay is the process by which an unstable atom releases energy and matter to reach a stable form. This only applies to radioactive tracers and may cause a relatively large amount of concentration loss in the fluids.

The decay process of an atom is statistically random and unpredictable. However, if the number of atoms is large enough, the rate of decay can be formulated:

$$\frac{dN}{dt} = -\lambda N \,, \tag{2.5}$$

where N is the number of atoms and λ is the decay constant defined by:

$$\lambda = \frac{ln2}{t_{1/2}}, \tag{2.6}$$

where $t_{1/2}$ is the half-life of the radioactive tracer. Half-life is the time interval required for one-half of the atomic nuclei of a radioactive sample to decay and it is a constant for a specific radioactive isotope.

Integration of Eq. (2.5) gives the standard equation for exponential radioactive decay:

$$N(t) = N_0 e^{-\lambda t}, \tag{2.7}$$

where N_0 is the initial number of atoms and $N(t)$ is the number of atoms after time t.

2.3 Waves

In physics, a wave is usually described as a disturbance that travels through a medium as an energy transport phenomenon. The wave discussed in this thesis however, refers to the tracer concentration change that propagates through the permeable media. Waves can be divided into the following types based on the change of shape while propagating (Lax, 1957).

1）Rarefaction waves

The shape of a rarefaction wave remains unchanged while propagating and all the points maintain the same relative position as shown in Figure 2.2. This may happen in single phase flow when only convection and linear adsorption is present, which makes the different concentrations travel with the same velocity.

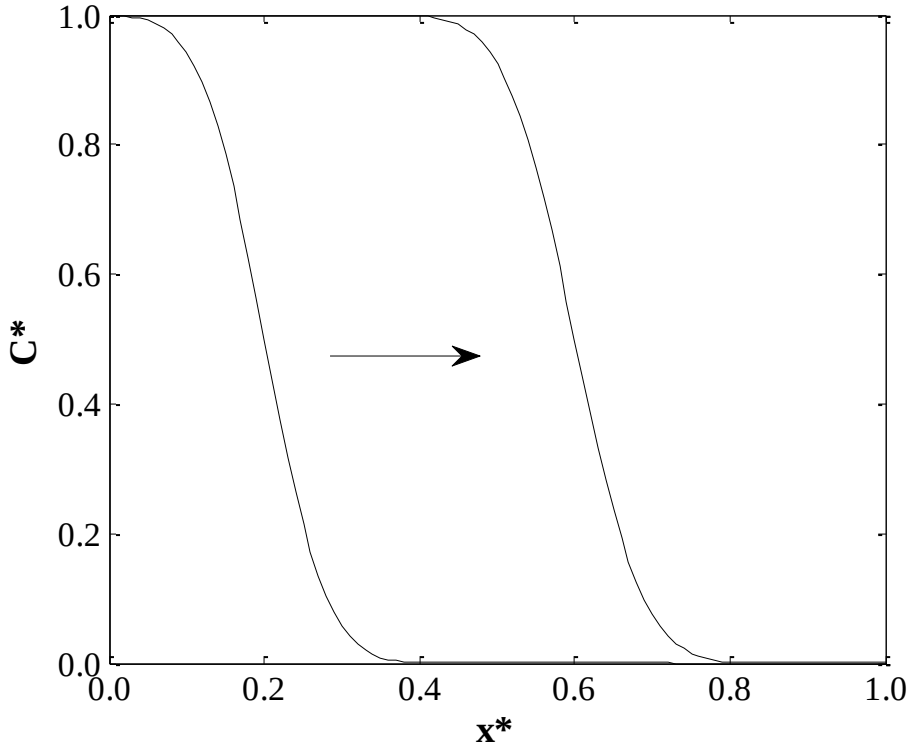

Figure 2.2: Rarefaction wave

2）Self-sharpening waves and shock waves

The shape of a self-sharpening wave shrinks upon propagation which means the neighboring compositions get closer. Shock waves take shape when discontinuities happen as a result of self-sharpening waves. If slower waves (closer to the initial conditions) form ahead of faster waves, a leading shock wave will originate when faster waves catch up to the slower waves. The formation of a shock wave is shown in Figure 2.3 and this phenomenon happens only when the dispersion term is missing (Section 4.1.2).

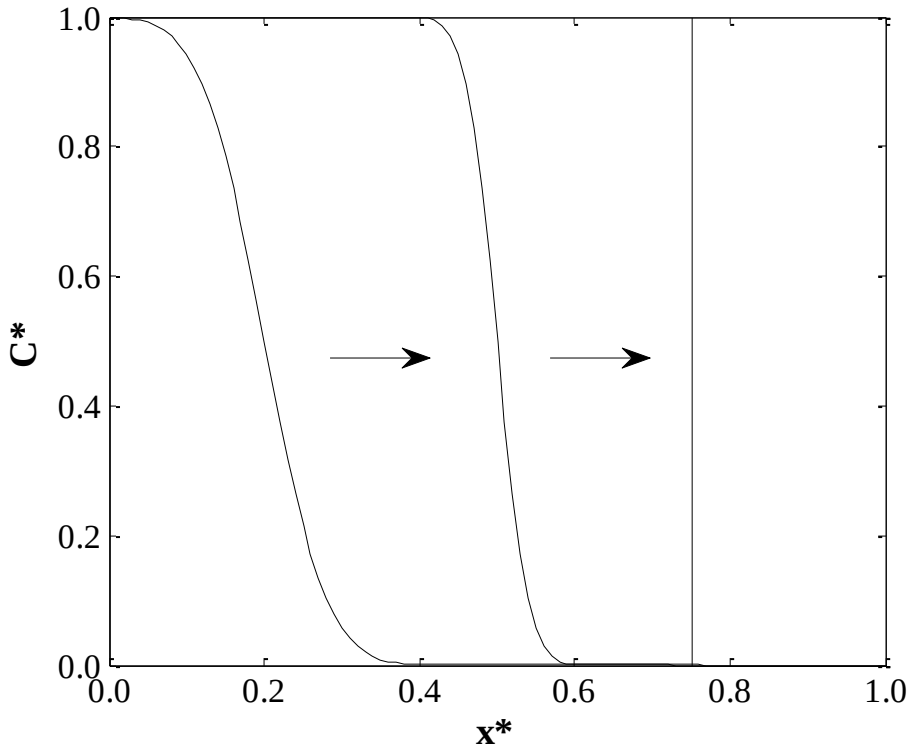

Figure 2.3: Formation of shock waves

3）Diffusive waves

The shock wave happens when the dispersion term is missing, which is a simplification for an analytical solution. In real cases, dispersion can never be avoided. The effect of dispersion enlarges the mixing zone and results in diffusive waves shown in Figure 2.4.

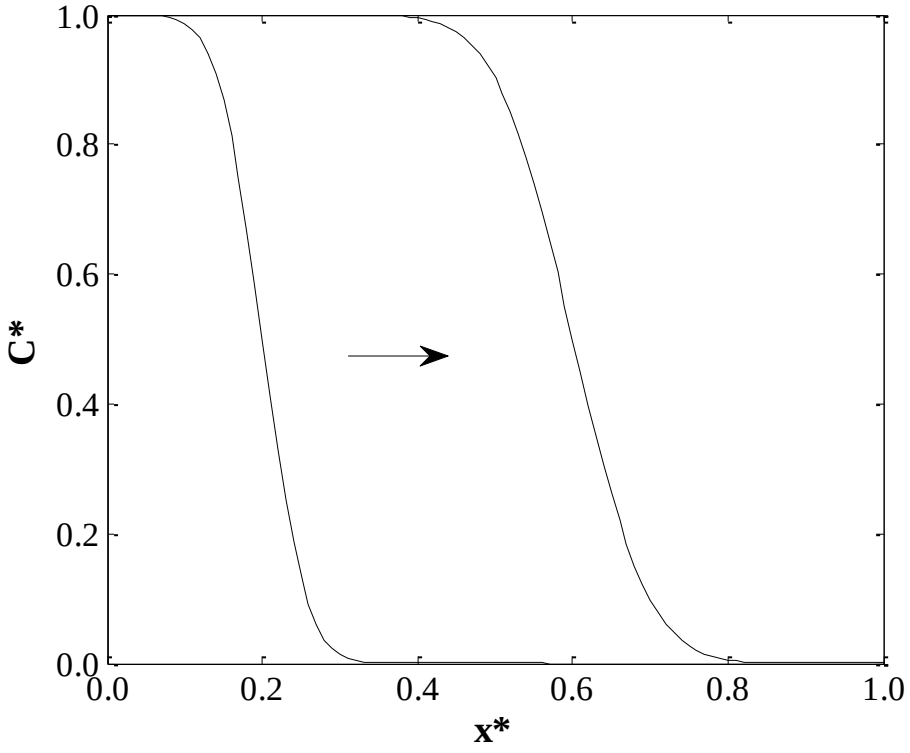

Figure 2.4: Diffusive wave

Chapter 3 Mathematical Method Development and Results

3.1 Mathematical Background

In this chapter, useful mathematical concepts and theories related to this thesis are discussed. The mass conservation for components in multiphase flow, the fractional flow theory and the relative permeability are introduced, all of which are applied in the tracer models in Chapter 4

3.1.1 Mass Conservation

The mass conservation for components in multiphase flow is developed by Bear (1972). In his development, he included accumulation term, flux term and source term. These are all discussed in this section.

The mass conservation equation for each component in each phase is given as:

$$\frac{\partial W_{ij}}{\partial t} + \vec{\nabla} \cdot \vec{N}_{ij} - R_{ij} = 0 \qquad i = 1, \dots, N_c \quad j = 1, \dots, N_p \,, \tag{3.1}$$

where W_{ij} is the component concentration in units of mass of i in phase j per bulk volume (kg/m^3), which is the accumulation term; $\vec{N}_{ij}$ is the mass flux term ($kg \cdot m^{-2} \cdot s^{-1}$); R_{ij} is the source term ($kg \cdot m^{-3} \cdot s^{-1}$), N_c is the number of components and N_p is the number of phases.

For one-dimensional flow, Eq. (3.1) is simplified to:

$$\frac{\partial W_{ij}}{\partial t} + \frac{\partial N_{ij}}{\partial x} - R_{ij} = 0 \qquad i = 1, \dots, N_c \quad j = 1, \dots, N_p \,. \tag{3.2}$$

The terms in Eq. (3.2) are discussed in detail below.

Accumulation term

Let V be the bulk volume. Then, the volume occupied by fluid phase j is $\emptyset S_j V$ and the volume occupied by the solid phase is $(1-\emptyset)V$, where $\emptyset$ is porosity and S_j is the saturation of phase j.

Define ε_j as the volume fraction occupied by fluid phase j. Then ε_j can be formulated as the volume of phase j divided by the bulk volume V:

$$\varepsilon_j = \emptyset S_j \text{ for fluid phases,} \tag{3.3}$$

and

$$\varepsilon_j = 1 - \emptyset \text{ for solid phase.} \tag{3.4}$$

Then, the total mass of phase j can be expressed as $\rho_j \varepsilon_j V$ where ρ_j is the density of phase j.

We define ω_{ij} to be the mass fraction of component i in phase j, which is the mass of component i in phase j divided by total mass of phase j:

$$\omega_{ij} = \frac{W_{ij} V}{\rho_j \varepsilon_j V} = \frac{W_{ij}}{\rho_j \varepsilon_j} \,. \tag{3.5}$$

Thus, the accumulation term W_{ij} is expressed as:

$$W_{ij} = \varepsilon_j \rho_j \omega_{ij} = \varepsilon_j C_{ij} \,, \tag{3.6}$$

where $C_{ij} = \rho_j \omega_{ij}$ is the mass concentration of component i in phase j (kg/m^3).

Flux term

As a component is transported through porous media by the mechanism of convection or hydrodynamic dispersion, the flux is the sum of the two mechanisms. As both convection and hydrodynamic dispersion have already been discussed in section 2.2, the flux term can be obtained by summing Eq. (2.1) and Eq. (2.2):

$$N_{ij} = u_j C_{ij} - \varepsilon_j D_{ij} \frac{\partial C_{ij}}{\partial x} \,, \tag{3.7}$$

where u_j is volumetric flux of phase j (m/s) and D_{ij} is overall dispersion coefficient of component i in phase j (m^2/s).

Source term

The source term R_{ij} is the generation or vanish rate of component i in phase j due to chemical or biological reactions. R_{ij} is formulated based on the following relationship:

$$R_{ij} = \varepsilon_j r_{ij} \,, \tag{3.8}$$

where r_{ij} is the reaction rate of component i in phase j ($kg \cdot m^{-3} \cdot s^{-1}$).

For radioactive tracers, the reaction rate for radioactive decay is given by $r_{ij} = -\lambda C_{ij}$ which was reformulated from Eq. (2.5) in section 2.2.

Combining the source term for a radioactive tracer is given by:

$$R_{ij} = -\varepsilon_j \lambda C_{ij} \,. \tag{3.9}$$

Substitution of Eq. (3.6), Eq. (3.7) and Eq. (3.9) into Eq. (3.2) gives the one-dimensional mass conservation equation for component i in phase j:

$$\frac{\partial(\varepsilon_j C_{ij})}{\partial t} + \frac{\partial(u_j C_{ij})}{\partial x} - \varepsilon_j D_{ij} \frac{\partial^2 C_{ij}}{\partial x^2} + \varepsilon_j \lambda C_{ij} = 0 \,. \tag{3.10}$$

In this thesis, only one tracer exists, i.e., this is a one-component system. The conservation equations for the tracer in each phase can be written as:

Water phase: $$\frac{\partial}{\partial t}(\emptyset S_w C_w) + \frac{\partial}{\partial x}(u_w C_w) - \emptyset S_w D_w \frac{\partial^2 C_w}{\partial x^2} + \emptyset S_w \lambda C_w = 0 \,. \tag{3.11}$$

Oil phase: $$\frac{\partial}{\partial t}(\emptyset S_o C_o) + \frac{\partial}{\partial x}(u_o C_o) - \emptyset S_o D_o \frac{\partial^2 C_o}{\partial x^2} + \emptyset S_o \lambda C_o = 0 \,. \tag{3.12}$$

Solid phase: $$\frac{\partial}{\partial t}[(1-\emptyset) C_s] = 0 \,. \tag{3.13}$$

Then, the general two-phase, single-tracer conservation equation can be obtained by summing the above three equations:

$$\emptyset \frac{\partial}{\partial t}[K C_w (1 - S_w) + C_w S_w] + (1-\emptyset)\frac{\partial Cs}{\partial t} + u_T \frac{\partial}{\partial x}[K C_w (1 - f_w) + C_w f_w]$$

$$-\emptyset \frac{\partial}{\partial x}\left[S_w D_w \frac{\partial C_w}{\partial x} + (1 - S_w) D_o K \frac{\partial C_w}{\partial x}\right] + \emptyset\lambda[S_w C_w + K C_w (1 - S_w)] = 0 \,, \tag{3.14}$$

where $K = {C_o}/{C_w}$ is the partitioning coefficient, $u_T = u_w + u_o =$constant the total volumetric flux and $f_w = {u_w}/{u_T}$ is the fractional flow function.

3.1.2 Relative Permeability and the Corey Model

Absolute permeability refers to the permeability of rock when saturated with one fluid, i.e., 100% saturation of one fluid. Effective permeability is the permeability of a fluid when more than one fluid saturates the rock. Relative permeability is defined as the ratio of the effective permeability of a given fluid to the absolute permeability of the rock:

$$k_{rj} = \frac{k_j}{k}\,, \tag{3.15}$$

where k_{rj} is the relative permeability of phase j, k_j is the effective permeability of phase j and k is the absolute permeability.

In an oil-water system, the relative permeabilities of both water (k_{rw}) and oil (k_{ro}) are functions of water saturation S_w. The Corey model is an empirical prediction model for relative permeability calculations (Corey *et al*., 1954):

$$k_{rw} = a_w(\bar{S}_w)^{n_w}\,, \tag{3.16}$$

$$k_{ro} = a_o(1 - \bar{S}_w)^{n_o}\,, \tag{3.17}$$

where

$$\bar{S}_w = \frac{S_w - S_{wc}}{1 - S_{wc} - S_{or}}, \tag{3.18}$$

and a_w, a_o, n_w and n_o are empirical constants. Furthermore, S_{wc} is the connate water saturation and S_{or} is the residual oil saturation.

Both oil relative permeability and water relative permeability can be plotted as functions of water saturation if a_w, a_o, n_w, n_o, S_{wc} and S_{or} are given. Figure 3.1 shows one example of relative permeability curves ($a_w = 0.4$, $a_o = 0.9$, $n_w = 3$, $n_o = 3$, $S_{wc} = 0.2$ and $S_{or} = 0.2$).

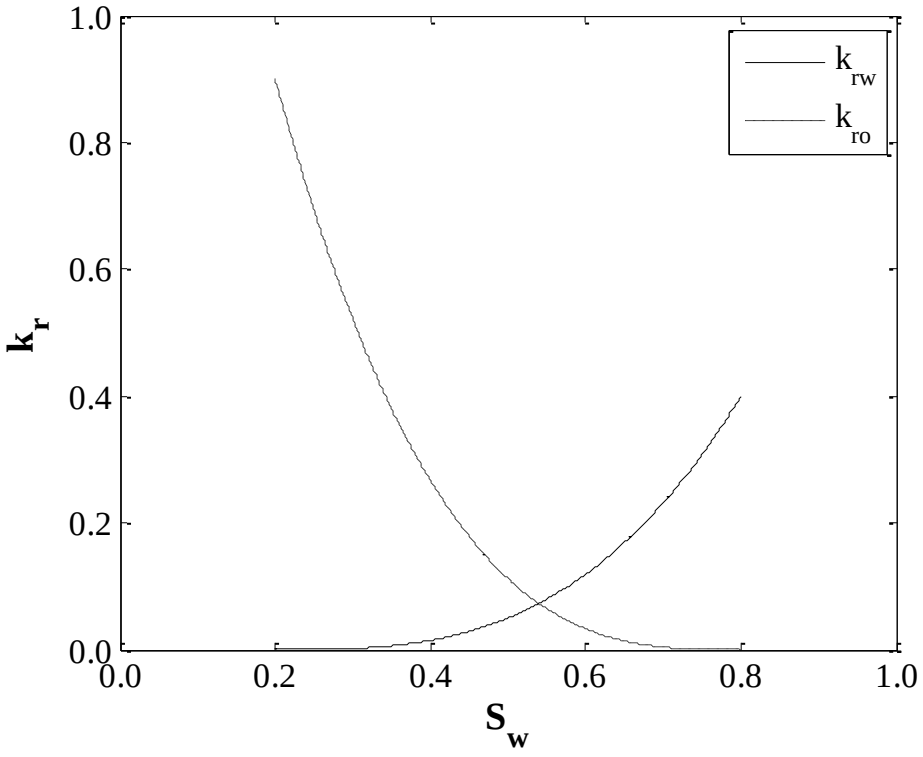

Figure 3.1: Relative permeability curves

3.1.3 Fractional Flow Theory

In 1942, the Buckley-Leverett theory is developed for waterflooding. Since then, it has been applied to areas of enhanced oil recovery. The fractional flow of a phase is defined as the flow rate of a particular phase divided by the total flow rate. When considering an oil-water displacement with a dipping angle α, the fractional flow of water in an oil-water system can be determined as shown below (Buckley and Leverett, 1942; Johansen, 2008).

First, applying Darcy's law to oil and water:

$$u_o = -\frac{kk_{ro}}{\mu_o}\left(\frac{\partial P_o}{\partial x} + \rho_o g sin\alpha\right), \tag{3.19}$$

$$u_w = -\frac{kk_{rw}}{\mu_w}\left(\frac{\partial P_w}{\partial x} + \rho_w g sin\alpha\right), \tag{3.20}$$

where μ_o, μ_w, ρ_o, ρ_w are the viscosity and density of oil and water, respectively. Here, u_o is the oil flux and u_w is the water flux.

Let P_o and P_w be the pressures of the oil phase and water phase, respectively, and assume the system is water-wet. Then, P_c, which is the capillary pressure between oil phase and water phases, is defined by:

$$P_c = P_o - P_w\,. \tag{3.21}$$

Substitution of Eq. (3.21) into Eq. (3.19) gives:

$$u_o = -\frac{kk_{ro}}{\mu_o}\left(\frac{\partial(P_w + P_c)}{\partial x} + \rho_o g sin\alpha\right). \quad (3.22)$$

We define the phase mobility by:

$$\lambda_w = \frac{kk_{rw}}{\mu_w}, \quad (3.23)$$

$$\lambda_o = \frac{kk_{ro}}{\mu_o}. \quad (3.24)$$

Then, Eq. (3.22) and Eq. (3.20) become:

$$u_o = -\lambda_o\left(\frac{\partial P_w}{\partial x} + \frac{\partial P_c}{\partial x} + \rho_o g sin\alpha\right), \quad (3.25)$$

$$u_w = -\lambda_w\left(\frac{\partial P_w}{\partial x} + \rho_w g sin\alpha\right). \quad (3.26)$$

Therefore,

$$u_T = u_o + u_w = -\lambda_o\left(\frac{\partial P_w}{\partial x} + \frac{\partial P_c}{\partial x} + \rho_o g sin\alpha\right) - \lambda_w\left(\frac{\partial P_w}{\partial x} + \rho_w g sin\alpha\right). \quad (3.27)$$

From Eq. (3.26):

$$\frac{\partial P_w}{\partial x} = -\frac{u_w}{\lambda_w} - \rho_w g sin\alpha. \quad (3.28)$$

Substitution of Eq. (3.28) into Eq. (3.27) gives:

$$u_T = -\lambda_T\left(-\frac{u_w}{\lambda_w} - \rho_w g sin\alpha\right) - \lambda_o\frac{\partial P_c}{\partial x} - \lambda_o\rho_o g sin\alpha - \lambda_w\rho_w g sin\alpha, \quad (3.29)$$

where

$$\lambda_T = \lambda_w + \lambda_o. \quad (3.30)$$

Rearranging Eq. (3.29) gives,

$$u_w = \lambda_w \left(\frac{u_T + \lambda_o \frac{\partial P_c}{\partial x} + \lambda_o \rho_o g sin\alpha + \lambda_w \rho_w g sin\alpha}{\lambda_T} - \rho_w g sin\alpha \right). \quad (3.31)$$

Then, the fractional flow function for water is defined as,

$$f_w = \frac{u_w}{u_T} = \frac{\lambda_w}{\lambda_T} + \frac{\lambda_o \lambda_w}{u_T \lambda_T} \frac{\partial P_c}{\partial x} - \frac{\lambda_o \lambda_w}{u_T \lambda_T} \Delta \rho g sin\alpha \,. \quad (3.32)$$

Throughout the thesis, we consider only horizontal flow; hence Eq. (3.32) reduces to:

$$f_w = \frac{u_w}{u_T} = \frac{\lambda_w}{\lambda_T} + \frac{\lambda_o \lambda_w}{u_T \lambda_T} \frac{\partial P_c}{\partial x} \,. \quad (3.33)$$

Let,

$$F_w = \frac{\lambda_w}{\lambda_T} \,, \quad (3.34)$$

then,

$$f_w = \frac{u_w}{u_T} = F_w + \frac{\lambda_o \lambda_w}{u_T \lambda_T} \frac{\partial P_c}{\partial x} \,. \quad (3.35)$$

Eq. (3.34) can be written as:

$$F_w = \frac{\lambda_w}{\lambda_T} = \frac{1}{1 + \frac{\mu_w}{\mu_o} \frac{k_{ro}}{k_{rw}}} \,, \quad (3.36)$$

which is a special format of fractional flow function when capillary pressure is not considered.

From the Corey Model discussed in the previous section (Corey, 1954):

$$\frac{k_{ro}}{k_{rw}} = \frac{a_o(1 - \frac{S_w - S_{wc}}{1 - S_{wc} - S_{or}})^{n_o}}{a_w(\frac{S_w - S_{wc}}{1 - S_{wc} - S_{or}})^{n_w}} . \tag{3.37}$$

Substituting Eq. (3.37) into Eq. (3.36) gives:

$$F_w = \frac{1}{1 + \frac{\mu_w}{\mu_o} \frac{a_o(1 - \frac{S_w - S_{wc}}{1 - S_{wc} - S_{or}})^{n_o}}{a_w(\frac{S_w - S_{wc}}{1 - S_{wc} - S_{or}})^{n_w}}} . \tag{3.38}$$

An example of the fractional flow (F_w) is plotted in Figure 3.2 corresponding to Figure 3.1, and is shown with its common S-shape.

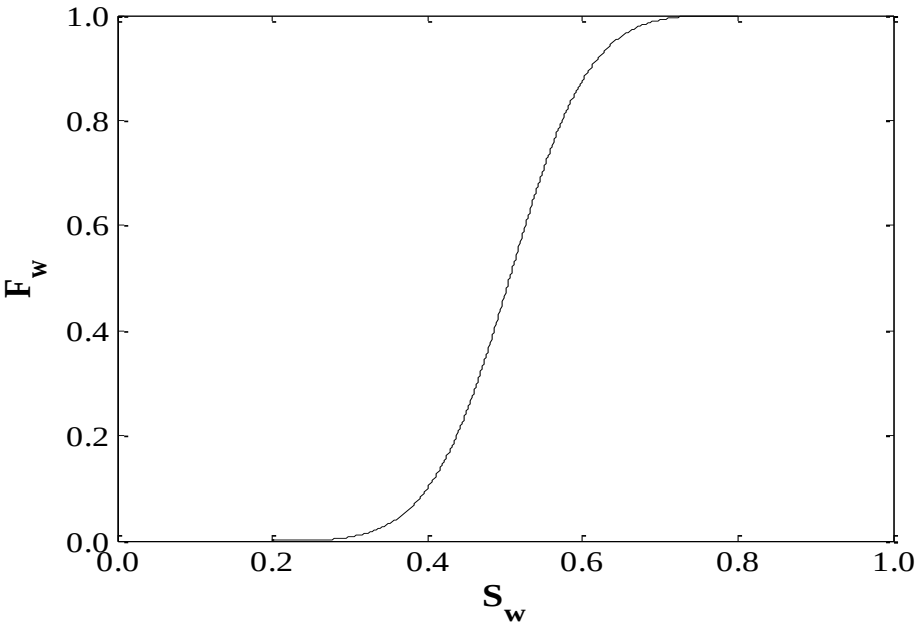

Figure 3.2: Fractional flow function

3.2 One-Dimensional, Single-Phase Single Tracer Modeling

In this section, a miscible displacement model is discussed for single-component tracer flow, which means the tracer mixes with the original phase in all proportions and the system acts as single phase. As this is a one-dimensional tracer slug displacement, we describe the leading edge and the trailing edge of the tracer slug. Simplifications are made through different assumptions and either analytical methods or numerical methods are applied for specific situations.

The general single-phase, one-dimensional conservation equation for a tracer flow is derived based on the following assumptions:

1) The tracer is ideal, i.e. the properties of the carrying phase are not affected by the tracer.
2) The flow is single phase, which means neither fractional flow effects nor capillary pressure effects are considered.
3) The flow is one dimensional.
4) Both fluid and rock are incompressible.
5) The process is isothermal.
6) The flow is horizontal (no gravity effect).

As discussed in Chapter 2, tracer flow is governed by the following mechanisms: 1) Convection; 2) Hydrodynamic dispersion (diffusion and dispersion); 3) Adsorption; and 4) Radioactive Decay. A general one-dimensional, single-phase tracer

conservation equation is obtained by substituting $S_w = 1$ in the two-phase tracer conservation equation, i.e., Eq. (3.14) to give:

$$\emptyset \frac{\partial C}{\partial t} + (1 - \emptyset) \frac{\partial C_S}{\partial t} + u_T \frac{\partial C}{\partial x} - \emptyset D \frac{\partial^2 C}{\partial x^2} + \emptyset \lambda C = 0 \,, \tag{3.39}$$

where C is the mass concentration of tracer (kg/m^3), C_S is the sorbed concentration of tracer (kg/m^3), u_T is the total volumetric flux (m/s), x is the distance (m), t is the time (s), $\emptyset$ is porosity, D is hydrodynamic dispersion coefficient (m^2/s) and λ is the decay constant (s^{-1}).

After the equation is introduced, the main task is to find the solution of concentration as a function of position and time for the general single-phase one-dimensional tracer flow equation, Eq. (3.39). Although the complete model, Eq. (3.39) lacks an analytical solution, additional assumptions are made to make this possible. Analytical methods for solving the convection dispersion equation and the convection adsorption equation are introduced in Section 3.2.1 and Section 3.2.2, which give better understanding of the tracer flow behavior. Other complex equations can only be solved by numerical methods and were implemented in Matlab codes by the author (Section 3.2.3 and Section 3.2.4).

3.2.1 Convection Dispersion Model

The analytical method to solve the convection dispersion equation is described below (Bird *et al*., 1960; Johansen, 2008).

When the convection term and the dispersion term are non-zero, Eq. (4.39) becomes:

$$\emptyset \frac{\partial C}{\partial t} + u_T \frac{\partial C}{\partial x} - \emptyset D \frac{\partial^2 C}{\partial x^2} = 0\,, \tag{3.40}$$

The above equation is known as the convection dispersion equation.

Dimensionless variables x^*, t^* and C^* are defined to simplify the equation:

$$x^* = \frac{x}{L}\,, \tag{3.41}$$

$$t^* = \frac{u_T t}{\emptyset L}\,, \tag{3.42}$$

$$C^* = \frac{C - C_R}{C_L - C_R}\,, \tag{3.43}$$

where C_L is the left-end concentration of the system (kg/m^3) and C_R is the right-end concentration of the system (kg/m^3). L is the distance between injection well and production well (m).

Applying the dimensionless variables yields:

$$\frac{\partial C^*}{\partial t^*} + \frac{\partial C^*}{\partial x^*} - \frac{1}{N_{pe}} \frac{\partial^2 C^*}{\partial x^{*2}} = 0, \tag{3.44}$$

where

$$N_{pe} = \frac{u_T L}{\emptyset D}\,, \tag{3.45}$$

is the Peclet number, which is used to define the ratio of convective mass transfer over

dispersion mass transfer. A large Peclet number means that convection is relatively dominant in the fluid flow.

In the case of injecting a slug of tracer into a horizontal reservoir, as shown in Figure 3.3, the boundary condition for the leading edge is: $C^*(x,0) = 0;\ C^*(0,t) = 1$ and the trailing edge is: $C^*(x,0) = 1;\ C^*(0,t) = 0$.

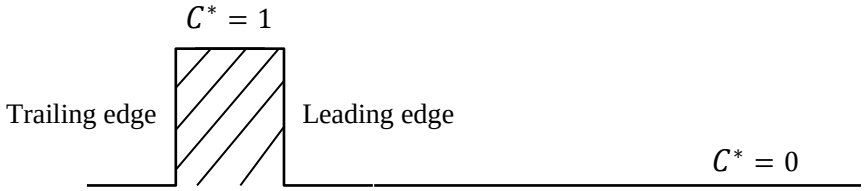

Figure 3.3: Overview of tracer injection in a horizontal reservoir

The convection term in Eq. (3.44) can be taken out by transforming from Eulerian coordinates to Lagrangian coordinates. The Eulerian coordinates correspond to spatial points and the Lagrangian coordinates correspond to material points. Therefore, by assuming the reference point travels with the same velocity as the convection wave, the convection term is vanishing. To reach this target, the following transform is introduced:

$$\xi = x^* - t^*\,, \tag{3.46}$$

$$\tau = t^*\,. \tag{3.47}$$

Applying the chain rule:

$$\frac{\partial C^*}{\partial t^*} = -\frac{\partial C^*}{\partial \xi} + \frac{\partial C^*}{\partial \tau}\,, \tag{3.48}$$

$$\frac{\partial C^*}{\partial x^*} = \frac{\partial C^*}{\partial \xi}\,. \tag{3.49}$$

Substitution of Eq. (3.48) and Eq. (3.49) into Eq. (3.44) gives the convection dispersion equation based on dimensionless Lagrangian coordinates:

$$\frac{\partial C^*}{\partial \tau} = \frac{1}{N_{pe}} \frac{\partial^2 C^*}{\partial \xi^2}\,. \tag{3.50}$$

Then, the Boltzmann Transformation is introduced to convert the partial differential equation above to an ordinary differential equation which can be easily solved. A variable η is defined as a combination of ξ and τ:

$$\eta = \frac{\xi}{2\sqrt{\tau/N_{pe}}}\,. \tag{3.51}$$

The partial derivatives of η are:

$$\frac{\partial \eta}{\partial \tau} = -\frac{\eta}{2\sqrt{\tau/N_{pe}}}\,, \tag{3.52}$$

$$\frac{\partial \eta}{\partial \xi} = \frac{1}{2\sqrt{\tau/N_{pe}}}\,. \tag{3.53}$$

Then, the partial derivatives of C^* can be expressed in terms of η by applying the chain rule again:

$$\frac{\partial C^*}{\partial \xi} = \frac{\partial C^*}{\partial \eta}\frac{\partial \eta}{\partial \xi} = \frac{1}{2\sqrt{\tau/N_{pe}}}\frac{\partial C^*}{\partial \eta}, \tag{3.54}$$

$$\frac{\partial^2 C^*}{\partial \xi^2} = \frac{1}{4\tau/N_{pe}}\frac{\partial^2 C^*}{\partial \eta^2}, \tag{3.55}$$

$$\frac{\partial C^*}{\partial \tau} = \frac{\partial C^*}{\partial \eta}\frac{\partial \eta}{\partial \tau} = -\frac{\eta}{2\tau}\frac{\partial C^*}{\partial \eta}. \tag{3.56}$$

Inserting these expressions into Eq. (3.50) gives:

$$-\frac{\eta}{2\tau}\frac{\partial C^*}{\partial \eta} = \frac{1}{N_{pe}}\frac{1}{4\tau/N_{pe}}\frac{\partial^2 C^*}{\partial \eta^2}. \tag{3.57}$$

The variable τ can be eliminated and η is the only variable in the equation, which means the equation is reduced to an ordinary differential equation successfully:

$$2\eta\frac{dC^*}{d\eta} + \frac{d^2C^*}{d\eta^2} = 0, \tag{3.58}$$

with the following boundary conditions:

$$C^*(\infty) = 0, \tag{3.59}$$

$$C^*(-\infty) = 1. \tag{3.60}$$

To reduce this second-order ordinary differential equation to first-order ordinary differential equations, another variable is defined:

$$\delta = \frac{dC^*}{d\eta}. \tag{3.61}$$

Then, Eq. (3.58) becomes:

$$2\eta\delta + \frac{d\delta}{d\eta} = 0\,. \tag{3.62}$$

The above equation can be easily solved as follows:

$$\delta = \alpha e^{-\eta^2}, \tag{3.63}$$

then,

$$\frac{dC^*}{d\eta} = \alpha e^{-\eta^2}\,. \tag{3.64}$$

After integration,

$$C^*(\eta) = C^*(0) + \alpha \int_0^{\eta} e^{-\eta^2}\, d\eta\,. \tag{3.65}$$

Combining the boundary conditions, α and $C^*(0)$ is calculated:

$$\alpha = -\frac{1}{\sqrt{\pi}}\,, \tag{3.66}$$

$$C^*(0) = -\frac{\sqrt{\pi}}{2}\alpha = \frac{1}{2}\,. \tag{3.67}$$

Then, the concentration distribution can be expressed as a function of η:

$$C^*(\eta) = \frac{1}{2}\left[1 - erf(\eta)\right], \tag{3.68}$$

where

$$erf(\eta) = \frac{2}{\sqrt{\pi}} \int_0^{\eta} e^{-\eta^2}\, d\eta\,, \tag{3.69}$$

is a special function in mathematics called the Error Function, the values of which are shown in Table 3.1.

Table 3.1: Error Function table

x	$erf(x)$	x	$erf(x)$
0.00	0.0000	0.90	0.7969
0.05	0.0564	0.95	0.8208
0.10	0.1124	1.00	0.8427
0.15	0.1680	1.10	0.8802
0.20	0.2227	1.20	0.9103
0.25	0.2763	1.30	0.9340
0.30	0.3206	1.40	0.9523
0.35	0.3793	1.50	0.9661
0.40	0.4203	1.60	0.9763
0.45	0.4754	1.70	0.9838
0.50	0.5205	1.80	0.9890
0.55	0.5633	1.90	0.9927
0.60	0.6039	2.00	0.9953
0.65	0.6420	2.10	0.9970
0.70	0.6778	2.20	0.9981
0.75	0.7111	2.30	0.9988
0.80	0.7421	2.40	0.9993
0.85	0.7707	2.50	0.9996

The final form of the solution is obtained by back substituting the dimensionless variables into Eq. (3.68),

$$C(x,t) = C_R + \frac{1}{2}(C_L - C_R)\left[1 - erf\left(\frac{x-t}{2\sqrt{t/N_{pe}}}\right)\right], \qquad (3.70)$$

and also the dimensionless form is shown below,

$$C^* = \frac{1}{2}\left[1 - erf\left(\frac{x^* - t^*}{2\sqrt{t^*/N_{pe}}}\right)\right]. \tag{3.71}$$

The above dimensionless concentration equation is plotted in Figure 3.4, which gives an overview of concentration propagation for a fixed Peclet number: $N_{pe} = 200$ and different times: $t_1^* = 0.2$, $t_2^* = 0.4$, $t_3^* = 0.7$. The figure shows that the leading edge propagates along the x direction as a diffusive wave, which is caused by dispersion only.

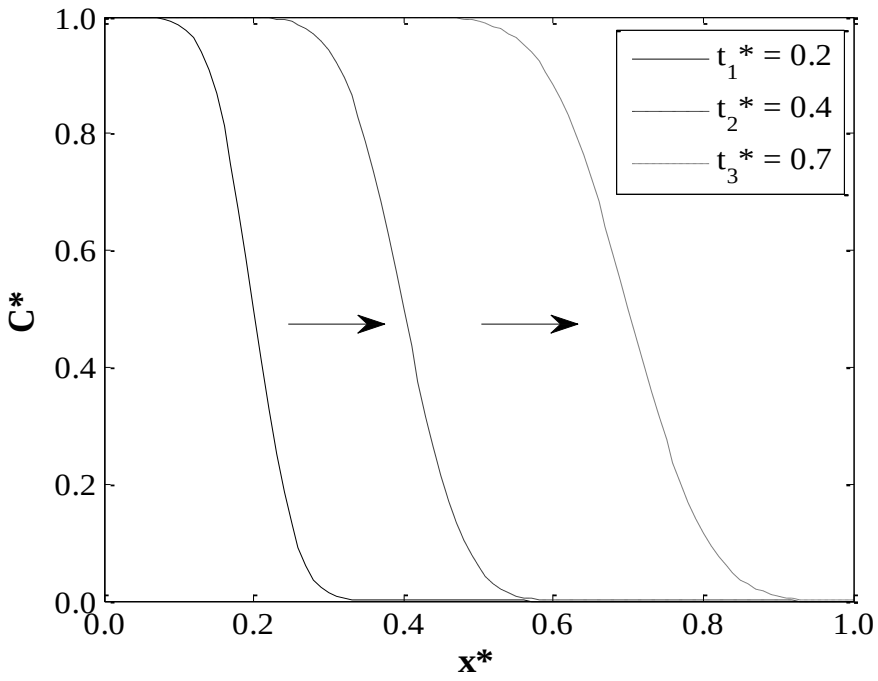

Figure 3.4: Leading edge of dimensionless concentration distribution (C^*) propagates over time for $N_{pe} = 200$

Figure 3.5 is plotted for the dimensionless concentration distribution at a constant dimensionless time $t^* = 0.4$ with different Peclet numbers: $N_{pe1} = 50$, $N_{pe2} = 200$,

$N_{pe3} = 1000$. The figure shows that the size of the mixing zone increases as the Peclet number decreases. This is because N_{pe} is defined as the ratio of convection rate over dispersion rate, therefore a smaller N_{pe} means dispersion is more significant, i.e., the mixing zone grows faster.

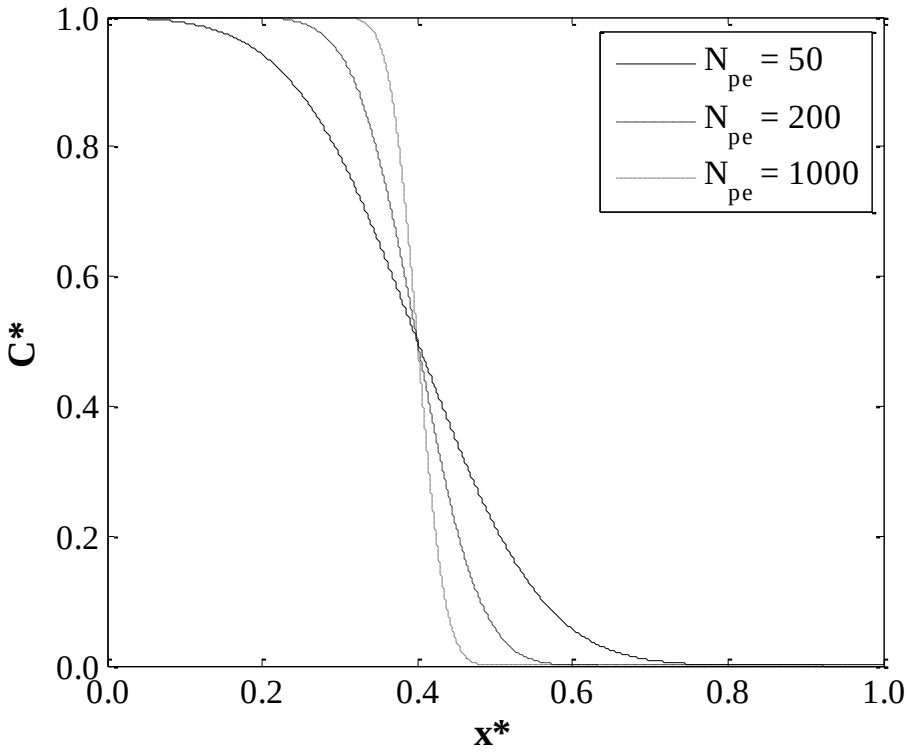

Figure 3.5: Leading edge of dimensionless concentration distribution (C^*) with different Peclet numbers

The trailing edge can be solved similarly as the leading edge. The only difference is to change the boundary conditions to $C^*(x, 0) = 1$; $C^*(0, t) = 0$. The final form of solution is:

$$C(x,t) = C_R + \frac{1}{2}(C_L - C_R)\left[1 + erf\left(\frac{x-t}{2\sqrt{t/N_{pe}}}\right)\right], \tag{3.72}$$

and also the dimensionless form:

$$C^* = \frac{1}{2}\left[1 + erf\left(\frac{x^* - t^*}{2\sqrt{t^*/N_{pe}}}\right)\right]. \tag{3.73}$$

The dimensionless concentration is also plotted as shown in Figure 3.6 for $N_{pe} = 200$ with three time steps: $t_1^* = 0.2$, $t_2^* = 0.4$, $t_3^* = 0.7$.

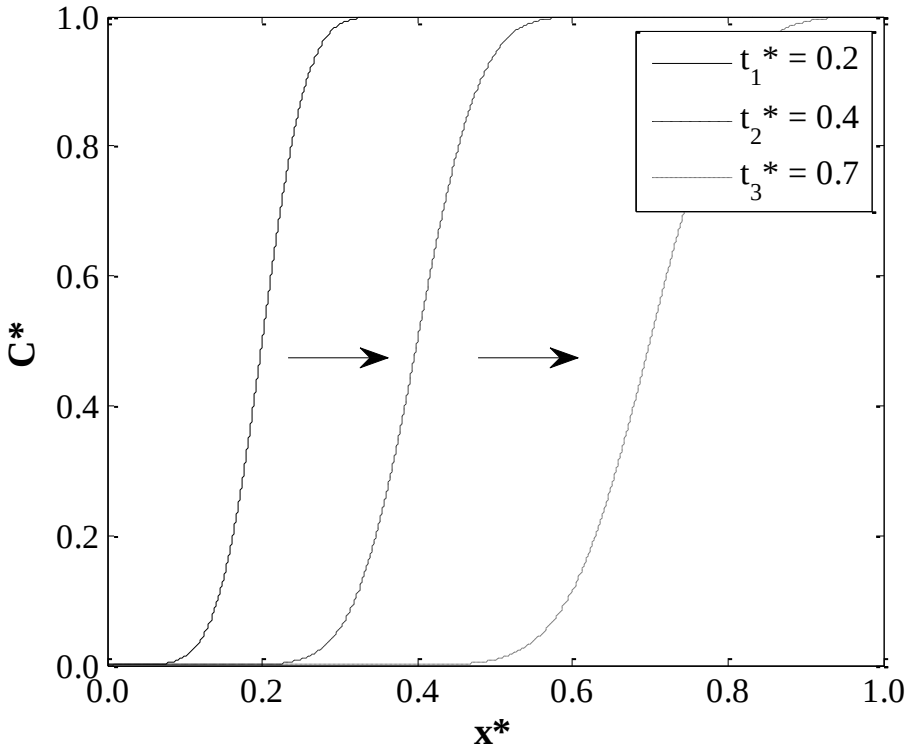

Figure 3.6: Trailing edge of dimensionless concentration distribution (C^*) propagates over time for $N_{pe} = 200$

After the concentration distributions are obtained for the leading and trailing edges,

the distinctive shape of the tracer slug collapse time (i.e., the time when the trailing edge of tracer slug catches with the leading edge) can be calculated based on Eq. (3.71) and Eq. (3.73).

The dimensionless tracer slug size (the time interval of tracer injection) is defined beforehand as:

$$\Delta t^* = {t_l}^* - {t_t}^* , \tag{3.74}$$

where ${t_l}^*$ is the dimensionless travelling time of the leading edge, i.e., the length of time after the tracer slug is injected; and ${t_t}^*$ is the dimensionless travelling time of the trailing edge, i.e., the length of time after stopping tracer slug injection. Therefore, Δt expresses the duration of tracer injection and it is one of the key factors that affect the tracer slug collapse time.

As both the trailing edge and the leading edge act as diffusive waves, the concentration profile would collapse when the trailing edge catches up with the leading edge. Three tracer slugs are plotted in Figure 3.7 for the following three time steps listed in Table 3.2, which gives a brief view of the tracer dimensionless concentration distribution over time. For the case shown in Figure 3.7, $N_{pe} = 1000$, $\Delta t^* = 0.2$.

Table 3.2: Time steps for Figure 3.7

Time step 1	Time step 2	Time step 3
$t_{t1}{}^* = 0.1$	$t_{t2}{}^* = 0.35$	$t_{t3}{}^* = 0.55$
$t_{l1}{}^* = 0.3$	$t_{l2}{}^* = 0.55$	$t_{l3}{}^* = 0.75$

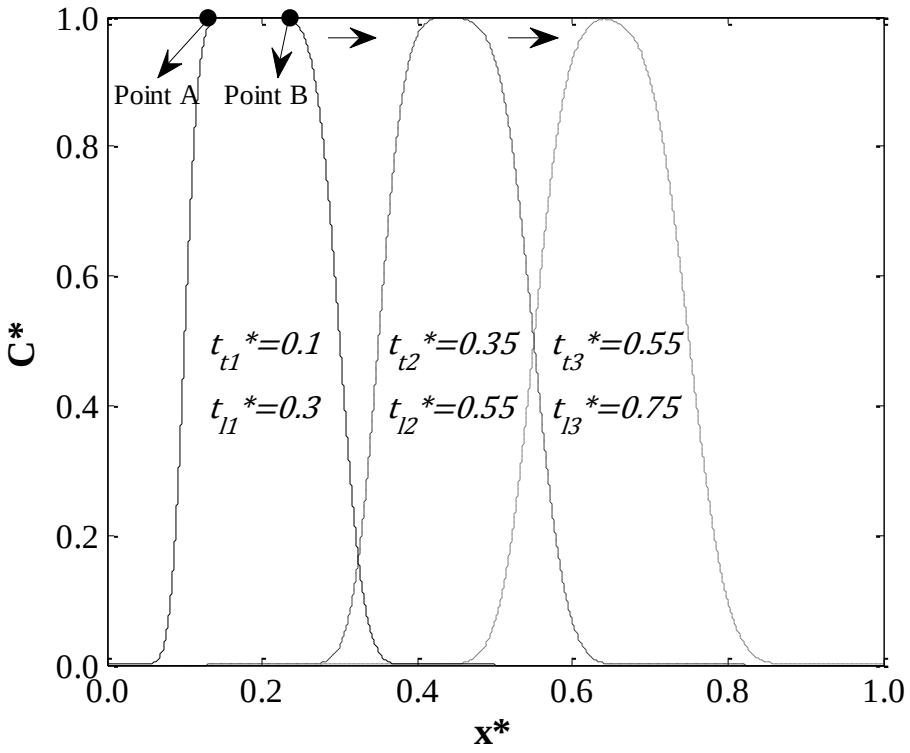

Figure 3.7: Tracer slug propagation for convection dispersion equation for $N_{pe} = 1000$

Actually, many series of $t_l{}^*$ and $t_t{}^*$ were tried by trial and error and it was found that at $t_l{}^* = 0.75$, $t_t{}^* = 0.55$, Point A starts to catch up with Point B in Figure 3.7, and this is the collapse time that the trailing edge starts to catch up with the leading edge.

This collapse time can also be calculated manually. As illustrated in Figure 3.7, the concentration of both Point A and Point B are close to 1.0 and were both chosen to be

0.995 for approximate calculation. The collapse happens when the travel distance of Point A equals to the travel distance of Point B. Hence, the collapse time can be calculated based on this relationship:

$$x_A{}^* = x_B{}^* , \tag{3.75}$$

where $x_A{}^*$ is the travel distance of Point A and $x_B{}^*$ is the travel distance of Point B.

For Point A on the trailing edge:

$$\frac{1}{2}\left[1 + erf\left(\frac{x_A{}^* - t_t{}^*}{2\sqrt{t_t{}^*/N_{pe}}}\right)\right] = 0.995 . \tag{3.76}$$

Thus,

$$erf\left(\frac{x_A{}^* - t_t{}^*}{2\sqrt{t_t{}^*/N_{pe}}}\right) = 0.99 . \tag{3.77}$$

Checking the value of error function in Table 3.1 gives:

$$\frac{x_A{}^* - t_t{}^*}{2\sqrt{t_t{}^*/N_{pe}}} \cong 2 . \tag{3.78}$$

Therefore,

$$x_A{}^* = 4\sqrt{t_t{}^*/N_{pe}} + t_t{}^* . \tag{3.79}$$

The travel distance of Point B can be obtained in the same way:

$$x_B{}^* = -4\sqrt{t_l{}^*/N_{pe}} + t_l{}^* . \tag{3.80}$$

Substituting Eq. (3.79) and Eq. (3.80) into Eq. (3.75) gives:

$$4\sqrt{t_t{}^*/N_{pe}} + t_t{}^* = -4\sqrt{t_l{}^*/N_{pe}} + t_l{}^* , \tag{3.81}$$

which can be simplified to:

$$\sqrt{t_l{}^*} - \sqrt{t_t{}^*} = \frac{4}{\sqrt{N_{pe}}} . \tag{3.82}$$

Substituting $\Delta t^* = t_l{}^* - t_t{}^*$ gives:

$$\sqrt{t_l{}^*} - \sqrt{t_l{}^* - \Delta t^*} = \frac{4}{\sqrt{N_{pe}}} . \tag{3.83}$$

The collapse time $t_l{}^*$ for various Δt^* and N_{pe} can be calculated using the above equation.

Applying the values used in the case above, and calculating the collapse time using Eq. (3.83) gives: $t_l{}^* = 0.73$ and $t_t{}^* = t_l{}^* - \Delta t^* = 0.53$, which is almost the same as the results obtained from Matlab. The result from Matlab was obtained by trial method and observations of the result; the result from calculation is a manual calculation. However, both the results reflect the collapse time properly.

In summary, the solution of tracer profile from convection dispersion equation acts as a diffusive wave, which is caused by dispersion. The collapse time obtained using

analytical method coincides with the trial and observation method from Matlab.

3.2.2 Convection Adsorption Model

In this section, the convection adsorption equation is solved analytically:

$$\emptyset \frac{\partial C}{\partial t} + (1 - \emptyset) \frac{\partial Cs}{\partial t} + u_T \frac{\partial C}{\partial x} = 0 \,, \tag{3.84}$$

where Cs is the adsorption concentration, which represents the interaction between the stationary phase and the flowing phase. The Langmuir adsorption isotherm (Figure 3.8) was chosen which has already been discussed in Chapter 2:

$$C_S = \frac{aC}{1 + bC} \,, \tag{3.85}$$

where a and b are empirical constants. The unit of b is m^3/kg and a is dimensionless.

The tracer model with Langmuir adsorption is a special case of polymer flooding. The convection adsorption tracer results in this thesis therefore follow from the polymer case, which was solved and analyzed by Johansen and Winther in 1988 (Johansen and Winther, 1988).

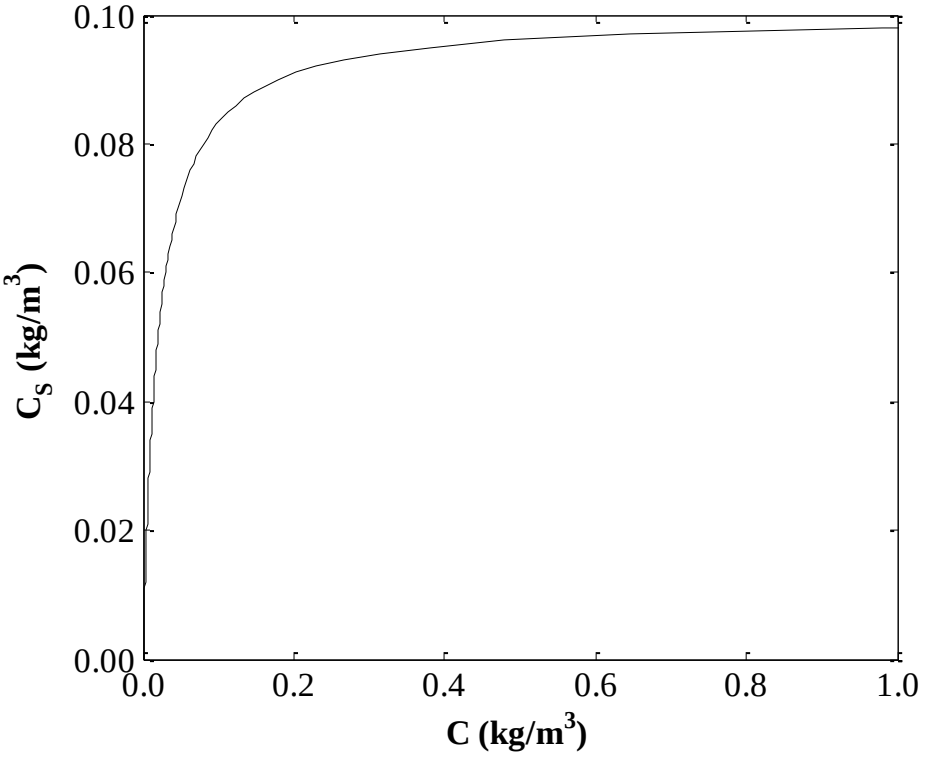

Figure 3.8: Langmuir adsorption isotherm (C_S)

Applying chain rule to Eq. (3.84) gives:

$$(1+\frac{1-\emptyset}{\emptyset}\frac{dC_S}{dC})\frac{\partial C}{\partial t}+\frac{u_T}{\emptyset}\frac{\partial C}{\partial x}=0. \tag{3.86}$$

Applying the same dimensionless variables as the above section gives:

$$\left[1+\frac{1-\emptyset}{\emptyset}\frac{dC_S}{dC}\right]\frac{\partial C^*}{\partial t^*}+\frac{\partial C^*}{\partial x^*}=0\,. \tag{3.87}$$

In this section, the same case of injecting a slug of tracer into a horizontal reservoir is discussed for the same boundary conditions. The boundary conditions for leading edge are: $C^*(\mathrm{x},0)=0;\ C^*(0,\mathrm{t})=1$ and for trailing edge are: $C^*(\mathrm{x},0)=1;\ C^*(0,\mathrm{t})=0$.

The total derivative $\frac{dC^*}{dt^*}$ of concentration is:

$$\frac{\partial C^*}{\partial t^*} + \frac{dx^*}{dt^*}\frac{\partial C^*}{\partial x^*} = \frac{dC^*}{dt^*}\,. \tag{3.88}$$

Then, comparing Eq. (3.87) and Eq. (3.88) gives:

$$\frac{dC^*}{dt^*} = 0, \tag{3.89}$$

$$\frac{dx^*}{dt^*} = \frac{1}{1 + \frac{1-\emptyset}{\emptyset}\frac{dC_S}{dC}}\,. \tag{3.90}$$

According to Eq. (3.89) and Eq. (3.90), any given value of C^* propagates with a characteristic constant velocity given by Eq. (3.90). Hence, the propagation velocity $v(C)^*$ is:

$$v(C)^* = \frac{1}{1 + \frac{1-\emptyset}{\emptyset}\frac{dC_S}{dC}} = \frac{1}{1 + \frac{1-\emptyset}{\emptyset}\frac{a}{\{1 + b[C^*(C_L - C_R) + C_R]\}^2}}\,. \tag{3.91}$$

Figure 3.9 is plotted for the dimensionless propagation velocities of different tracer concentrations with $\emptyset = 0.2$, $C_L = 10\ kg/m^3$, $C_R = 0$ and Langmuir parameters: $a = 10$, $b = 10\ m^3/kg$. The propagation velocity increases smoothly from the low concentration to the high concentration.

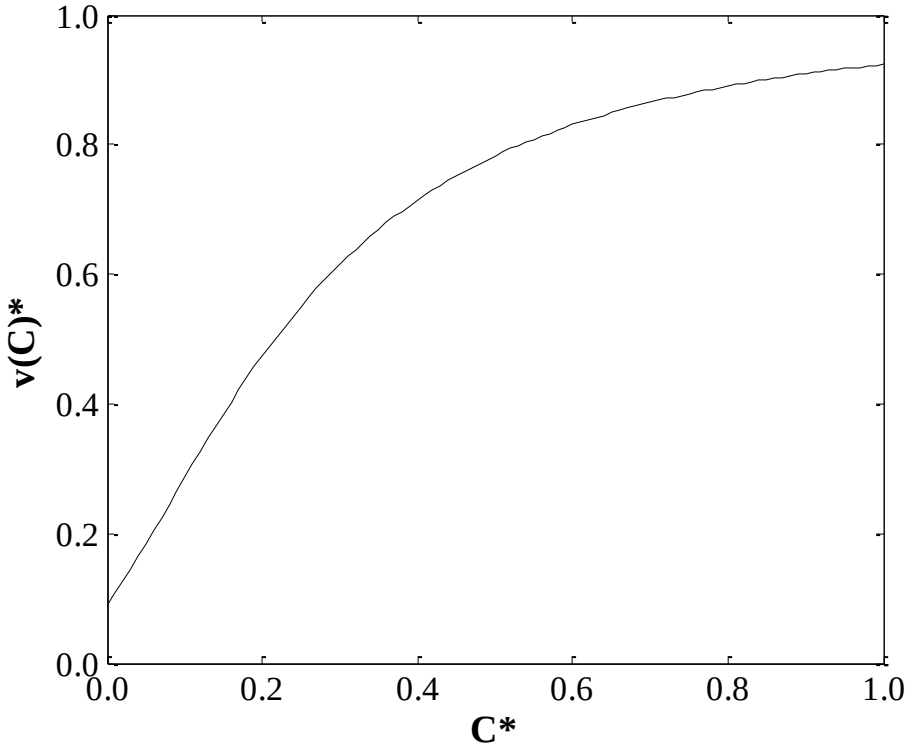

Figure 3.9: Dimensionless propagation velocities ($v(C)^*$) of different concentrations

After the velocity is calculated, the location of the concentration can be obtained by multiplying the propagation velocity with time t^*:

$$x^* = \frac{1}{1 + \frac{1-\emptyset}{\emptyset}\frac{a}{\{1+b[C^*(C_L - C_R) + C_R]\}^2}} t^* . \qquad (3.92)$$

Keeping the same Langmuir parameters and choosing three time steps: ${t_1}^* = 0.1$, ${t_2}^* = 0.4$, ${t_3}^* = 0.8$, the plot of the concentration distribution as a function of position is shown in Figure 3.10. The expanding shape is caused by adsorption.

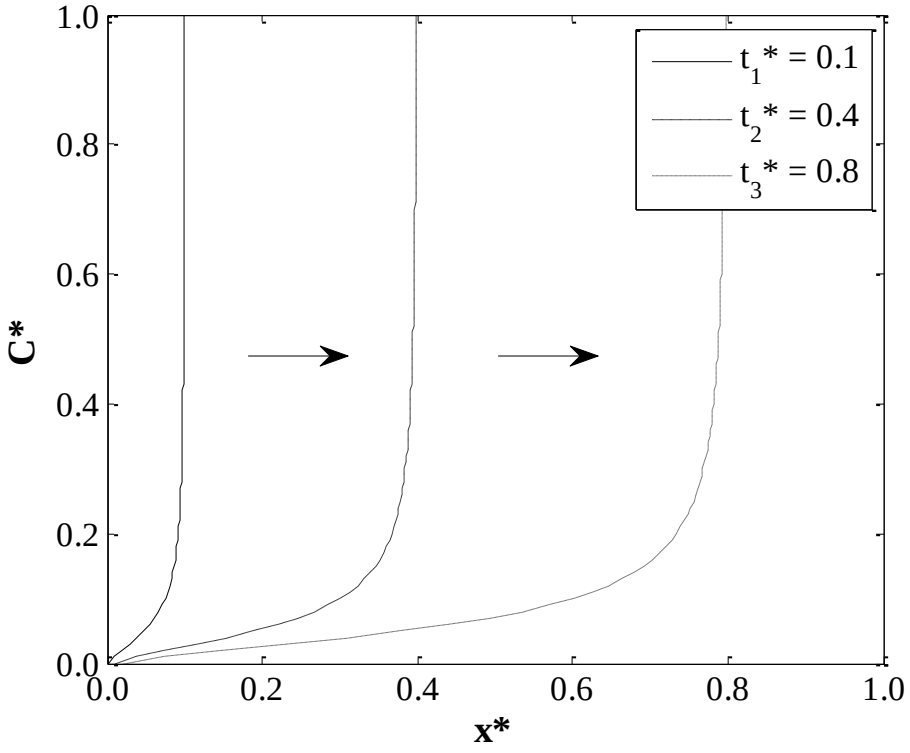

Figure 3.10: Dimensionless concentration distributions (C^*) for trailing edge as a function of position at three time steps

Figure 3.11 shows the flowing concentration for $t^* = 0.8$ with the boundary conditions for trailing edge. The concentration moves continuously as a function of position.

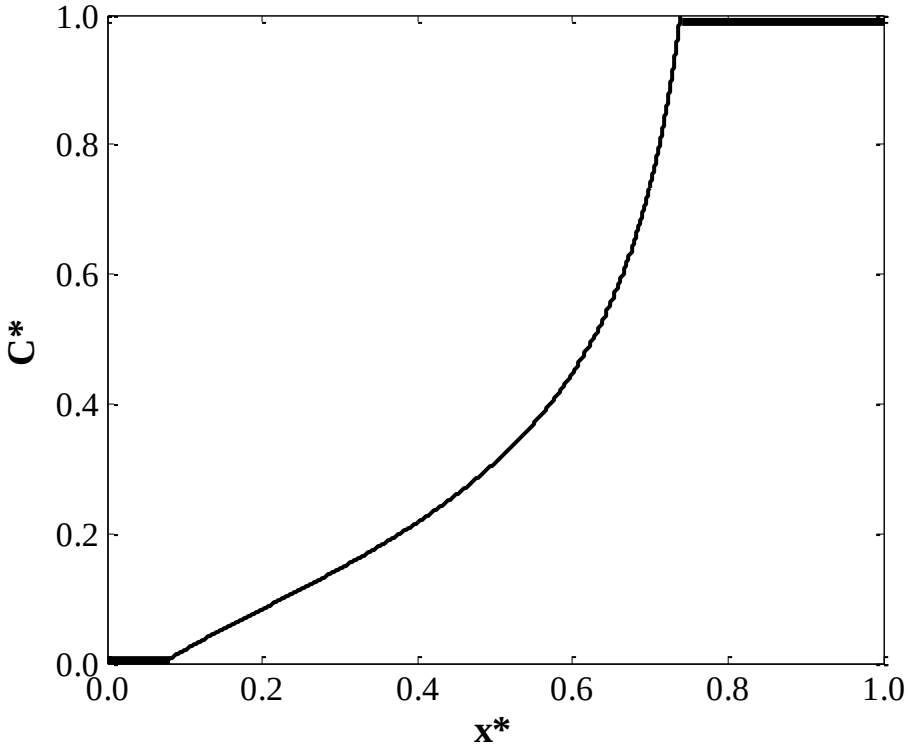

Figure 3.11: Dimensionless Concentration distribution (C^*) for trailing edge with boundary conditions for convection adsorption model

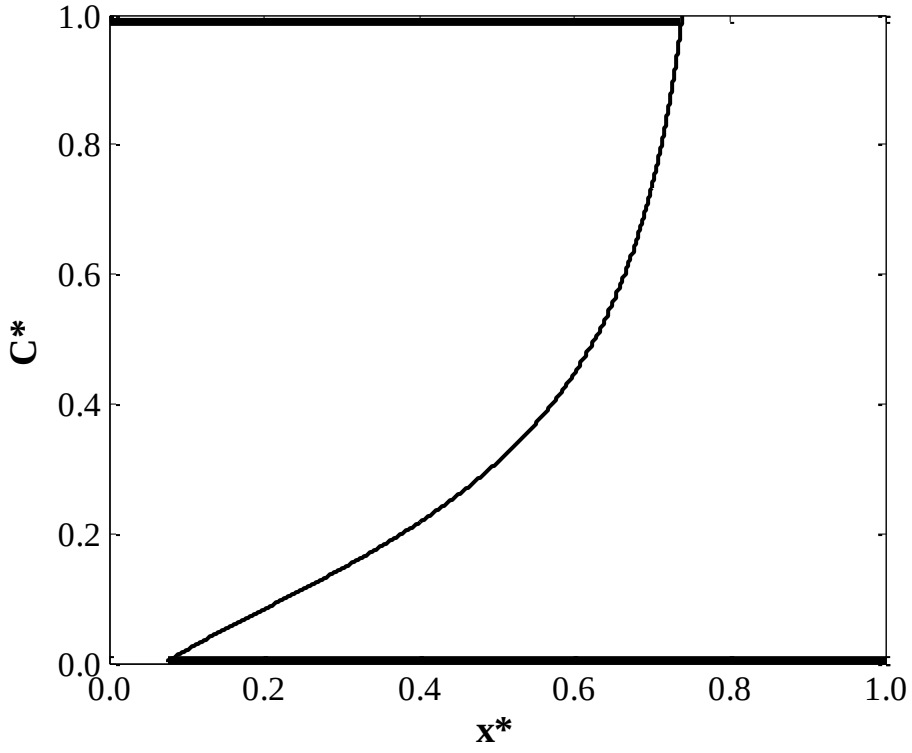

Figure 3.12: Dimensionless concentration distribution (C^*) for leading edge with boundary conditions for convection adsorption model

Instead of a continuous change in concentration as for the trailing edge, the leading edge is as a shock. Trying to use the same procedure to plot the leading edge, we obtain Figure 3.12.

If can be seen from Figure 3.12 clearly that for x^* values between 0.07 and 0.74, there are three concentration values for each position, which cannot be true physically. The main reason for this phenomenon is the absence of the dispersion term. However, the problem can be solved by treating the leading edge as a shock, which is a self-sharpening wave with a discontinuous change in concentration. The shock is drawn in

Figure 3.13 as a dashed vertical line connecting the initial condition and the inlet condition together.

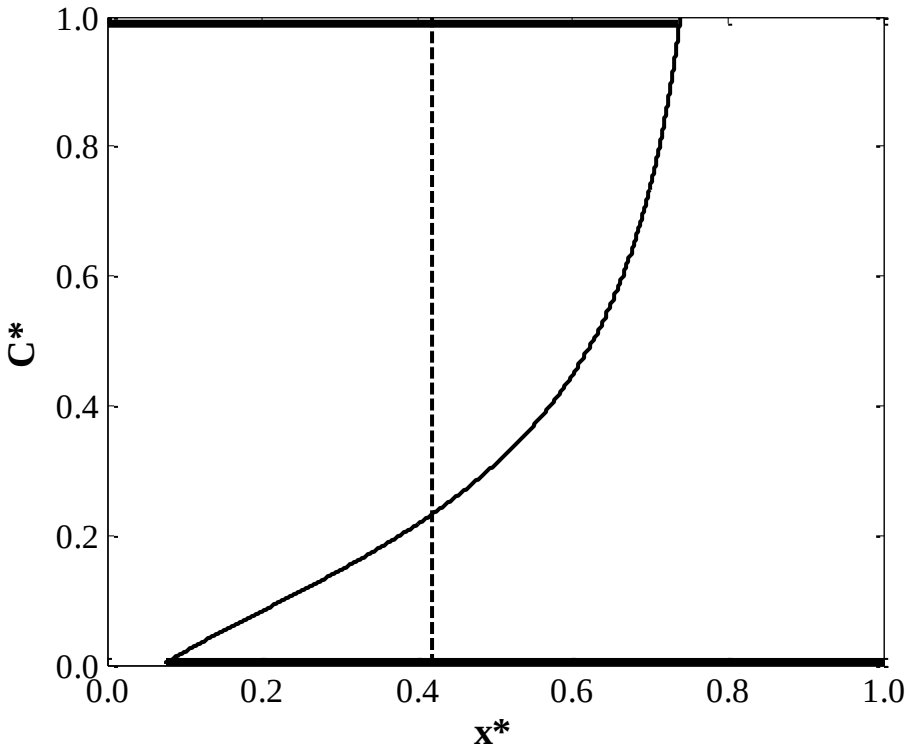

Figure 3.13: Dimensionless leading edge concentration distribution (C^*) as a function of position for convection adsorption model

After the shock is defined, the shock velocity can be calculated shown in the following steps.

First, recall Eq. (3.90) :

$$\frac{dx^*}{dt^*} = \frac{1}{1 + \frac{1-\emptyset}{\emptyset}\frac{dC_S}{dC}}. \tag{3.93}$$

Then, the shock velocity is obtained based on the Rankine-Hugoniot relation which

represents material balance across the shock wave (Johansen and Winther, 1988):

$$v_{\Delta C}{}^{*} = \frac{1}{1 + \frac{1-\emptyset}{\emptyset}\frac{\Delta C_S}{\Delta C}} = \frac{1}{1 + \frac{C_{SL} - C_{SR}}{C_L - C_R}}, \tag{3.94}$$

where 'L', 'R' represent the left-end and right-end values of the shock, respectively.

From Eq. (3.85):

$$C_{SL} = \frac{aC_L}{1 + bC_L}, \tag{3.95}$$

$$C_{SR} = \frac{aC_R}{1 + bC_R}. \tag{3.96}$$

For a tracer slug injection,

$$C_R = 0. \tag{3.97}$$

Substituting Eq. (3.95), Eq. (3.96) and Eq. (3.97) to Eq. (3.94) gives:

$$v_{\Delta C}{}^{*} = \frac{1}{1 + \frac{1-\emptyset}{\emptyset}\frac{a}{1 + bC_L}}. \tag{3.98}$$

Obviously, for constant a, b and C_L, the shock velocity stays constant. The shock propagation with $\emptyset = 0.2$, $C_L = 10\ kg/m^3$ and Langmuir parameters: $a = 10$, $b = 10\ m^3/kg$ is shown in Figure 3.14 for three time steps: $t_1{}^{*} = 0.3$, $t_2{}^{*} = 0.6$, $t_3{}^{*} = 1.0$.

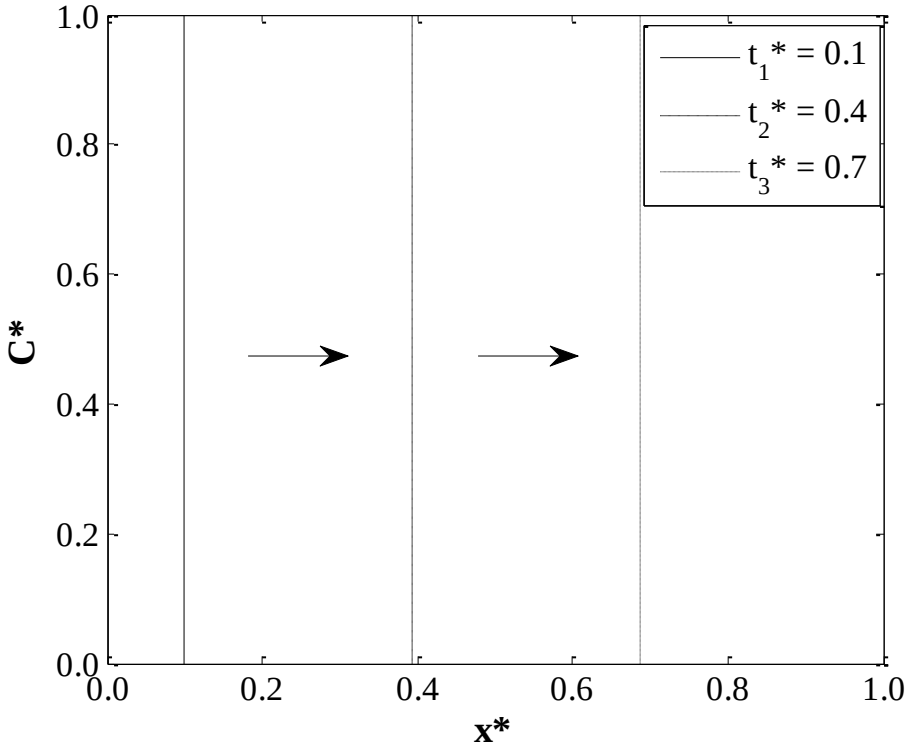

Figure 3.14: Dimensionless concentration distributions (C^*) for leading shock as a function of position for convection adsorption model

As the trailing edge acts as a spreading wave with a growing width and the leading edge forms a shock with constant velocity, the tracer slug would collapse when the trailing edge catches up with the leading edge.

The tracer slug collapse time of the trailing edge and leading shock were investigated by trial and error. The results are shown in Figure 3.15. It was found that at $t_l^* = 0.7$, $t_t^* = 0.5$, the trailing edge starts to catch up with the leading edge which is the tracer slug collapse time. This collapse time was found by numerical simulation. However, the collapse time can also be obtained by analytical calculation discussed below.

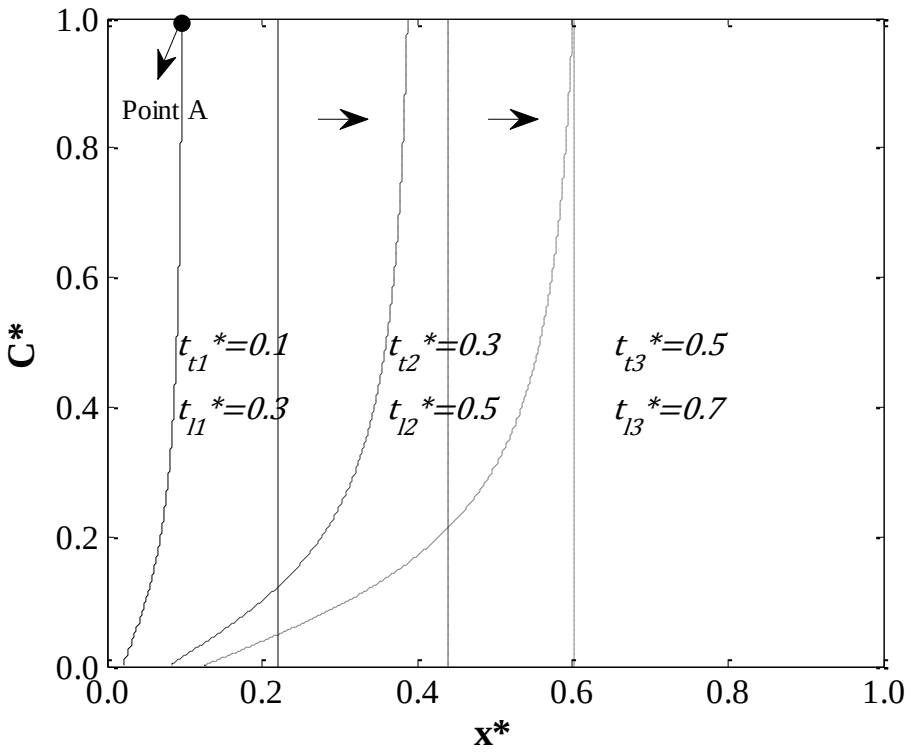

Figure 3.15: Tracer slug propagation for convection adsorption equation

As illustrated in the above figure, the trailing edge is spreading along the x direction with time while the leading edge propagates as a shock. The collapse happens when the point on the trailing edge with a dimensionless concentration equals to 1.0 (Point A in Figure 3.15) hits the leading edge. That is to say, when the collapse happens, the travel distance of Point A equals to the travel distance of the leading shock. Hence, the

breakthrough time can be calculated based on this relationship.

$$x_A{}^* = x_{shock}{}^* , \tag{3.99}$$

where $x_A{}^*$ is the travel distance of point A and $x_{shock}{}^*$ is the travel distance of the leading shock.

For Point A ($C^* = 1.0$),

$$x_A{}^* = \frac{1}{1 + \frac{1-\emptyset}{\emptyset}\frac{a}{\{1 + b[(C_L - C_R) + C_R]\}^2}} t_t{}^*$$

$$= \frac{1}{1 + \frac{1-\emptyset}{\emptyset}\frac{a}{\{1 + b[(C_L - C_R) + C_R]\}^2}} (t_l{}^* - \Delta t^*) . \tag{3.100}$$

Substituting $C_R = 0$ to Eq. (3.100) gives:

$$x_A{}^* = \frac{1}{1 + \frac{1-\emptyset}{\emptyset}\frac{a}{(1 + bC_L)^2}} (t_l{}^* - \Delta t^*) . \tag{3.101}$$

For the leading shock,

$$x_{shock}{}^* = v_{\Delta C}{}^* t_l{}^* = \frac{1}{1 + \frac{1-\emptyset}{\emptyset}\frac{a}{1 + bC_L}} t_l{}^* . \tag{3.102}$$

Therefore,

$$\frac{1}{1 + \frac{1-\emptyset}{\emptyset}\frac{a}{(1 + bC_L)^2}} (t_l{}^* - \Delta t^*) = \frac{1}{1 + \frac{1-\emptyset}{\emptyset}\frac{a}{1 + bC_L}} t_l{}^* . \tag{3.103}$$

In the above equation, the only unknown is t_l^* which can be solved easily by substituting other parameters.

Then, applying the values in the above case study, i.e., $\emptyset = 0.2$, $a = 10$, $b = 10\ m^3/kg$, $C_L = 10\ kg/m^3$, $\Delta t^* = 0.2$ to Eq. (3.103) to calculate the collapse time gives: $t_l^* = 0.701$, $t_t^* = 0.501$.

Comparing this to the result obtained from Matlab ($t_l^* = 0.7$, $t_t^* = 0.5$), shows good agreement.

The above explanation and analysis concludes that the trailing edge of the tracer profile from convection adsorption equation acts as a spreading wave, while the leading edge of the tracer profile acts as a shock wave. The collapse time obtained using analytical method shows excellent agreement with the collapse time obtained through trial and observation method from Matlab. The analytical method is time saving compared to the observation method, but can only be applied to the models that have analytical solutions. The observation method can be applied to all the models, which have either analytical solutions or numerical solutions.

3.2.3 Convection Dispersion Adsorption Model

In this section, convection, dispersion and adsorption are all considered resulting the following equation:

$$\emptyset \frac{\partial C}{\partial t} + (1 - \emptyset) \frac{\partial Cs}{\partial t} + u_T \frac{\partial C}{\partial x} - \emptyset D \frac{\partial^2 C}{\partial x^2} = 0 \,. \tag{3.104}$$

This equation is a second order parabolic partial differential equation satisfied by a function $C(x, t)$ dependent on two free variables (space and time) and it can be solved using numerical methods. In this section, a finite difference method is applied to convert the differential equation to an approximating difference equation.

First, both the Peclet number and the dimensionless variables are applied to Eq. (3.104) as in the previous section:

$$\left[1 + \frac{1 - \emptyset}{\emptyset} \frac{a}{\{1 + b[C^*(C_L - C_R) + C_R]\}^2}\right] \frac{\partial C^*}{\partial t^*} = \frac{1}{N_{pe}} \frac{\partial^2 C^*}{\partial x^{*2}} - \frac{\partial C^*}{\partial x^*} \,. \tag{3.105}$$

Then, we discretize the domain into a grid of evenly spaced points and each point is defined in (x, t) space shown in Figure 3.16.

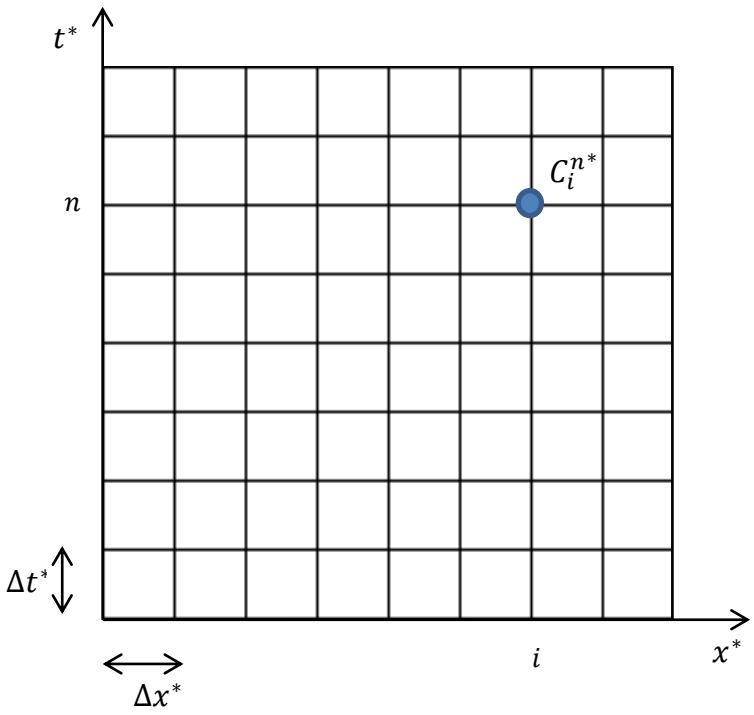

Figure 3.16: Domain in (x^*,t^*) space

As can be seen clearly in Figure 3.16, each point is characterized by:

$$x_i{}^* = x_0{}^* + i\Delta x^* \; ; i = 0,\cdots, i_{max} \, , \tag{3.106}$$

$$t_n{}^* = t_0{}^* + n\Delta t^* \; ; n = 0,\cdots, n_{max} \, , \tag{3.107}$$

$$C_i^{n^*} = C^*(x_i{}^*, t_n{}^*) \, . \tag{3.108}$$

Here, Δx^* is the space step length and Δt^* is the time step length.

Then, the finite difference approximation for Eq. (3.105) is given by:

$$\frac{C_i^{n+1^*} - C_i^{n^*}}{\Delta t^*}\left[1 + \frac{1-\emptyset}{\emptyset}\frac{a}{\{1 + b[C_i^{n^*}(C_L - C_R) + C_R]\}^2}\right]$$

$$= \frac{1}{N_{pe}} \frac{C_{i+1}^{n}{}^{*} - 2C_i^{n*} + C_{i-1}^{n}{}^{*}}{\Delta x^{*2}} - \frac{C_{i+1}^{n}{}^{*} - C_{i-1}^{n}{}^{*}}{2\Delta x^{*}} . \quad (3.109)$$

This is an explicit scheme because the space derivatives and the adsorption are evaluated at time level n.

Rearranging Eq. (3.109) gives:

$$C_i^{n+1*} = \frac{\Delta t^{*}}{1 + \frac{1-\emptyset}{\emptyset} \frac{a}{\{1 + b[C_i^{n*}(C_L - C_R) + C_R]\}^2}}$$

$$\left[\frac{1}{N_{pe}} \frac{C_{i+1}^{n}{}^{*} - 2C_i^{n*} + C_{i-1}^{n}{}^{*}}{\Delta x^{*2}} - \frac{C_{i+1}^{n}{}^{*} - C_{i-1}^{n}{}^{*}}{2\Delta x^{*}}\right] + C_i^{n*} \quad (3.110)$$

Then, we input code to Matlab according to the above equation. By choosing grid size and time step size, and applying the boundary conditions, we are able to get the results.

The grid size and time step size chosen are 1000 and 200. Usually, a small time step would help to get less numerical smearing and numerical instability. We plot the concentration distribution combining the boundary conditions in Matlab for leading edge, $C^{*}(\mathrm{x}, 0) = 0$; $C^{*}(0, \mathrm{t}) = 1$ shown in Figure 3.17, and the trailing edge with boundary conditions $C^{*}(\mathrm{x}, 0) = 1$; $C^{*}(0, \mathrm{t}) = 0$, shown in Figure 3.18. The values chosen for the parameters are $\emptyset = 0.2$, $N_{pe} = 100$, $a = 1.5$, $b = 30\ m^3/kg$, $C_L = 100\ kg/m^3$, $C_R = 0$ and three time steps: ${t_1}^{*} = 0.2$, ${t_2}^{*} = 0.4$, ${t_3}^{*} = 0.7$.

Figure 3.19 shows how the model is solved sequentially using finite difference

methods. The numerical modeling of all the models that presented in this thesis applies the same approach.

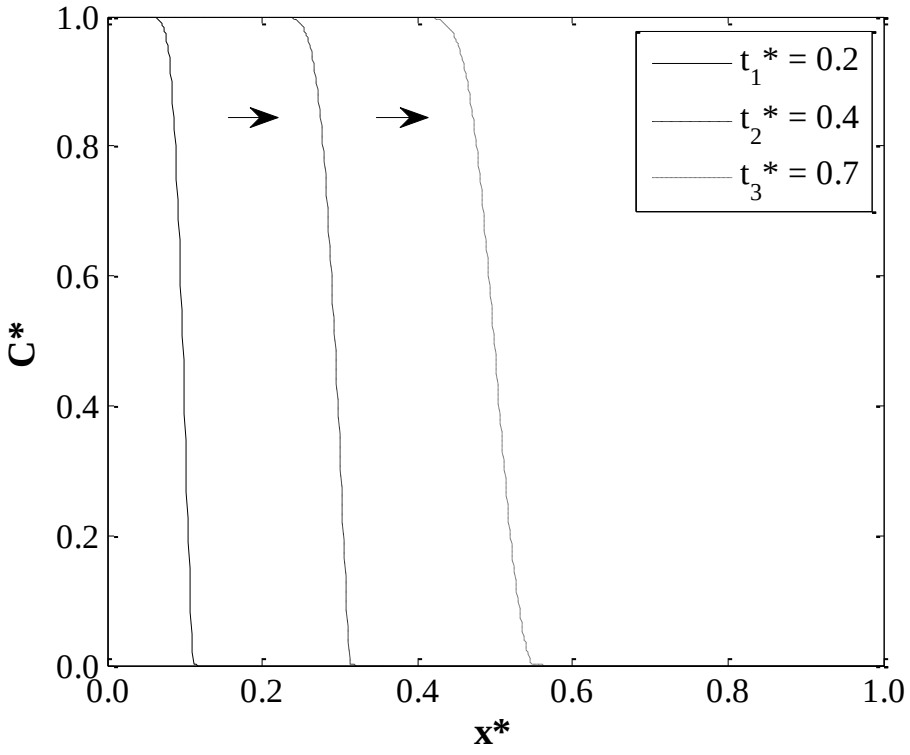

Figure 3.17: Leading edge of concentration distribution (C^*) over time

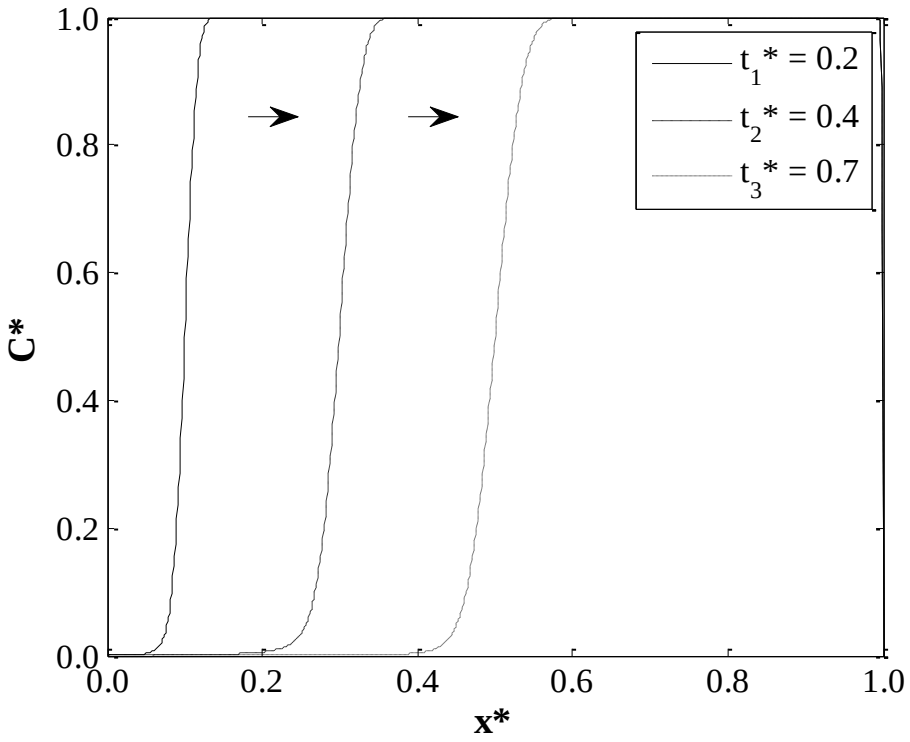

Figure 3.18: Trailing edge of concentration distribution (C^*) over time

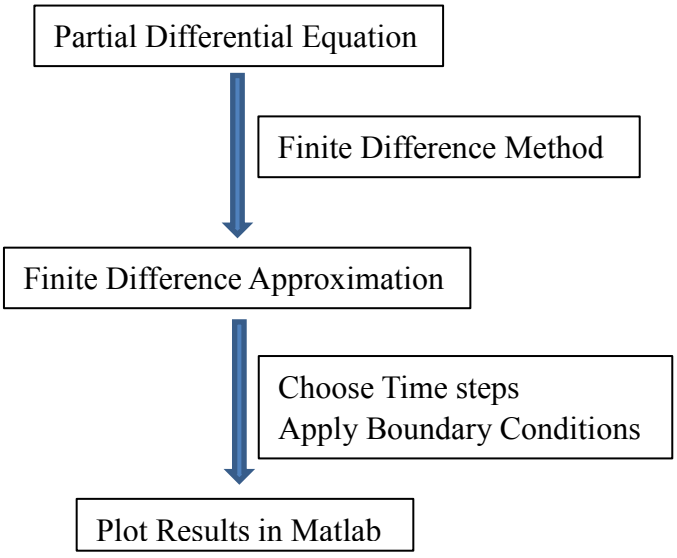

Figure 3.19: Finite Difference Method to Solve the Models

In order to see the difference between the convection dispersion scenario and

convection dispersion adsorption scenario, the leading edge of adsorption condition and non-adsorption condition at $t^* = 0.7$ are plotted in the same plot shown in Figure 3.20.

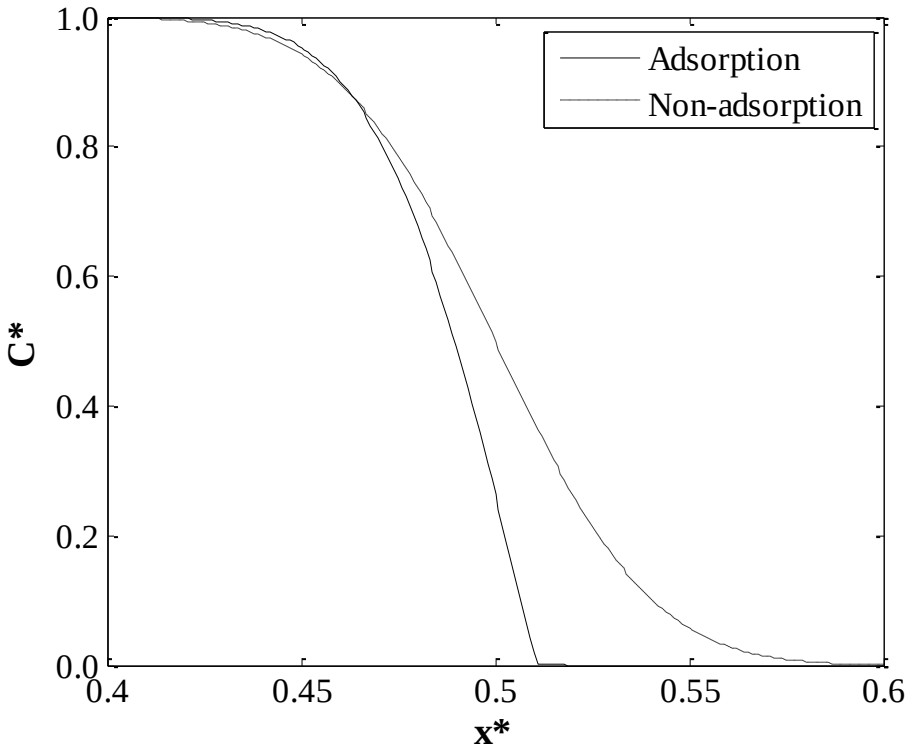

Figure 3.20: Comparison of dimensionless concentration distribution (C^*) between adsorption and non-adsorption scenario

Figure 3.20 shows that, when adsorption is added, the concentration decreases because of the effect of adsorption. As for the adsorption case, some of the tracer attached to the solid phase, which results in a faster rate of tracer concentration loss.

In conclusion, for convection dispersion adsorption equation, the tracer slug is delayed by adsorption when compared with convection dispersion equation due to the

concentration loss caused by adsorption.

3.2.4 Convection Dispersion Adsorption Radioactive Decay Model

The convection dispersion adsorption radioactive equation is with all the four terms considered and it is the complete model for one-dimensional single-phase tracer flow.

$$\emptyset \frac{\partial C}{\partial t} + (1-\emptyset)\frac{\partial Cs}{\partial t} + u_T \frac{\partial C}{\partial x} - \emptyset D \frac{\partial^2 C}{\partial x^2} + \emptyset \lambda C = 0\,. \tag{3.111}$$

This equation can be solved similarly as Eq. (3.110) in the above section by using finite difference method.

First, the dimensionless form is given using the same dimensionless variables as above,

$$\left[1 + \frac{1-\emptyset}{\emptyset}\frac{a}{\{1+b[C^*(C_L - C_R) + C_R]\}^2}\right]\frac{\partial C^*}{\partial t^*}$$

$$= \frac{1}{N_{pe}}\frac{\partial^2 C^*}{\partial x^{*2}} - \frac{\partial C^*}{\partial x^*} - M[C^*(C_L - C_R) + C_R]\,, \tag{3.112}$$

where

$$M = \frac{\lambda \emptyset L}{u}\,, \tag{3.113}$$

is a dimensionless constant defined for simplification. If the medium and the fluid flow rate are defined, M depends only on the radioactive tracer type defined by the decay constant λ (s^{-1}).

Applying finite difference method gives:

$$C_i^{n+1^*} = C_i^{n^*} + \frac{\Delta t^*}{1 + \frac{1-\emptyset}{\emptyset}\frac{a}{\{1+b[C_i^{n^*}(C_L - C_R) + C_R]\}^2}}$$

$$\left[\frac{1}{N_{pe}}\frac{C_{i+1}^{n}{}^{*} - 2C_i^{n^*} + C_{i-1}^{n}{}^{*}}{\Delta x^{*2}} - \frac{C_{i+1}^{n}{}^{*} - C_{i-1}^{n}{}^{*}}{2\Delta x^*} - M[C_i^{n^*}(C_L - C_R) + C_R]\right]. \quad (3.114)$$

Plot $C^*(x^*, t^*)$ combining the boundary conditions for leading edge and trailing edge shown in Figure 3.21 and Figure 3.22 respectively. The values chosen for the plots are $\emptyset = 0.2$, $N_{pe} = 100$, $M = 0.0008$, $a = 1.5$, $b = 30\, m^3/kg$, $C_L = 100\, kg/m^3$, $C_R = 0$ and steps: $t_1{}^* = 0.2$, $t_2{}^* = 0.4$, $t_3{}^* = 0.7$.

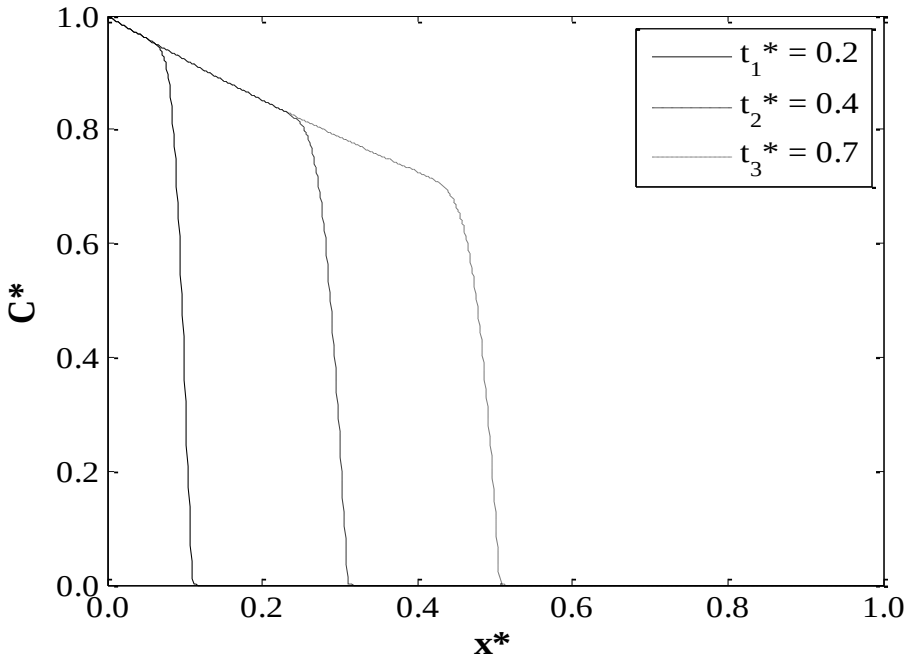

Figure 3.21: Leading edge of dimensionless concentration distribution (C^*) over time for $M = 0.0008$

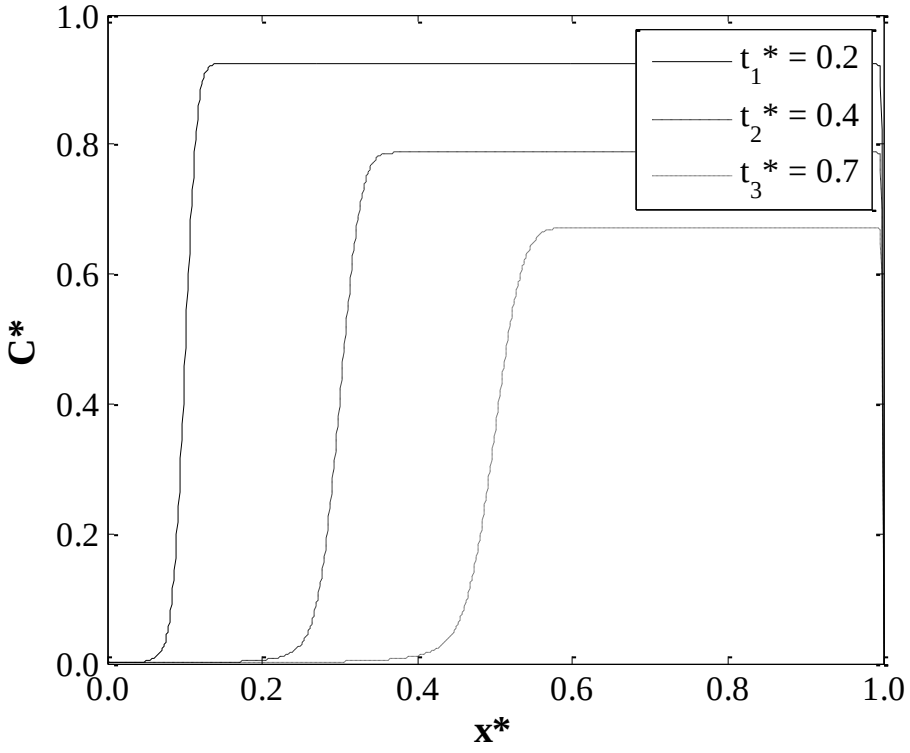

Figure 3.22: Trailing edge of dimensionless concentration distribution (C^*) over time for $M = 0.0008$

Figure 3.21 and Figure 3.22 have a significant difference compared with all the plots in the previous sections. The difference is that the concentration distribution is much lower than 1.0 because of the radioactive decay which happens at the beginning of the tracer injection.

As explained above, the decay constant λ is the only factor that affects the constant M if the medium and the fluid flow rate are selected. Hence, for different types of radioactive tracer injected into the same flowing medium with the same fluid flow rate, different types of radioactive tracers will give different values of constant M.

Ploting $C^*(x^*, t^*)$ for $\emptyset = 0.2$, $N_{pe} = 100$, $a = 1.5$, $b = 30\, m^3/kg$ at time step $t^* = 0.7$ for $M_1 = 0.0000$, $M_2 = 0.0008$, $M_3 = 0.0020$, $M_4 = 0.0050$ for leading edge are shown in Figure 3.23.

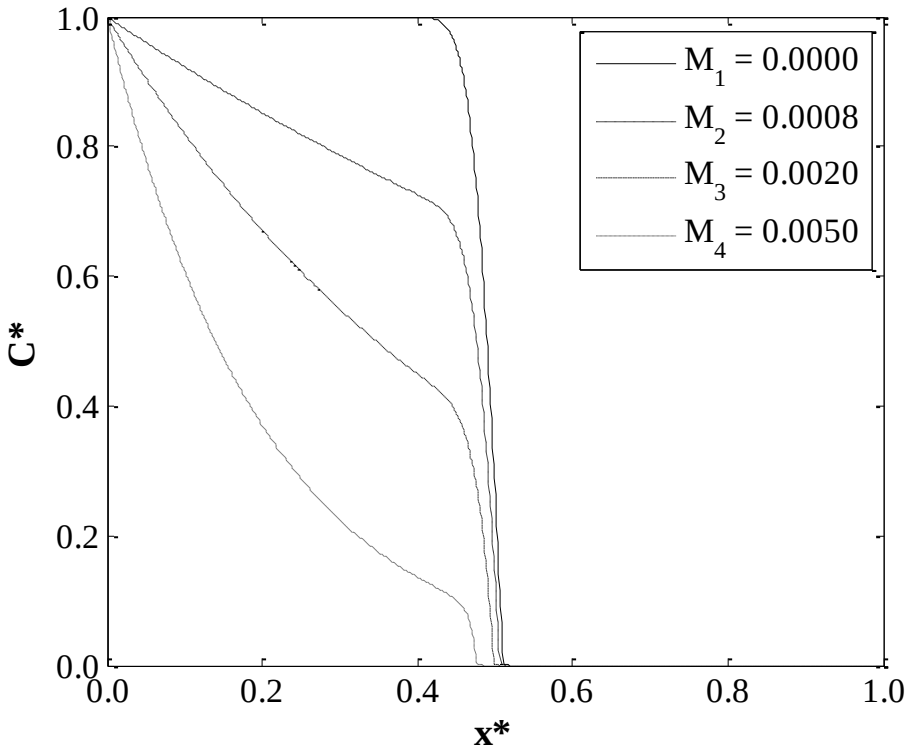

Figure 3.23: Leading edge of dimensionless concentration distribution (C^*) for different decay constants

As shown in Figure 3.23, the concentration distribution is relatively high for a small value of M. This holds true, because a large half-life $t_{1/2}$ means that the speed of radioactive decay is slow, so that the concentration distribution is relatively high and a large half-life $t_{1/2}$ results in a small value of constant M according to Eq. (3.113) and Eq. (2.6). For $M_1 = 0.0000$ which represents the case that there's no radioactive

decay, the concentration loss is very small compared to the radioactive cases. We can draw the conclusion that the effect of radioactive decay is severe and it can cause a large concentration loss.

The concentration distribution for the trailing edge with different values of M is also plotted shown in Figure 3.24 and the result is similar with the leading edge.

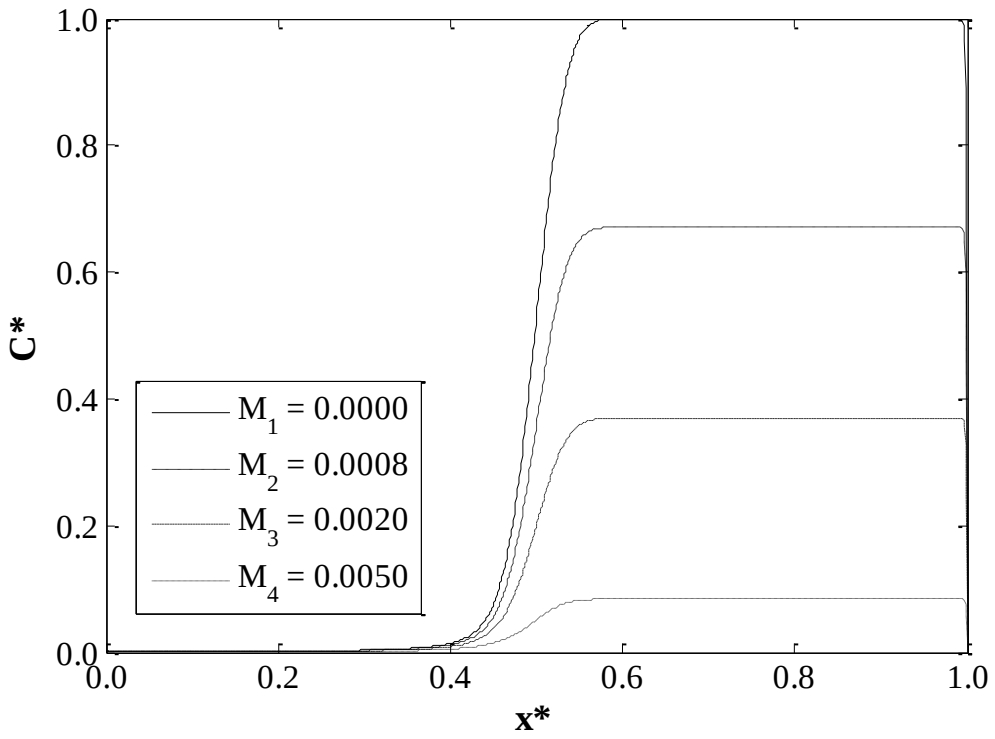

Figure 3.24: Trailing edge of dimensionless concentration distribution (C^*) for different decay constants

In conclusion, the tracer profile from the convection dispersion adsorption radioactive decay equation has a large tracer concentration loss because of the radioactive decay effect. The effect of radioactive decay on tracer concentration is severe and the smaller

the half-life, the larger the concentration loss.

3.3 One-Dimensional, Two-Phase Tracer Modeling

In this section, the flow of two phases and a partitioning tracer is discussed, i.e., the tracer partitions between the two phases. This two-phase tracer model is based on the following assumptions:

1) The tracers are ideal so that the fluid properties are not affected.
2) The flow is one dimensional.
3) Both phases and rock are incompressible.
4) The process is isothermal.
5) The flow is horizontal (no gravity effect).

The general form of the two-phase tracer flow model has already been discussed in Section 3.1. Then, incorporating the tracer flow model with the fractional flow function gives the conservation equations for oil, water and tracer shown below.

Water conservation:

$$\emptyset \frac{\partial S_w}{\partial t} + u_T \frac{\partial f_w}{\partial x} = 0. \tag{3.115}$$

Oil conservation:

$$u_T = u_w + u_o = \text{constant}. \tag{3.116}$$

Tracer conservation:

$$\emptyset\frac{\partial}{\partial t}[KC_w(1-S_w)+C_wS_w]+(1-\emptyset)\frac{\partial Cs}{\partial t}+u_T\frac{\partial}{\partial x}[KC_w(1-f_w)+C_wf_w]$$

$$-\emptyset\frac{\partial}{\partial x}\left[S_wD_w\frac{\partial C_w}{\partial x}+(1-S_w)D_oK\frac{\partial C_w}{\partial x}\right]+\emptyset\lambda[S_wC_w+KC_w(1-S_w)]=0, \quad (3.117)$$

where

$$f_w=\frac{u_w}{u_T}=F_w+\frac{\lambda_o\lambda_w}{u_T\lambda_T}\frac{\partial P_c}{\partial x}, \quad (3.118)$$

and

$$F_w=\frac{\lambda_w}{\lambda_T}=\frac{1}{1+\frac{\mu_w}{\mu_o}\frac{k_{ro}}{k_{rw}}}, \quad (3.119)$$

as already discussed in Section 3.1.3 and C_w is the tracer concentration in the water phase.

The above is the two-phase tracer model. Throughout this section, the system is assumed to be horizontal for simplicity and initially filled with oil at connate water saturation. Then, the tracer is injected with a water slug.

3.3.1 Convection Partitioning Model

In this section, only convection and partitioning between phases are applied and capillary pressure is negligible in order to simplify Eq. (3.115) to Eq. (3.117). The following is the simplified two-phase tracer model. This model can be solved using an

analytical method. The convection partitioning tracer model results here follow from the more general compositional model from gas injection which was solve and analyzed by Johansen *et al.* in 2005 (Johansen *et al*., 2005).

Water conservation: $$\emptyset \frac{\partial S_w}{\partial t} + u_T \frac{\partial F_w}{\partial x} = 0. \tag{3.120}$$

Oil conservation: $$u_T = u_w + u_o = \text{constant}\,. \tag{3.121}$$

Tracer conservation: $$\emptyset \frac{\partial}{\partial t}[KC_w(1 - S_w) + C_w S_w]$$

$$+u_T \frac{\partial}{\partial x}[KC_w(1 - F_w) + C_w F_w] = 0\,. \tag{3.122}$$

First, we consider Eq. (3.120), the water fractional flow function.

Introducing the following dimensionless variables:

$$x^* = \frac{x}{L}\,, \tag{3.123}$$

$$t^* = \frac{u_T t}{\emptyset L}\,, \tag{3.124}$$

gives:

$$\frac{\partial S_w}{\partial t^*} + \frac{dF_w}{dS_w}\frac{\partial S_w}{\partial x^*} = 0\,. \tag{3.125}$$

Using the total derivative of S_w with respect to t^*:

$$\frac{\partial S_w}{\partial t^*} + \frac{dx^*}{dt^*}\frac{\partial S_w}{\partial x^*} = \frac{dS_w}{dt^*}\,, \tag{3.126}$$

and comparing Eq. (3.125) and Eq. (3.126) gives:

$$\frac{dS_w}{dt^*} = 0\,, \tag{3.127}$$

$$\frac{dx^*}{dt^*} = \frac{dF_w}{dS_w}\,. \tag{3.128}$$

From Eq. (3.127) and Eq. (3.128), the water saturation is constant over time and the propagation velocity of a constant water saturation is given by:

$$v(S_w)^* = \frac{dF_w}{dS_w}\,. \tag{3.129}$$

Note that the velocity is the dimensionless velocity. This velocity is given by the slope of the tangent in the fractional flow plot.

Recall Eq. (3.38):

$$F_w = \frac{1}{1 + \frac{\mu_w}{\mu_o}\,\frac{a_o(1 - \frac{S_w - S_{wc}}{1 - S_{wc} - S_{or}})^{n_o}}{a_w(\frac{S_w - S_{wc}}{1 - S_{wc} - S_{or}})^{n_w}}}\,. \tag{3.130}$$

In the plot of the fractional flow function in Figure 3.25, the following values are chosen: $\mu_w = 1\ cp$, $\mu_o = 2\ cp$, $a_w = 0.4$, $a_o = 0.9$, $n_w = 3$, $n_o = 3$, $S_{wc} = 0.2$, $S_{or} = 0.2$. The corresponding relative permeability curves are shown in Figure 3.26.

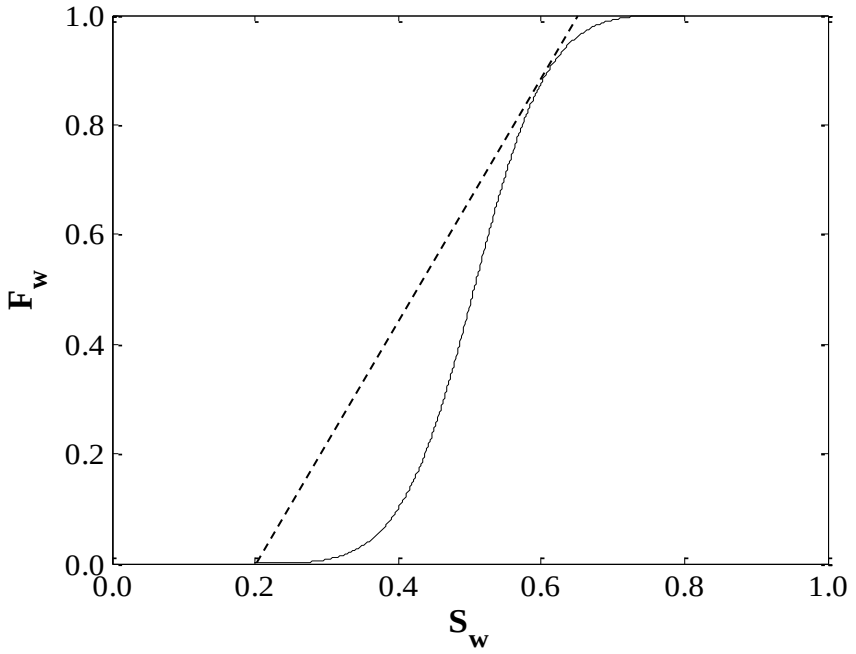

Figure 3.25: Fractional flow function

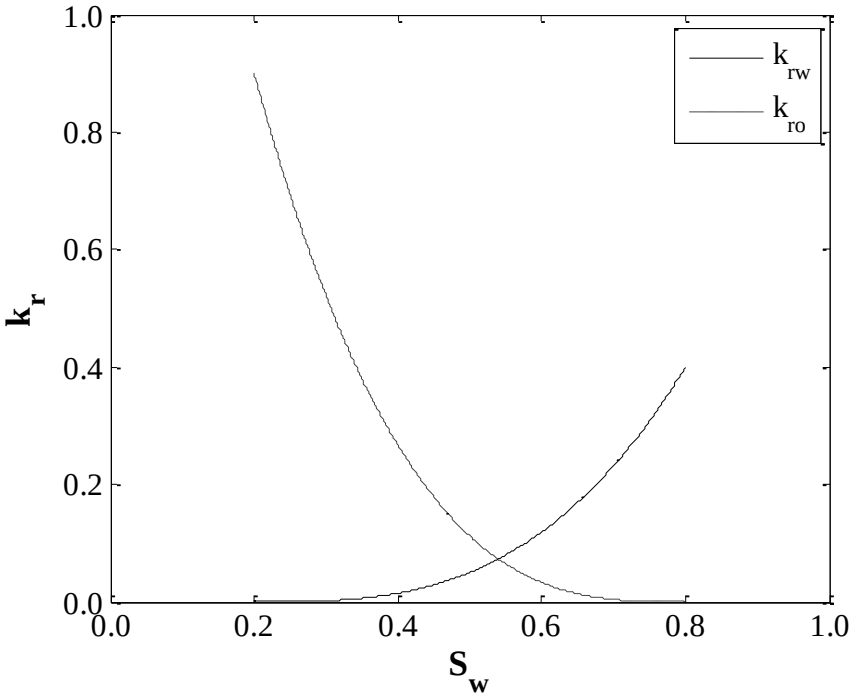

Figure 3.26: Relative permeability curve

According to Eq. (3.89), since saturation propagation velocity with time is constant,

the position of any given saturation at time t can be calculated by:

$$x^* = \frac{dF_w}{dS_w} t^* . \tag{3.131}$$

The derivative of F_w was calculated in Matlab, and the saturation distribution as a function of position is plotted for two time steps: ${t_1}^* = 0.4$, ${t_2}^* = 0.8$ in Figure 3.27.

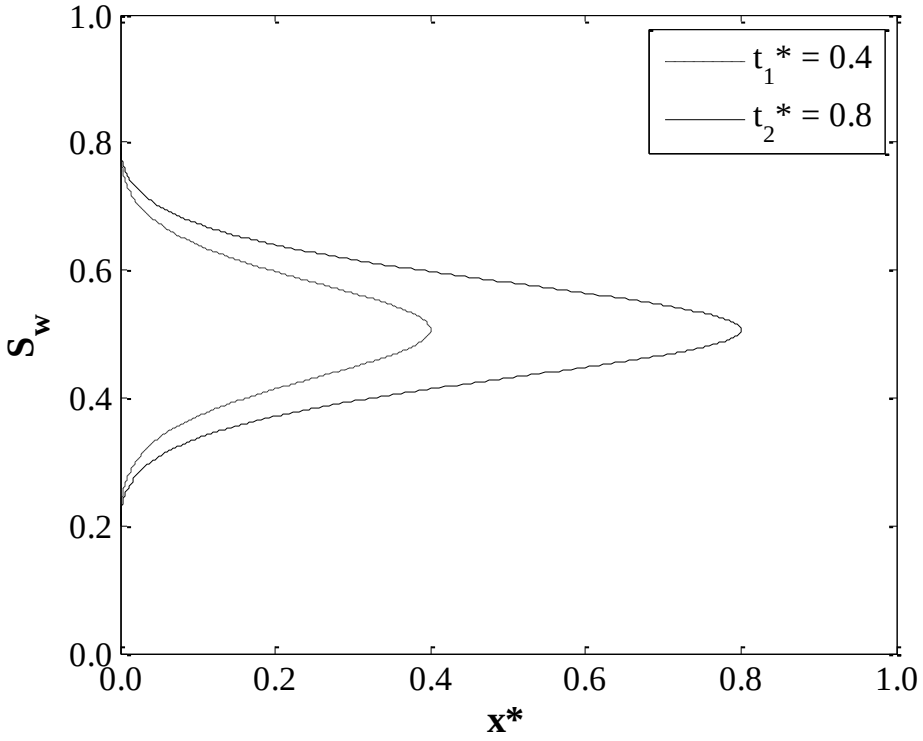

Figure 3.27: Saturation distribution as a function of position

Figure 3.27 cannot hold true physically, because one position must have only one saturation value. According to the Buckley-Leverett construction, this saturation is resolved by saturation discontinuities and a shock front is formed.

The shock front velocity can be calculated as the slope of the tangent drawn from S_{wc}

in Figure 3.25, because for the contact point of continuous saturation and the shock, the velocity should be the same. This gives:

$$v_{\Delta s} = \frac{\Delta F_w}{\Delta S_w}. \tag{3.132}$$

This is the Rankine-Hugoniot condition for mass concentration across the shock. From Eq. (3.132), the shock front velocity can be calculated as the slope of the tangent drawn from S_{wc} in Figure 3.25 and velocity for this case can be calculated which equals to 2.2. Then, the saturation profile for the given boundary conditions: $S(x,0) = 0.2;\ S(0,t) = 0.8$ is plotted in Figure 3.28.

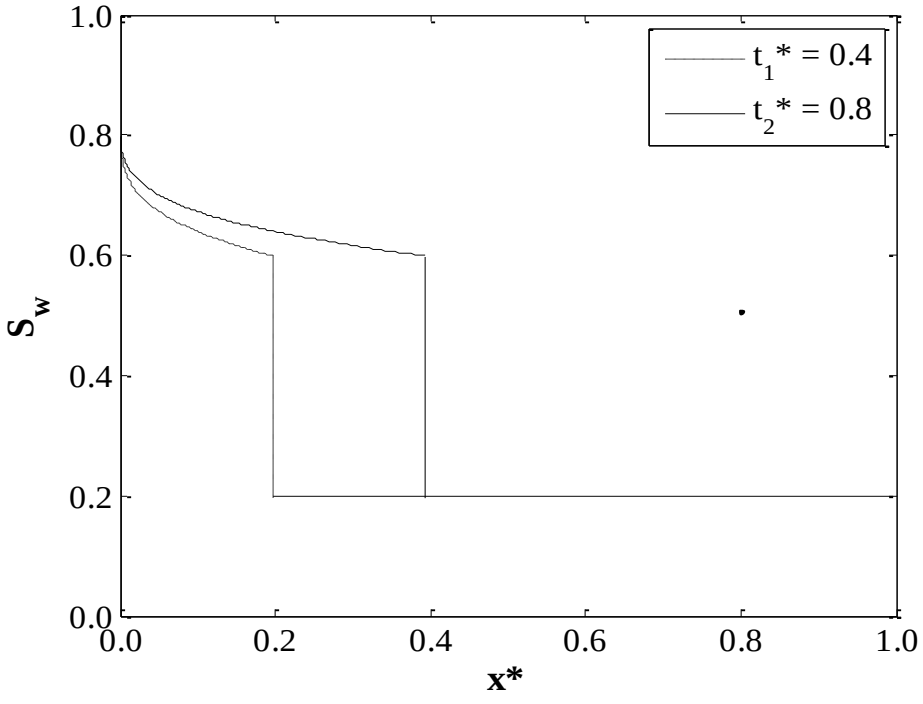

Figure 3.28: Saturation profile of leading edge

Up to this point, the calculation of water saturation distribution has been described.

Next, we describe the calculation of the tracer concentration.

Through formula expansion, Eq. (3.122) changes to:

$$K\frac{\partial C_w}{\partial t} + (1-K)\frac{\partial C_w}{\partial t}S_w + (1-K)\frac{\partial S_w}{\partial t}C_w + \frac{u_T}{\emptyset}\left[K\frac{\partial C_w}{\partial x} + (1-K)\frac{\partial C_w}{\partial x}F_w + (1-K)\frac{\partial F_w}{\partial x}C_w\right] = 0\,. \quad (3.133)$$

From Eq. (3.120) :

$$(1-K)\frac{\partial S_w}{\partial t}C_w + \frac{u_T}{\emptyset}(1-K)\frac{\partial F_w}{\partial x}C_w = 0\,. \quad (3.134)$$

Substituting into Eq. (3.133) gives:

$$\frac{\partial C_w}{\partial t} + \frac{u_T}{\emptyset}\frac{[K(1-F_w)+F_w]}{[K(1-S_w)+S_w]}\frac{\partial C_w}{\partial x} = 0\,. \quad (3.135)$$

Applying the same dimensionless variables as before gives:

$$\frac{\partial {C_w}^*}{\partial t^*} + \frac{[K(1-F_w)+F_w]}{[K(1-S_w)+S_w]}\frac{\partial {C_w}^*}{\partial x^*} = 0\,. \quad (3.136)$$

Similarly, the total derivative of ${C_w}^*$ with respect to t^*:

$$\frac{\partial {C_w}^*}{\partial t^*} + \frac{dx^*}{dt^*}\frac{\partial {C_w}^*}{\partial x^*} = \frac{d{C_w}^*}{dt^*}\,. \quad (3.137)$$

Comparing Eq. (3.136) and Eq. (3.137) gives:

$$\frac{d{C_w}^*}{dt^*} = 0\,, \quad (3.138)$$

$$\frac{dx^*}{dt^*} = \frac{[K(1-F_w)+F_w]}{[K(1-S_w)+S_w]} = \frac{F_w + \frac{K}{1-K}}{S_w + \frac{K}{1-K}}. \tag{3.139}$$

From Eq. (3.138) and Eq. (3.139), the concentration of tracer in the water phase is constant over time and $\frac{dx^*}{dt^*}$ is the propagation velocity of tracer concentration in the water phase, i.e.,

$$v(C_w)^* = \frac{F_w + \frac{K}{1-K}}{S_w + \frac{K}{1-K}}, \tag{3.140}$$

where we assume the partitioning coefficient K is constant. This coefficient can be measured in the laboratory at reservoir conditions and is considered to be known.

From Eq. (3.140), the concentration propagation velocities for different concentrations can be interpreted geometrically as the slope of lines connecting Point A $(-\frac{K}{1-K}, -\frac{K}{1-K})$ and points on the fractional flow curve, for example the slope of Line AB, AC and AD shown in Figure 3.29. Most tracers have K values between 0.1 and 10. In this case, $K = 3$ and $v(C_w) = \frac{F_w - 1.5}{S_w - 1.5}$ have been used.

Assume Line AB is the tangent of the fractional flow curve drawn from Point A and Point B which has saturation $S_w = S_w^*$ (S_w^* is the saturation value shown in Figure 3.29), the corresponding tracer velocity $v(C_w)$ is equal to $v(S_w)$ because the slope of Line AB is equal to the water saturation propagation velocity $\frac{dF_w}{dS_w}$. For an arbitrary point C in Figure 3.29 that has the saturation larger than S_w^*, $v(C_w) > v(S_w)$, which

indicates that the tracer concentration propagates faster than the water saturation. Thus, the tracer will then catch up with smaller water saturations which have relatively large velocities until the tracer moves together with S_w^*. Similarly, for the saturations smaller than S_w^*, the saturation, for example point D in Figure 3.29, the water saturation moves faster than the tracer concentration. Larger water saturations will overtake the tracer until it moves together with S_w^*.

In other words, the tracer will move together with a characteristic water saturation S_w^* and the velocity is the slope of the tangent drawn from point $(-\frac{K}{1-K}, -\frac{K}{1-K})$. The propagation velocity of tracer concentration calculated for this case is $v(C_w) = 0.67$ and travels with $S_w^* = 0.68$ which is shown in Figure 3.30.

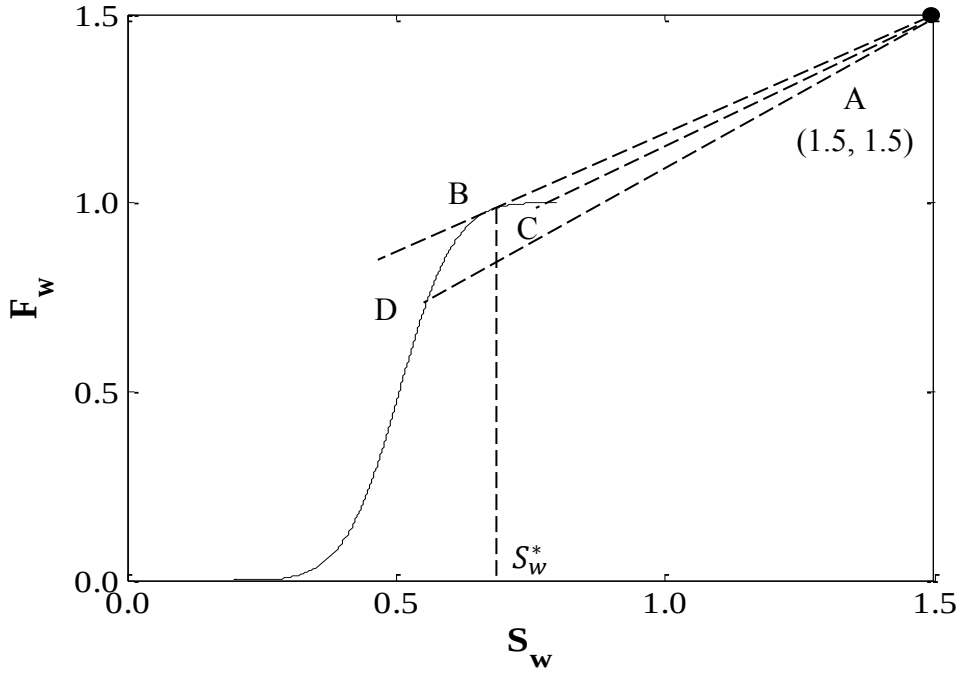

Figure 3.29: Construction to show tracer concentration velocity

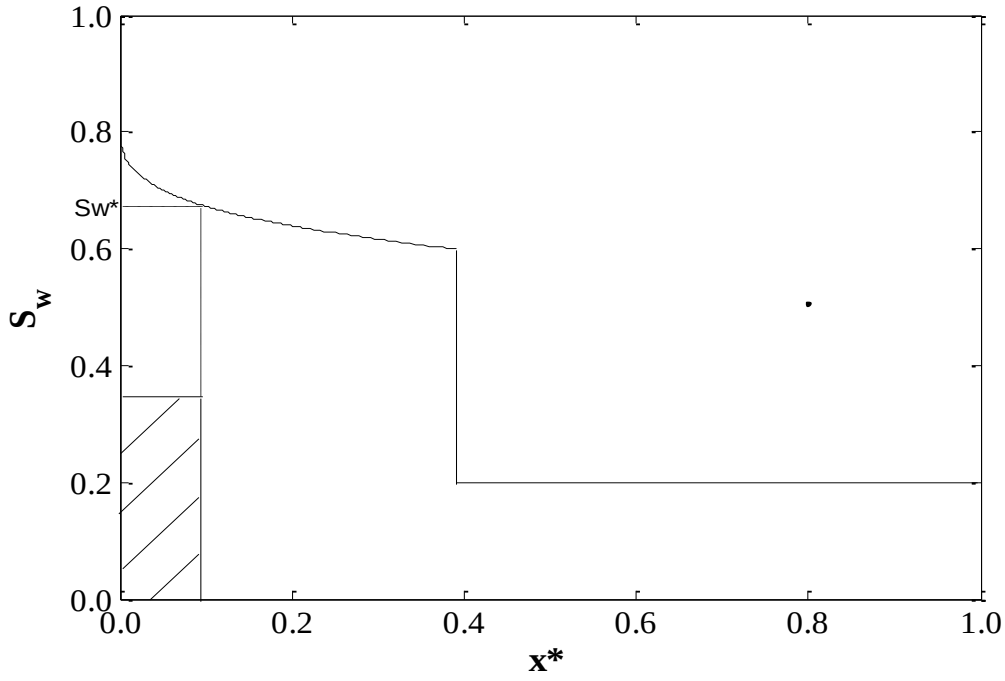

Figure 3.30: Propagation of saturation and tracer concentration

3.3.2 Convection Adsorption Partitioning Model

In this section, the adsorption term is added to the tracer convection partitioning equation. Assume this is a water-wet formation; therefore adsorption only happens from the water phase. Capillary pressure is assumed to be negligible.

Water conservation:
$$\emptyset \frac{\partial S_w}{\partial t} + u_T \frac{\partial F_w}{\partial x} = 0. \tag{3.141}$$

Oil conservation:
$$u_T = u_w + u_o = \text{constant}\,. \tag{3.142}$$

Tracer conservation:
$$\emptyset \frac{\partial}{\partial t}[KC_w(1 - S_w) + C_w S_w] + (1 - \emptyset)\frac{\partial Cs}{\partial t}$$
$$+u_T \frac{\partial}{\partial x}[KC_w(1 - F_w) + C_w F_w] = 0\,. \tag{3.143}$$

As the water fractional flow model stays the same, the water saturation distribution remains unchanged from the previous section.

For the tracer model, the problem solving process is similar as section 3.3.1. Rearranging Eq. (3.143) and applying Langmuir adsorption gives:

$$K\frac{\partial C_w}{\partial t} + (1 - K)\frac{\partial C_w}{\partial t}S_w + (1 - K)\frac{\partial S_w}{\partial t}C_w + \frac{1 - \emptyset}{\emptyset}\frac{a}{(1 + bC_w)^2}\frac{\partial C_w}{\partial t}$$
$$+\frac{u_T}{\emptyset}\left[K\frac{\partial C_w}{\partial x} + (1 - K)\frac{\partial C_w}{\partial x}F_w + (1 - K)\frac{\partial F_w}{\partial x}C_w\right] = 0\,. \tag{3.144}$$

Substituting Eq. (4.96) into the above equation gives:

$$\left[K + (1 - K)S_w + \frac{1 - \emptyset}{\emptyset}\frac{a}{(1 + bC_w)^2}\right]\frac{\partial C_w}{\partial t} + \frac{u_T}{\emptyset}[K + (1 - K)F_w]\frac{\partial C_w}{\partial x} = 0. \tag{3.145}$$

Therefore,

$$\frac{\partial C_w}{\partial t}+\frac{u_T}{\emptyset}\frac{[K+(1-K)F_w]}{[K+(1-K)S_w+\frac{1-\emptyset}{\emptyset}\frac{a}{(1+bC_w)^2}]}\frac{\partial C_w}{\partial x}=0\,. \qquad (3.146)$$

Applying the same dimensionless variables as before gives:

$$\frac{\partial {C_w}^*}{\partial t^*}+\frac{[K+(1-K)F_w]}{[K+(1-K)S_w+\frac{1-\emptyset}{\emptyset}\frac{a}{(1+bC_w)^2}]}\frac{\partial {C_w}^*}{\partial x^*}=0\,. \qquad (3.147)$$

The total derivative of ${C_w}^*$ with respect to t^*:

$$\frac{\partial {C_w}^*}{\partial t^*}+\frac{dx^*}{dt^*}\frac{\partial {C_w}^*}{\partial x^*}=\frac{d{C_w}^*}{dt^*}\,. \qquad (3.148)$$

Comparing Eq. (3.147) and Eq. (3.148) gives:

$$\frac{d{C_w}^*}{dt^*}=0\,, \qquad (3.149)$$

$$\frac{dx^*}{dt^*}=\frac{[K+(1-K)F_w]}{\left[K+(1-K)S_w+\frac{1-\emptyset}{\emptyset}\frac{a}{(1+bC_w)^2}\right]}$$

$$=\frac{F_w+\frac{K}{1-K}}{S_w+\frac{K}{1-K}+\frac{1-\emptyset}{\emptyset(1-K)}\frac{a}{(1+bC_w)^2}}\,. \qquad (3.150)$$

From Eq. (3.149) and Eq. (3.150), the concentration of tracer in the water phase is constant over time and $\frac{dx^*}{dt^*}$ is the propagation velocity of tracer concentration in the water phase, i.e.,

$$v(C_w)^* = \frac{F_w + \frac{K}{1-K}}{S_w + \frac{K}{1-K} + h_{(c)}}, \tag{3.151}$$

where

$$h_{(c)} = \frac{1-\emptyset}{\emptyset(1-K)} \frac{a}{(1+bC_w)^2}, \tag{3.152}$$

for simplicity.

From Eq. (3.151), the propagation velocity of a tracer is the slope of the tangent drawn from point $(-\frac{K}{1-K}, -\frac{K}{1-K} - h_{(c)})$ to the fractional flow function curve. According to Eq. (3.152), the values of $h_{(c)}$ changes when C_w changes. That is to say, different concentrations have different corresponding points from which tangent lines are drawn to calculate their velocities. In this case, $K = 3$, $a = 1.5$, $b = 10\, m^3/kg$, $\emptyset = 0.2$. The values of $h_{(c)}$ corresponding to C_w are calculated shown in Table 3.3.

According to the Table 3.3, as C_w changes from 0.00 to 1.00, the corresponding point $(-\frac{K}{1-K}, -\frac{K}{1-K} - h_{(c)})$ to draw tangents changes from Point A (4.5, 1.5) to Point B (1.52, 1.5) shown in Figure 3.31.

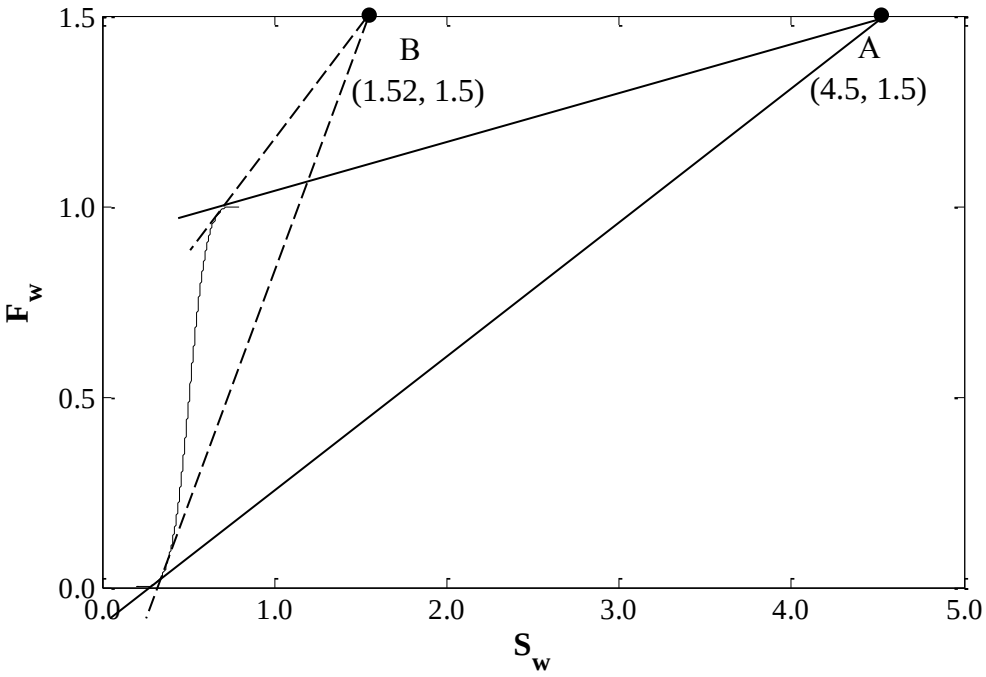

Figure 3.31: Construction to show tracer concentration velocity calculation

Table 3.3 shows the calculated velocity of the different concentrations at leading edge and trailing edge. It is shown that for both leading edge and trailing edge, the larger concentration moves faster, which results in a spreading wave along propagation.

Table 3.3: Velocity of concentrations at leading edge and trailing edge

Cw	$h(c)$	leading edge velocity	trailing edge velocity
0.00	-3.00	0.1326	0.3541
0.01	-2.48	0.1565	0.4028
0.03	-1.78	0.1988	0.5008
0.05	-1.33	0.2438	0.5879
0.07	-1.04	0.2829	0.6673
0.10	-0.75	0.3333	0.7684
0.15	-0.48	0.4051	0.8955
0.20	-0.33	0.4584	0.9842
0.25	-0.24	0.4986	1.0469
0.30	-0.19	0.5287	1.0923
0.40	-0.12	0.5668	1.1474
0.50	-0.08	0.5920	1.1786
0.70	-0.05	0.6186	1.2160
0.90	-0.03	0.6337	1.2354
1.00	-0.02	0.6392	1.2404

First, we will discuss the concentration propagation of the trailing edge.

Figure 4.32 is plotted for the propagation velocities of different tracer concentrations for the trailing edge. The propagation velocity increases smoothly from low to high concentrations.

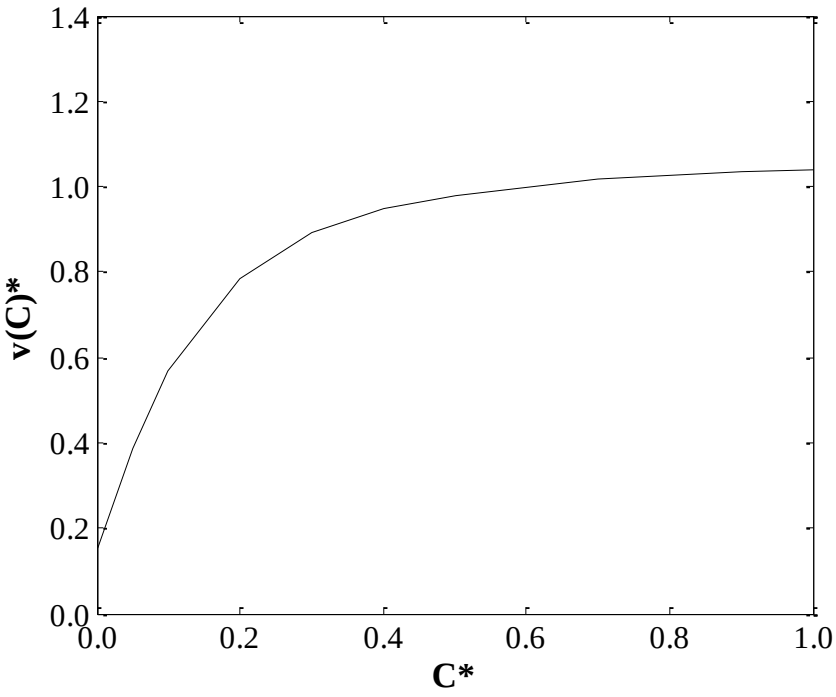

Figure 3.32: Dimensionless propagation velocity ($v(C)^*$) of concentration for trailing edge

After the velocities are calculated, the concentration propagation as a function of location can be obtained by multiplying the propagation velocities with time. Figure 3.33 shows the concentration distribution at different time steps.

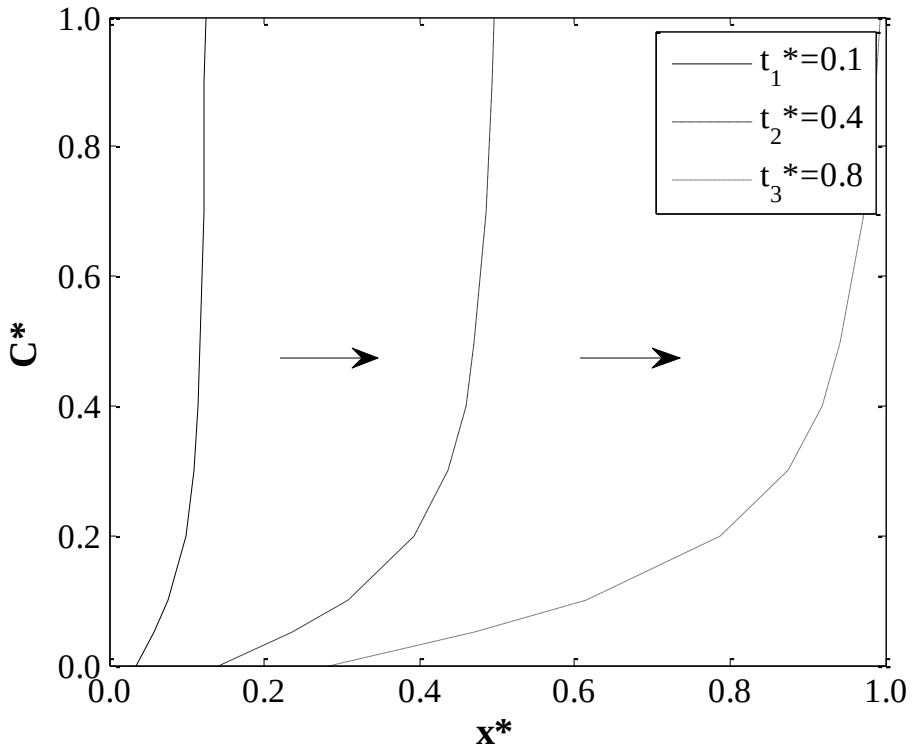

Figure 3.33: Dimensionless concentration distribution (C^*) for trailing edge as a function of position

Then, we apply trailing edge with boundary conditions. Figure 3.34 is the concentration for $t^* = 0.4$ with the boundary conditions of the trailing edge. The concentration moves continuously until if truncates at the boundary conditions which is physically correct.

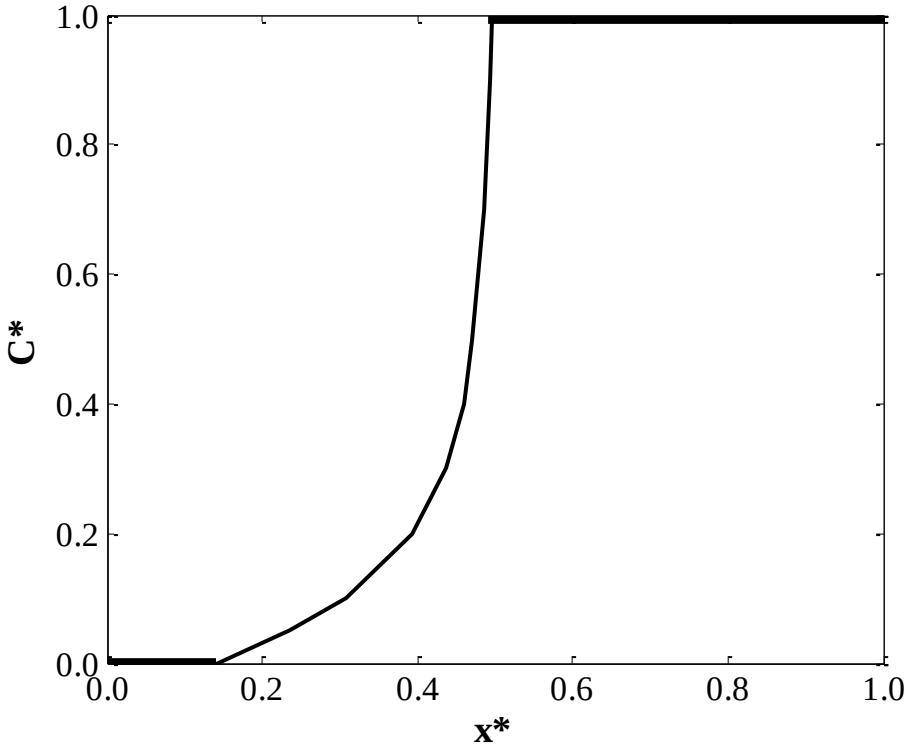

Figure 3.34: Dimensionless concentration distributions for trailing edge (C^*) as a function of position for $t^* = 0.4$

Then, if we reverse the inlet condition and the initial condition of trailing edge, the concentration distribution for the leading edge can be obtained. Figure 3.35 shows the concentration distribution of the leading edge at $t^* = 0.8$ with the boundary conditions.

From Figure 3.35, each positon has three different values between 0.1 and 0.5 which does not make sense physically. Thus, the leading edge should be treated as a shock wave, the dashed line shown in Figure 3.36.

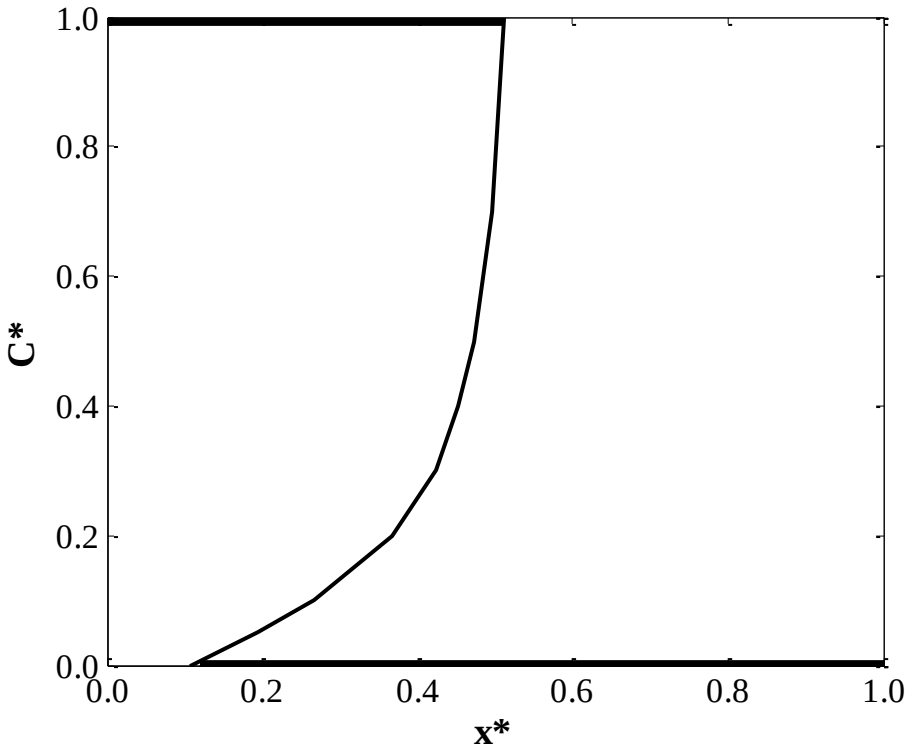

Figure 3.35: Dimensionless concentration distribution (C^*) for leading edge with boundary conditions for $t^* = 0.8$

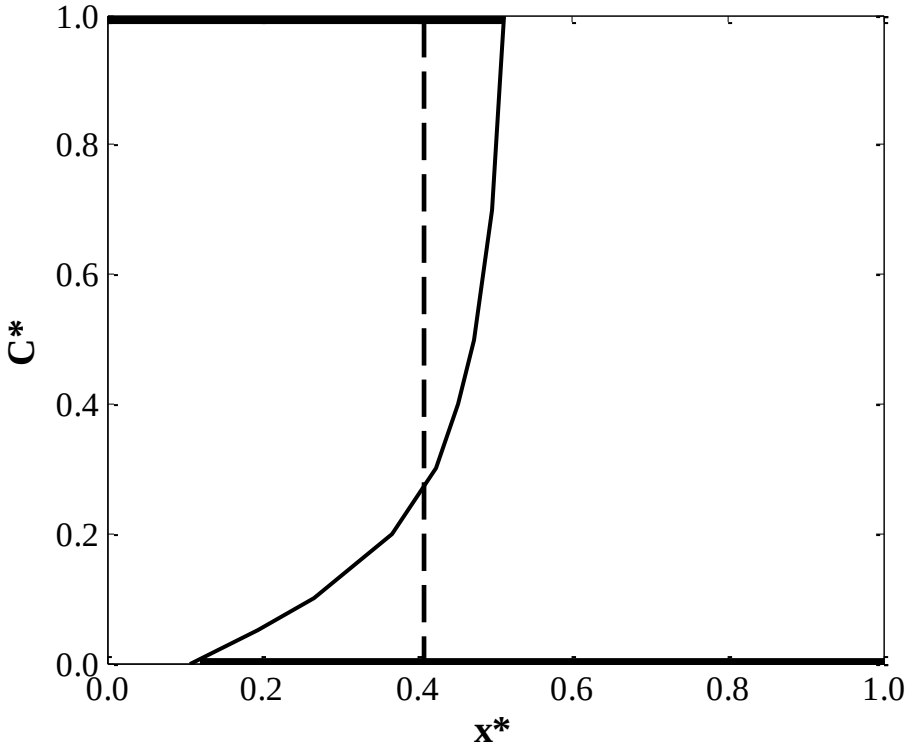

Figure 3.36: Dimensionless leading edge concentration distribution (C^*) as a function of position

3.3.3 Convection Adsorption Dispersion Partitioning and Radioactive Decay Model

The general model of two-phase tracer with all the factors included (partitioning between phases; dispersion; adsorption; radioactive decay) is solved numerically in this section. Recall Eq. (3.115), Eq. (3.116) and Eq. (3.117) :

Water conservation: $$\emptyset \frac{\partial S_w}{\partial t} + u_T \frac{\partial f_w}{\partial x} = 0. \quad (3.153)$$

Oil conservation: $$u_T = u_w + u_o = \text{constant}. \quad (3.154)$$

Tracer conservation: $$\emptyset \frac{\partial}{\partial t}[KC_w(1-S_w)+C_wS_w]+(1-\emptyset)\frac{\partial Cs}{\partial t}$$

$$+u_T\frac{\partial}{\partial x}[KC_w(1-f_w)+C_wf_w]-\emptyset\frac{\partial}{\partial x}\left[S_wD_w\frac{\partial C_w}{\partial x}+(1-S_w)D_oK\frac{\partial C_w}{\partial x}\right]$$

$$+\emptyset\lambda[S_wC_w+KC_w(1-S_w)]=0\,. \tag{3.155}$$

First, we apply the water fractional flow function.

Apply Eq. (3.118) and the same dimensionless variables (x^*, t^*) to Eq. (3.153) gives:

$$\frac{\partial S_w}{\partial t^*}+\frac{\partial F_w}{\partial x^*}=-\frac{1}{u_TL}\left(\frac{\partial N}{\partial x^*}\frac{\partial S_w}{\partial x^*}P_C'+\frac{\partial P_C'}{\partial x^*}\frac{\partial S_w}{\partial x^*}N+\frac{\partial S_w^2}{\partial x^{*2}}NP_C'\right), \tag{3.156}$$

where

$$N=\frac{\lambda_w\lambda_o}{\lambda_T}\,, \tag{3.157}$$

for simplification, and λ_w and λ_o are the phase mobility of water and oil which have already been discussed in section 3.1.3.

The capillary pressure P_C can be expressed as a function of the water saturation S_w following a hyperbolic relationship:

$$P_C=mS_w^2+pS_w+q\,, \tag{3.158}$$

where m, p, q are constants.

The following conditions are applied to calculate m, p, q:

$$P_C(S_w = 1) = 0\,, \tag{3.159}$$

$$P_C'(S_w = 1) = 0\,, \tag{3.160}$$

$$P_C(S_w = S_{wc} = 0.2) = 8 \times 10^6\,. \tag{3.161}$$

Then, the three constants are calculated and substitute into Eq. (3.148) gives:

$$P_C = 1.25 \times 10^7 S_w^2 + 2.5 \times 10^7 S_w + 1.25 \times 10^7\,. \tag{3.162}$$

According to the above equation, the capillary pressure P_C as a function of the water saturation S_w is plotted and shown in Figure 3.37.

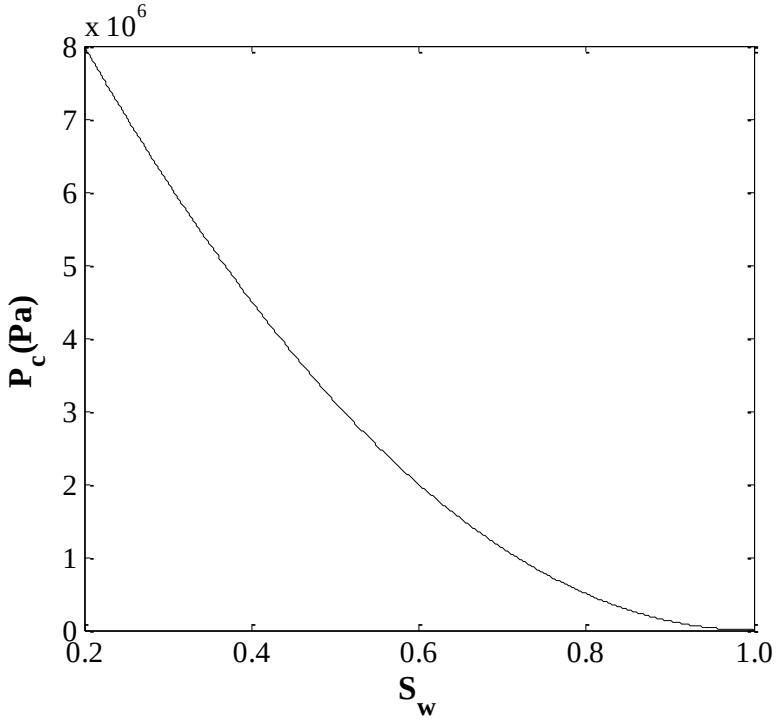

Figure 3.37: Capillary pressure as a function of water saturation

Then, we find the finite difference approximation for Eq. (3.156):

$$\frac{S_i^{n+1}-S_i^n}{\Delta t^*}+\frac{F_i^n-F_{i-1}^n}{\Delta x^*}=-\frac{1}{u_T L}\left[\frac{N_i^n-N_{i-1}^n}{\Delta x^*}\frac{S_{i+1}^n-S_{i-1}^n}{2\Delta x^*}P_{C_i}'^n\right.$$

$$\left.+\frac{P_{C_i}'^n-P_{C_{i-1}}'^n}{\Delta x^*}\frac{S_{i+1}^n-S_{i-1}^n}{2\Delta x^*}N_i^n+\frac{S_{i-1}^n-2S_i^n+S_{i+1}^n}{\Delta x^{*2}}P_{C_i}'^n N_i^n\right]. \qquad (3.163)$$

Rearranging the formula gives:

$$S_i^{n+1}=S_i^n-\Delta t^*\{\frac{F_i^n-F_{i-1}^n}{\Delta x^*}+\frac{1}{u_T L}\left[\frac{N_i^n-N_{i-1}^n}{\Delta x^*}\frac{S_{i+1}^n-S_{i-1}^n}{2\Delta x^*}P_{C_i}'^n\right.$$

$$\left.+\frac{P_{C_i}'^n-P_{C_{i-1}}'^n}{\Delta x^*}\frac{S_{i+1}^n-S_{i-1}^n}{2\Delta x^*}N_i^n+\frac{S_{i-1}^n-2S_i^n+S_{i+1}^n}{\Delta x^{*2}}P_{C_i}'^n N_i^n\right]\}. \qquad (3.164)$$

Plotting $S\ (x,t)$ as a function of x with boundary conditions: $S(x,0)=0.2;\ S(0,t)=0.8$ shown in Figure 3.38.

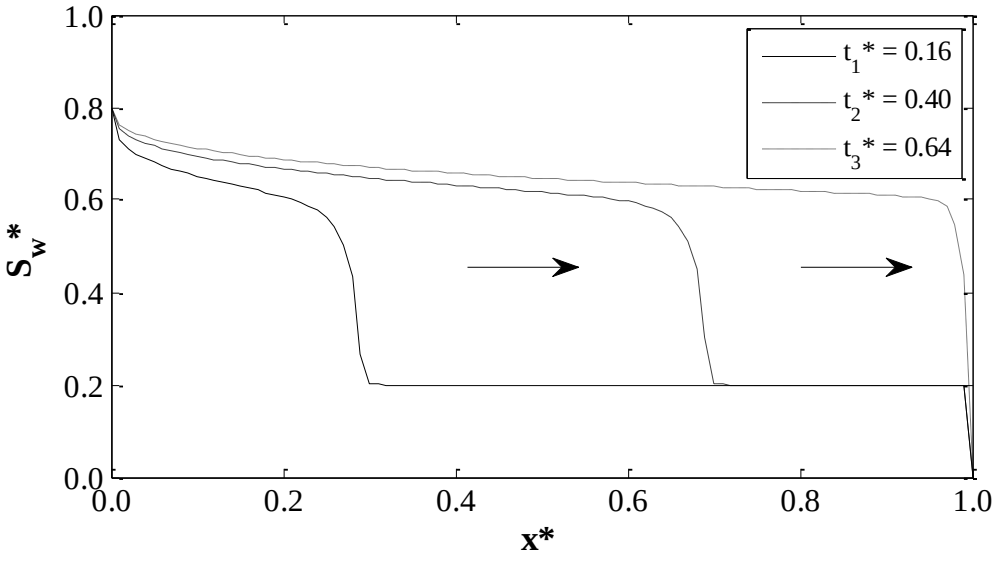

Figure 3.38: Saturation distribution

After the water saturation distribution is obtained, we consider the tracer concentration

equation.

First, substituting Eq. (3.118) and Langmuir adsorption to Eq. (3.155) gives:

$$\frac{\partial}{\partial t}[KC_w + (1-K)C_w S_w] + \frac{1-\emptyset}{\emptyset}\frac{a}{(1+bC_w)^2}\frac{\partial C_w}{\partial t}$$

$$+\frac{u_T}{\emptyset}\frac{\partial}{\partial x}\left[KC_w + (1-K)C_w\left(F_w + \frac{\lambda_o\lambda_w}{u_T\lambda_T}\frac{\partial P_c}{\partial x}\right)\right]$$

$$-\frac{\partial}{\partial x}\left[(D_w - KD_o)S_w\frac{\partial C_w}{\partial x} + KD_o\frac{\partial C_w}{\partial x}\right] + \emptyset\lambda[S_w C_w + KC_w(1-S_w)] = 0\,. \quad (3.165)$$

Then,

$$K\frac{\partial C_w}{\partial t} + (1-K)S_w\frac{\partial C_w}{\partial t} + (1-K)C_w\frac{\partial S_w}{\partial t} + \frac{1-\emptyset}{\emptyset}\frac{a}{(1+bC_w)^2}\frac{\partial C_w}{\partial t}$$

$$+\frac{u_T}{\emptyset}\left[K\frac{\partial C_w}{\partial x} + (1-K)f_w\frac{\partial C_w}{\partial x} + (1-K)C_w\frac{\partial F_w}{\partial x}\right] - (D_w - KD_o)\frac{\partial S_w}{\partial x}\frac{\partial C_w}{\partial x}$$

$$-(D_w - KD_o)S_w\frac{\partial^2 C_w}{\partial x^2} - KD_o\frac{\partial^2 C_w}{\partial x^2} + \lambda[S_w C_w + KC_w(1-S_w)] = 0\,. \quad (3.166)$$

Rearranging formula gives:

$$[K + (1-K)S_w]\frac{\partial C_w}{\partial t} + (1-K)C_w\frac{\partial S_w}{\partial t} + \frac{1-\emptyset}{\emptyset}\frac{a}{(1+bC_w)^2}\frac{\partial C_w}{\partial t}$$

$$+\frac{u_T}{\emptyset}[K + (1-K)F_w]\frac{\partial C_w}{\partial x} + \frac{u_T}{\emptyset}(1-K)C_w\frac{\partial F_w}{\partial x} - (D_w - KD_o)\frac{\partial S_w}{\partial x}\frac{\partial C_w}{\partial x}$$

$$-[(D_w - KD_o)S_w + KD_o]\frac{\partial^2 C_w}{\partial x^2} + \lambda[S_w C_w + KC_w(1-S_w)] = 0\,. \quad (3.167)$$

Applying the dimensionless variables to Eq. (3.165) gives:

$$\left[K+(1-K)S_w+\frac{1-\emptyset}{\emptyset}\frac{a}{\{1+b[C_w{}^*(C_L-C_R)+C_R]\}^2}\right]\frac{\partial C_w{}^*}{\partial t^*}$$

$$=-(1-K)[C_w{}^*(C_L-C_R)+C_R]\frac{\partial S_w}{\partial t^*}-[K+(1-K)F_w]\frac{\partial C_w{}^*}{\partial x^*}$$

$$-(1-K)[C_w{}^*(C_L-C_R)+C_R]\frac{\partial F_w}{\partial x^*}+\left(\frac{1}{N_{pew}}-K\frac{1}{N_{peo}}\right)\frac{\partial S_w}{\partial x^*}\frac{\partial C_w{}^*}{\partial x^*}$$

$$+\left[\left(\frac{1}{N_{pew}}-K\frac{1}{N_{peo}}\right)S_w+K\frac{1}{N_{peo}}\right]\frac{\partial^2 C_w{}^*}{\partial x^{*2}}-M\{S_w[C_w{}^*(C_L-C_R)+C_R]$$

$$+K(1-S_w)[C_w{}^*(C_L-C_R)+C_R]\}, \tag{3.168}$$

where

$$N_{pew}=\frac{u_T L}{\emptyset D_w}, \tag{3.169}$$

$$N_{peo}=\frac{u_T L}{\emptyset D_o}, \tag{3.170}$$

$$M=\frac{\lambda\emptyset L}{u_T}. \tag{3.171}$$

Then, find the finite difference approximation for Eq. (3.168):

$$\left[K+(1-K){S_{w_i}}^n+\frac{1-\emptyset}{\emptyset}\frac{a}{\left\{1+b\left[{C_{w_i}}^{n^*}(C_L-C_R)+C_R\right]\right\}^2}\right]\frac{{C_{w_i}}^{n+1^*}-{C_{w_i}}^{n^*}}{\Delta t^*}$$

$$=-(1-K)\left[{C_{w_i}}^{n^*}(C_L-C_R)+C_R\right]\frac{{S_{w_i}}^{n+1}-{S_{w_i}}^n}{\Delta t^*}$$

$$-\left[K+(1-K){F_{w_i}}^n\right]\frac{{C_{w_{i+1}}}^{n\ *}-{C_{w_{i-1}}}^{n\ *}}{2\Delta x^*}$$

$$-(1-K)\left[{C_{w_i}}^{n^*}(C_L-C_R)+C_R\right]\frac{{F_{w_i}}^n-{F_{w_{i-1}}}^n}{\Delta x^*}$$

$$+\left(\frac{1}{N_{pew}}-K\frac{1}{N_{peo}}\right)\frac{S_{w_{i+1}}^{\ n}-S_{w_{i-1}}^{\ n}}{\Delta x^*}\frac{C_{w_{i+1}}^{\ n\ *}-C_{w_{i-1}}^{\ n\ *}}{2\Delta x^*}$$

$$+\left[\left(\frac{1}{N_{pew}}-K\frac{1}{N_{peo}}\right)S_{w_i}^{\ n}+K\frac{1}{N_{peo}}\right]\frac{C_{w_{i+1}}^{\ n\ *}-2C_{w_i}^{\ n*}+C_{w_{i-1}}^{\ n\ *}}{\Delta x^{*2}}$$

$$-M\{S_{w_i}^{\ n}\left[C_{w_i}^{\ n*}(C_L-C_R)+C_R\right]+K\left(1-S_{w_i}^{\ n}\right)\left[C_{w_i}^{\ n*}(C_L-C_R)+C_R\right]\},\quad(3.172)$$

Rearranging formula gives:

$$C_{w_i}^{\ n+1*}=C_{w_i}^{\ n*}+\frac{\Delta t^*}{\left[K+(1-K)S_{w_i}^{\ n}+\frac{1-\emptyset}{\emptyset}\frac{a}{\left\{1+b\left[C_{w_i}^{\ n*}(C_L-C_R)+C_R\right]\right\}^2}\right]}$$

$$\times\{-(1-K)\left[C_{w_i}^{\ n*}(C_L-C_R)+C_R\right]\frac{S_{w_i}^{\ n+1}-S_{w_i}^{\ n}}{\Delta t^*}$$

$$-\left[K+(1-K)F_{w_i}^{\ n}\right]\frac{C_{w_{i+1}}^{\ n\ *}-C_{w_{i-1}}^{\ n\ *}}{2\Delta x^*}$$

$$-(1-K)\left[C_{w_i}^{\ n}(C_L-C_R)+C_R\right]\frac{F_{w_i}^{\ n}-F_{w_{i-1}}^{\ n}}{\Delta x^*}$$

$$+\left(\frac{1}{N_{pew}}-K\frac{1}{N_{peo}}\right)\frac{S_{w_{i+1}}^{\ n}-S_{w_{i-1}}^{\ n}}{\Delta x^*}\frac{C_{w_{i+1}}^{\ n\ *}-C_{w_{i-1}}^{\ n\ *}}{2\Delta x^*}$$

$$+\left[\left(\frac{1}{N_{pew}}-K\frac{1}{N_{peo}}\right)S_{w_i}^{\ n}+K\frac{1}{N_{peo}}\right]\frac{C_{w_{i+1}}^{\ n\ *}-2C_{w_i}^{\ n*}+C_{w_{i-1}}^{\ n\ *}}{\Delta x^{*2}}$$

$$-MS_{w_i}^{\ n}\left[C_{w_i}^{\ n*}(C_L-C_R)+C_R\right]-MK\left(1-S_{w_i}^{\ n}\right)\left[C_{w_i}^{\ n*}(C_L-C_R)+C_R\right]\},(3.173)$$

Plotting $C_w{}^*(x,t)$ combined with the boundary conditions for the leading edge: $C_w{}^*(x,0)=0$; $C_w{}^*(0,t)=1$ and trailing edge: $C_w{}^*(x,0)=1$; $C_w{}^*(0,t)=0$,

the propagation of tracer slug in the water phase is shown in Figure 3.38. For this case, the parameter used are $K = 0.2$, $\emptyset = 0.2$, $N_{pew} = 100$, $N_{peo} = 500$, $a = 1.5$, $b = 10\ m^3/kg$, $M = 0.0003$, $C_L = 100\ kg/m^3$, $C_R = 0$ with four time steps: ${t_1}^* = 0.16$, ${t_2}^* = 0.40$, ${t_3}^* = 0.64$, ${t_4}^* = 0.88$.

Figure 3.39 shows that as the tracer slug propagates along x direction, its shape spreads because of dispersion; there is also concentration loss as a result of adsorption, partitioning between phases and radioactive decay. Thus, the tracer slug dimensionless concentration could not reach 1.0.

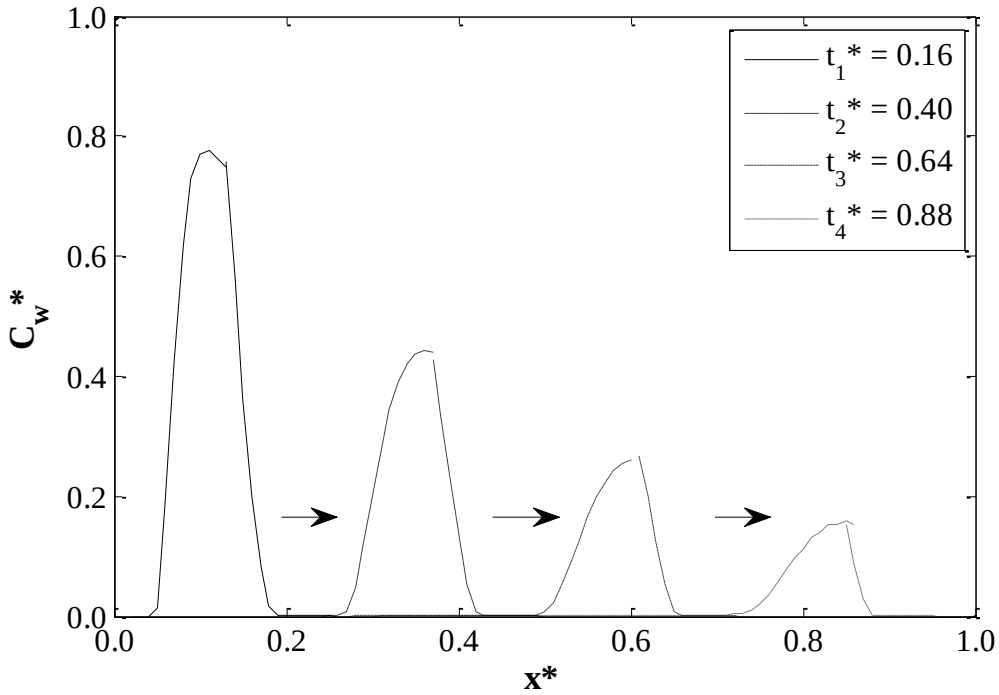

Figure 3.39: Tracer slug propagation in water phase

By comparing Figure 3.38 (water propagation) and Figure 3.39 (tracer slug propagation in the water phase), we can see that the tracer slug moves together with

water saturation along x direction, but relatively slow because of the retardation caused by partitioning between phases and adsorption. The water breaks through first, then the tracer slug breaks through.

The effects of decay constant and Peclet number on tracer slug propagation are discussed below. Figure 3.40, 3.41 and 3.42 are plotted for decay constants: $M_1 = 0.00006$, $M_2 = 0.0001$, $M_3 = 0.0003$, respectively for three time steps: ${t_1}^* = 0.2$, ${t_2}^* = 0.5$, ${t_3}^* = 0.8$.

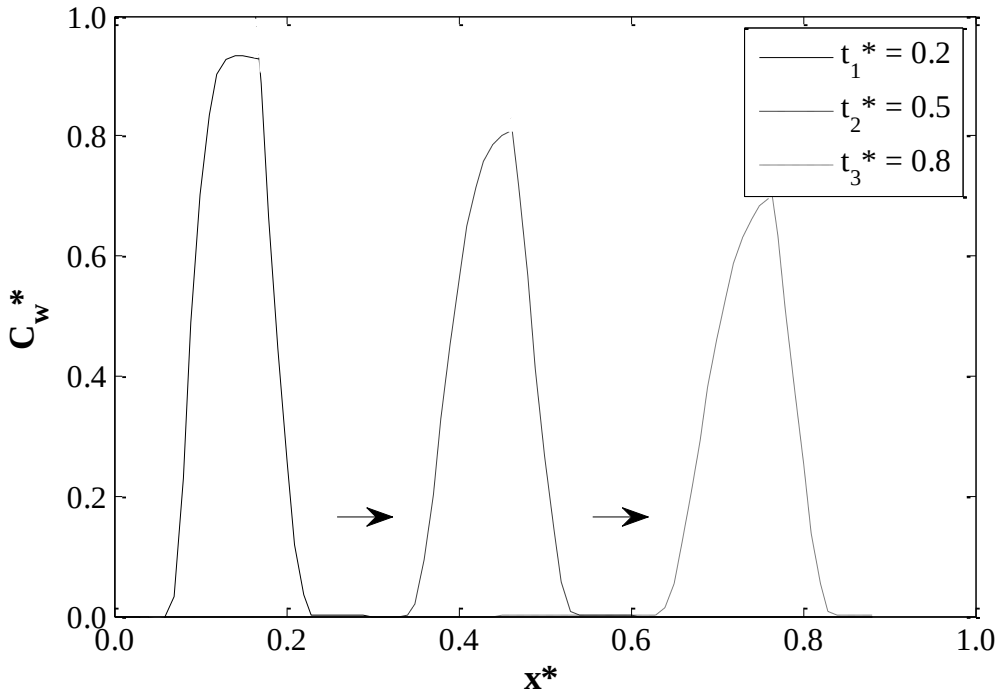

Figure 3.40: Tracer slug propagation in water phase for $M = 0.00006$

As can be seen from Figure 3.40, upon propagation, the tracer slug size has an observable decrease. When comparing with Figure 3.41 and Figure 3.42, the tracer slug concentration loss increases when the decay constant increases. At dimensionless

time step $t_3^* = 0.8$, the dimensionless concentration peak for $M = 0.00006$ is 0.7 shown in Figure 3.40; however, it becomes much lower equals to 0.55 for $M = 0.0001$ (Figure 3.41) and 0.18 for $M = 0.0003$ (Figure 3.42). This phenomenon is also observed and discussed in Section 3.2.4. A large decay constant *M* represents a large effect of radioactive decay, which results in a large concentration loss.

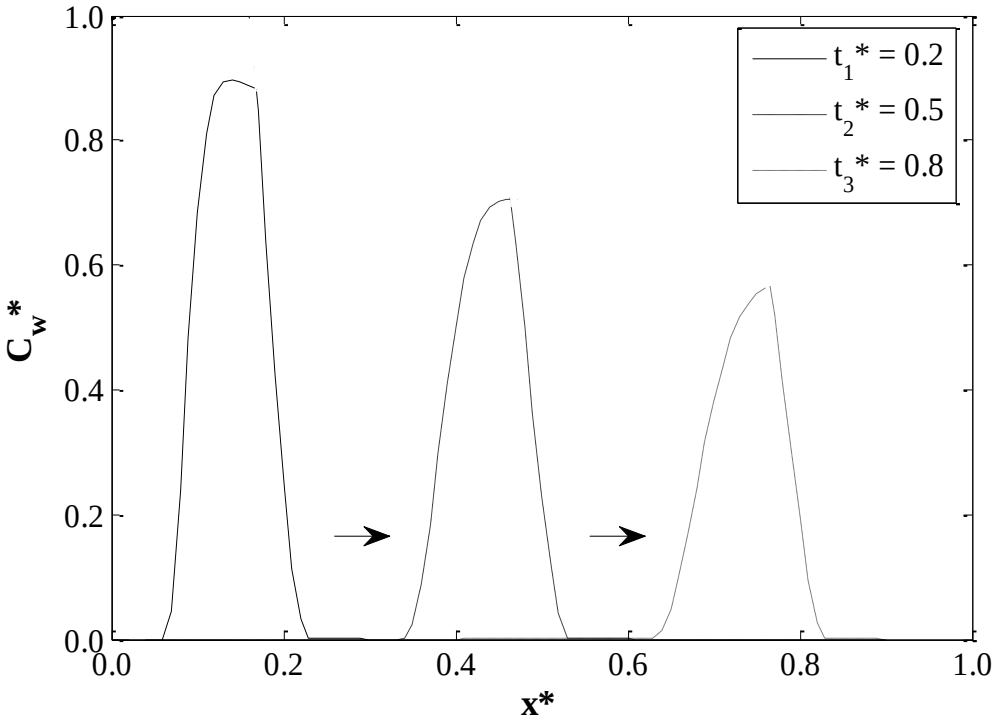

Figure 3.41: Tracer slug propagation in water phase for $M = 0.0001$

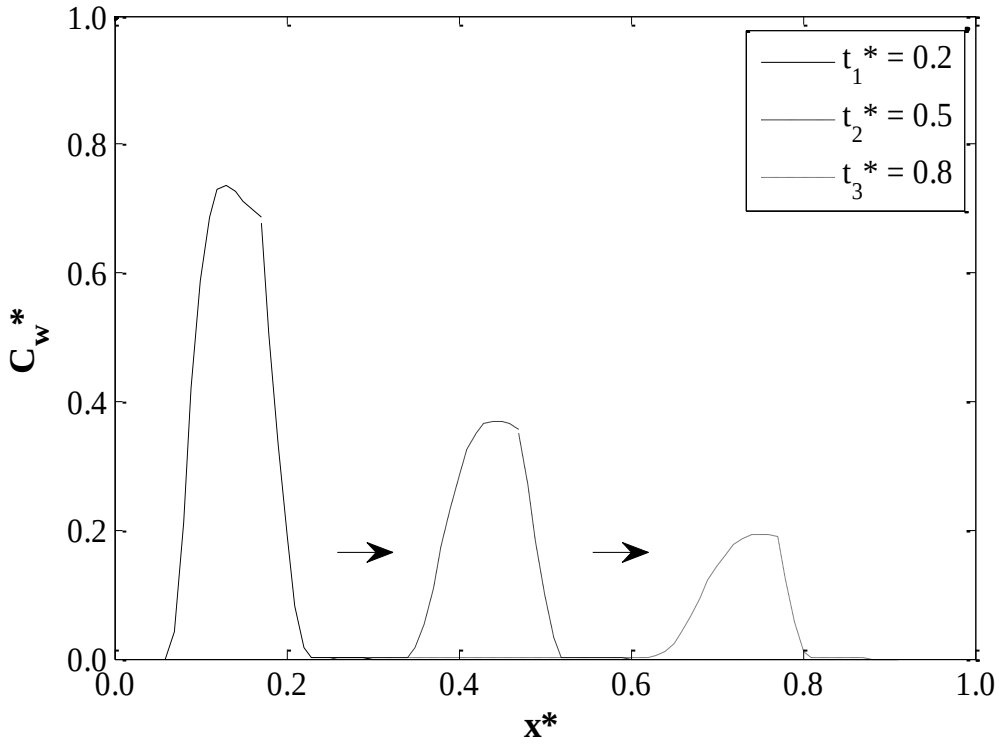

Figure 3.42: Tracer slug propagation in water phase for $M = 0.0003$

In order to investigate the effect of Peclet number, Figure 3.43, 3.44 and 3.45 are plotted for Peclet numbers: $N_{pe1} = 50$, $N_{pe2} = 100$, $N_{pe3} = 500$, respectively, for three time steps: ${t_1}^* = 0.2$, ${t_2}^* = 0.5$, ${t_3}^* = 0.8$. The dimensionless concentration peak of each time step is at the same level. The mixing zone decreases with the Peclet number increases, but the change is inconsequential. This is because the effect of Peclet number is not that severe when comparing to the large concentration loss caused by radioactive decay effect. Thus, we conclude that a small Peclet number results in a large tracer slug mixing zone; however, the effect is minor compared with other effects.

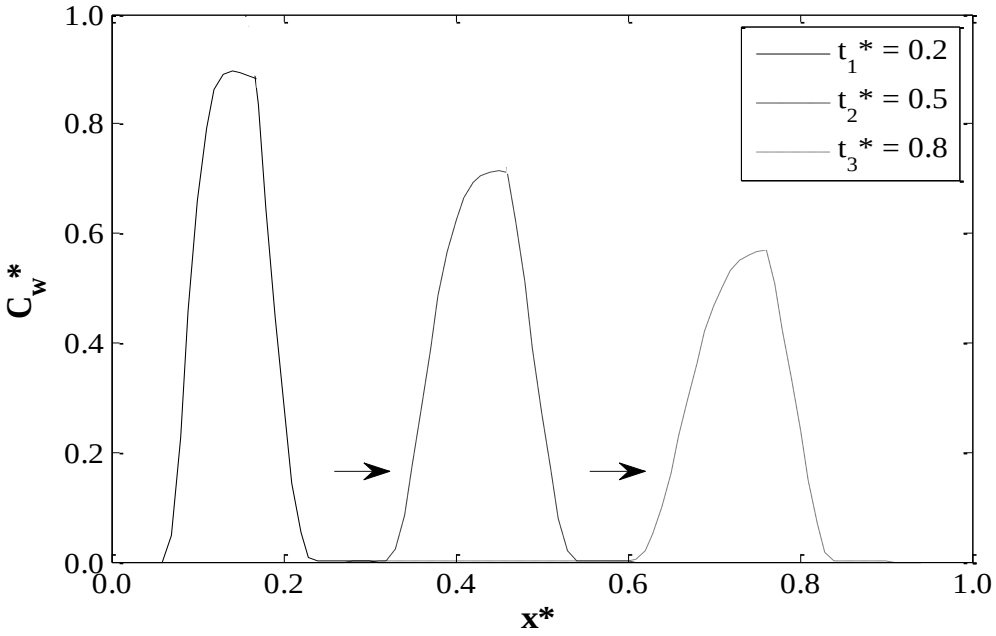

Figure 3.43: Tracer slug propagation in water phase for $N_{pe} = 50$

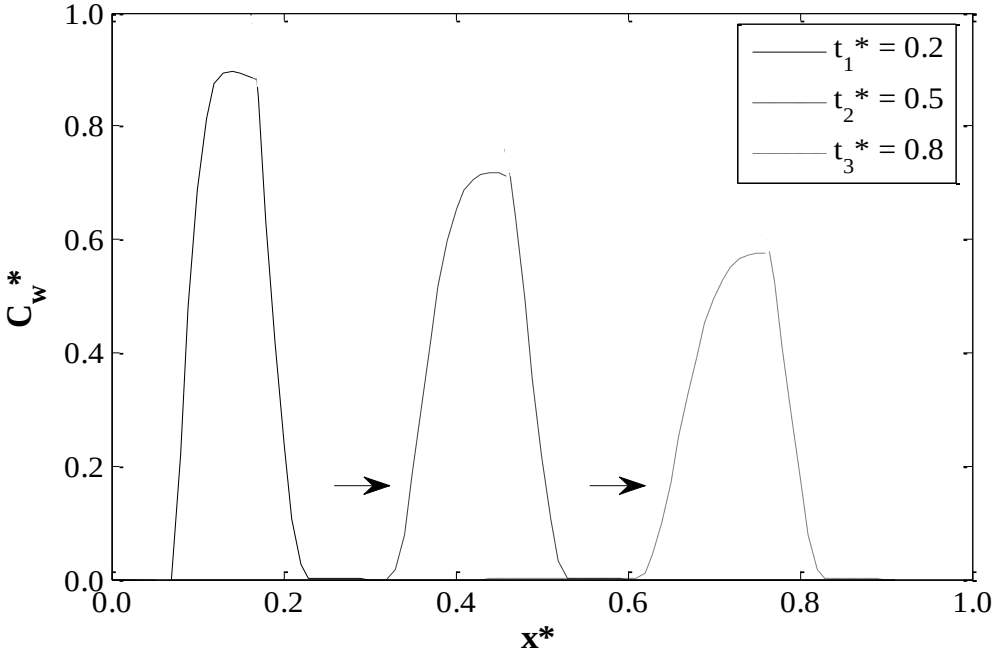

Figure 3.44: Tracer slug propagation in water phase for $N_{pe} = 100$

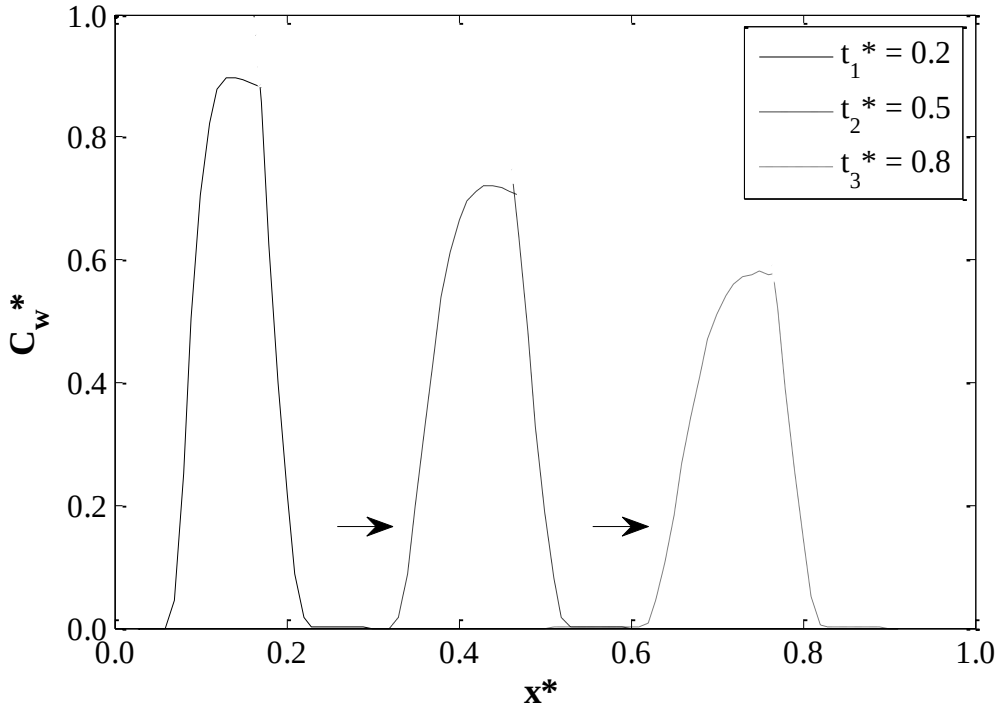

Figure 3.45: Tracer slug propagation in water phase for $N_{pe} = 500$

Chapter 4 Results and Discussion

4.1 Comparison of Models

The models in Chapter 3 are plotted at $t_1^* = 0.3$, $t_2^* = 0.5$ for the purpose of comparison shown below. The breakthrough time of each model (t_B^*) is also plotted in each figure to show the effects of flowing mechanisms on tracer breakthrough times.

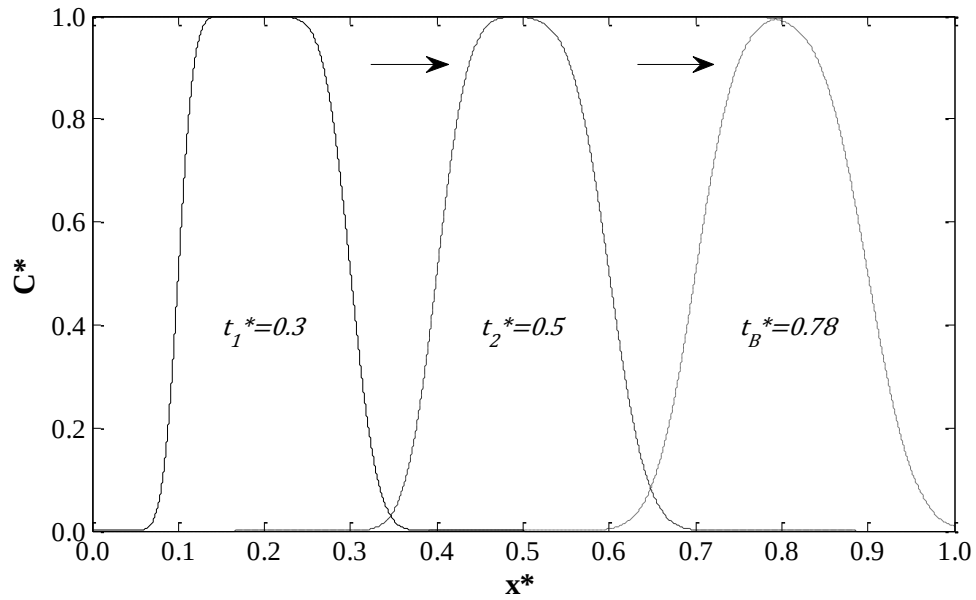

Figure 4.1: Tracer slug propagation for convection dispersion model

The tracer slug mixing zone increases upon propagation in the convection dispersion model in Figure 4.1 and breaks through at $t_B^* = 0.78$. Both the leading edge and trailing edge act as spreading waves, which is caused by dispersion. The tracer dimensionless concentration peak at every time step equals to 1.0.

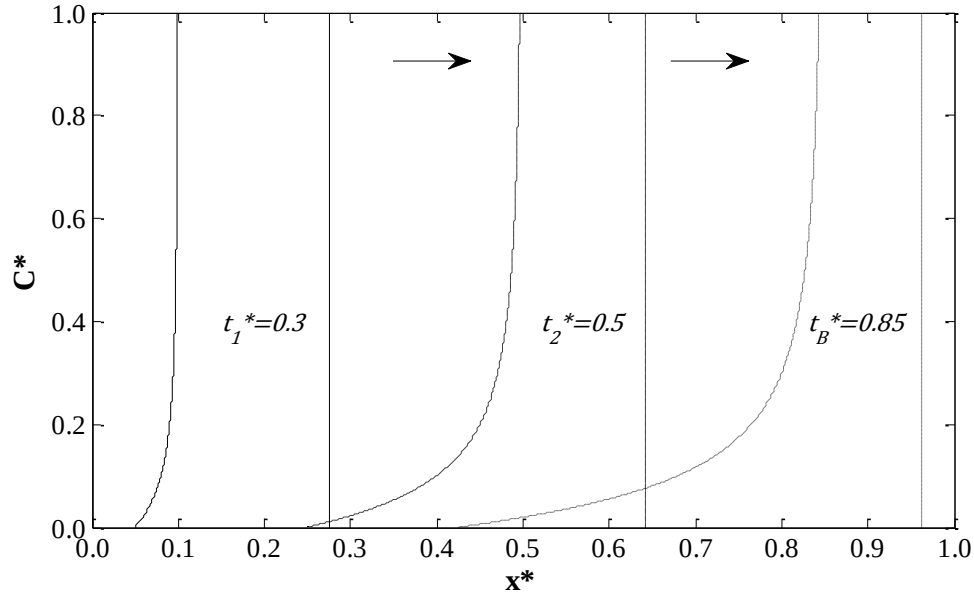

Figure 4.2: Tracer slug propagation for convection adsorption model

Figure 4.2 shows that the leading edge for convection adsorption model acts as shock while the trailing edge acts as a spreading wave, and the trailing edge starts to catch up with the leading edged upon propagation. The tracer dimensionless concentration peak still equals to 1.0, same as the previous case; however, the tracer slug size shrinks because of the concentration loss caused by adsorption. The tracer slug breakthrough time got delayed by adsorption ($t_B{}^* = 0.85$).

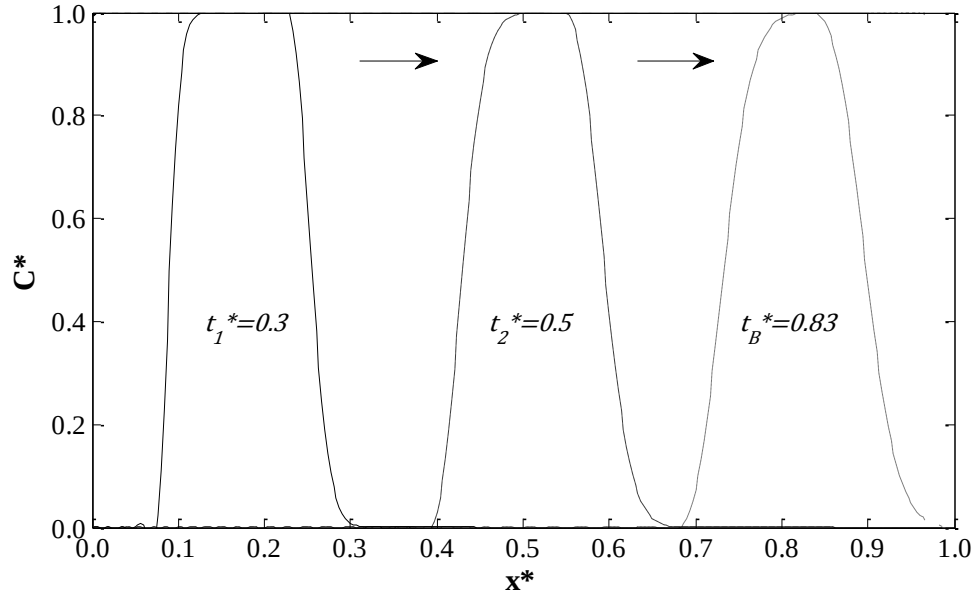

Figure 4.3: Tracer slug propagation for convection dispersion adsorption model

Figure 4.3 shows the tracer slug propagation when dispersion is added to the convection adsorption model. It is illustrated that both the leading edge and trailing edge of the tracer slug got smoothed by the effect of dispersion. The dimensionless concentration peak still equals to 1.0 for this case. The tracer slug breaks through earlier than the convection adsorption case at $t_B{}^* = 0.83$.

Figure 4.4 shows the convection dispersion adsorption radioactive decay model for tracer slug propagation. The tracer slug has a large concentration loss when radioactive decay effect is added. The tracer dimensionless concentration peak can never reach 1.0 because of the large concentration loss caused by radioactive decay. The tracer slug breakthrough time does not change much at $t_B{}^* = 0.84$.

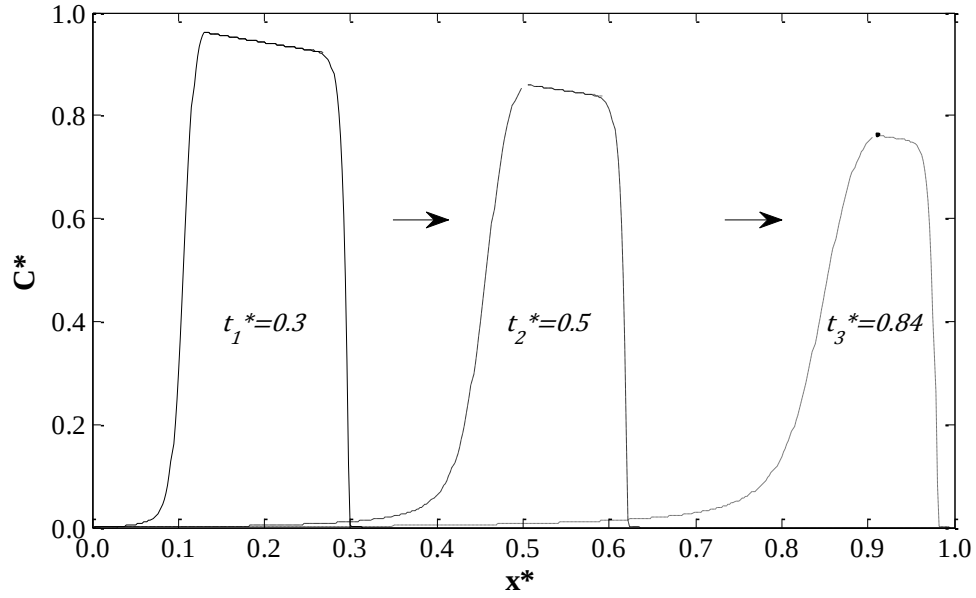

Figure 4.4: Tracer slug propagation for convection dispersion adsorption radioactive decay model

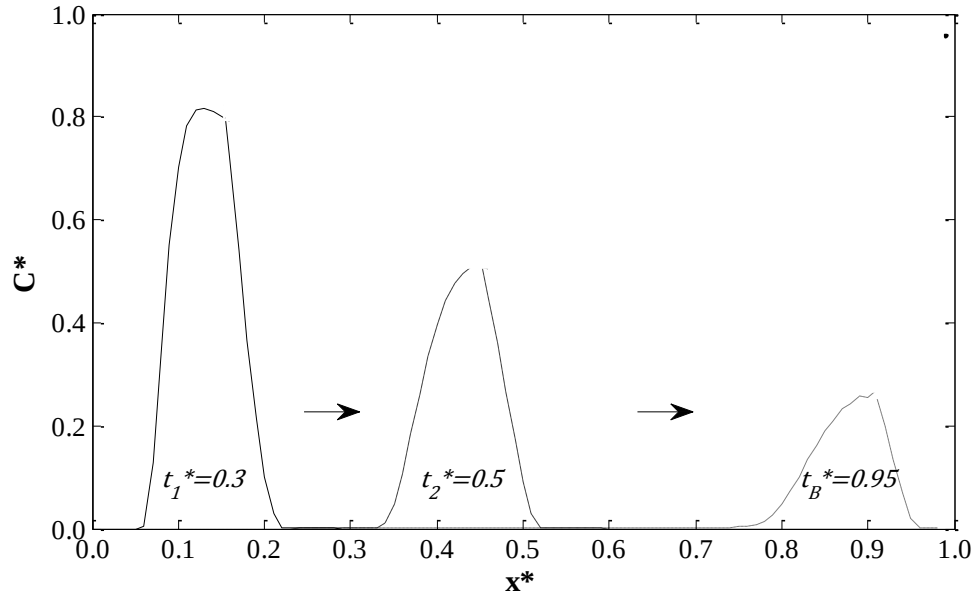

Figure 4.5: Tracer slug propagation for convection dispersion adsorption partitioning radioactive decay model

Figure 4.5 shows the tracer slug propagation for the two-phase complete model, which includes convection, dispersion, adsorption, partitioning between phases and radioactive decay. The tracer slug concentration peak got declined a lot when compared to Figure 4.4, which is caused by the effect of partitioning between phases. The dimensionless concentration peak is around 0.2 when the tracer slug got produced. The breakthrough time also got delayed at $t_B{}^* = 0.95$ as a result of partitioning.

4.2 Case Study

This case study is conducted using the two-phase tracer model discussed in the above chapter to interpret the profiles of tracer distributions with different input parameters.

4.2.1 Objectives

The objective of this case study is to discuss the effects of partitioning coefficient (K), adsorption type and wetting condition on tracer concentration distribution and breakthrough time. Twenty-seven runs were designed, using three different partitioning coefficients, three different adsorption models and three different wetting conditions. The concentration profiles and the tracer breakthrough times for different cases are compared followed by a sensitivity analysis of input parameters.

Table 4.1: Factors designed for case study

Partitioning coefficient (K)	0.1	0.5	0.9
Adsorption type (C_s)	Zero adsorption	Langmuir adsorption	Linear adsorption
Wetting condition	Water-wet	Intermediate-wet	Oil-wet

4.2.2 Input Parameters

The input partitioning coefficients and adsorption models are listed in Table 4.1. The input wetting conditions are more complex as wetting conditions affect the input imbibition capillary pressure curves and the input relative permeability curves. However, relative permeability curves are associated with capillary pressure curves and can be obtained from capillary curves through the Purcell approach (Purcell, 1949). In two-phase flow, the relative permeability of the wetting phase and non-wetting phase can be calculated use the following equations (Purcell, 1949; Kewen and Horne, 2006):

$$k_{r,wet} = \frac{\int_0^{S_w} dS_w/(P_c)^2}{\int_0^1 dS_w/(P_c)^2}, \tag{4.1}$$

$$k_{r,non-wet} = \frac{\int_{S_w}^1 dS_w/(P_c)^2}{\int_0^1 dS_w/(P_c)^2}, \tag{4.2}$$

where $k_{r,wet}$ and $k_{r,non-wet}$ are the wetting phase relative permeability and the non-wetting phase relative permeability, respectively. The wetting phase saturation is defined as S_w and P_c is the capillary pressure, which is a function of S_w.

Imbibition capillary pressure curves always have a point at which capillary pressure is

equal to zero, hence it is impossible to use the above Purcell method, a primary drainage capillary pressure is chosen to calculate the normalized relative permeability curves. Then, the normalized relative permeability curves are transformed to different shapes representing different wetting conditions. The detailed steps are shown below.

Step 1: use a parabolic equation to represent a leverett J-function curve:

$$J = 5{S_w}^2 - 10S_w + 5.357\,, \tag{4.3}$$

and the curve is shown in Figure 4.6 below.

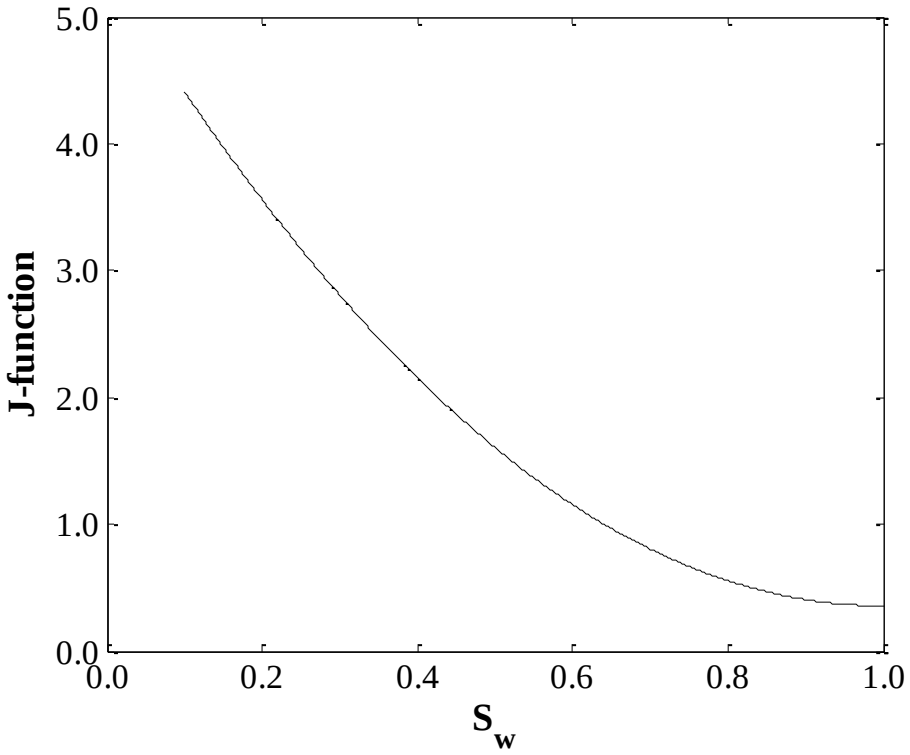

Figure 4.6: Leverett J-function curve

Step 2: use Eq. (4.1) and Eq. (4.2) to calculate the normalized relative permeability

and the curves are plotted in Figure 4.7.

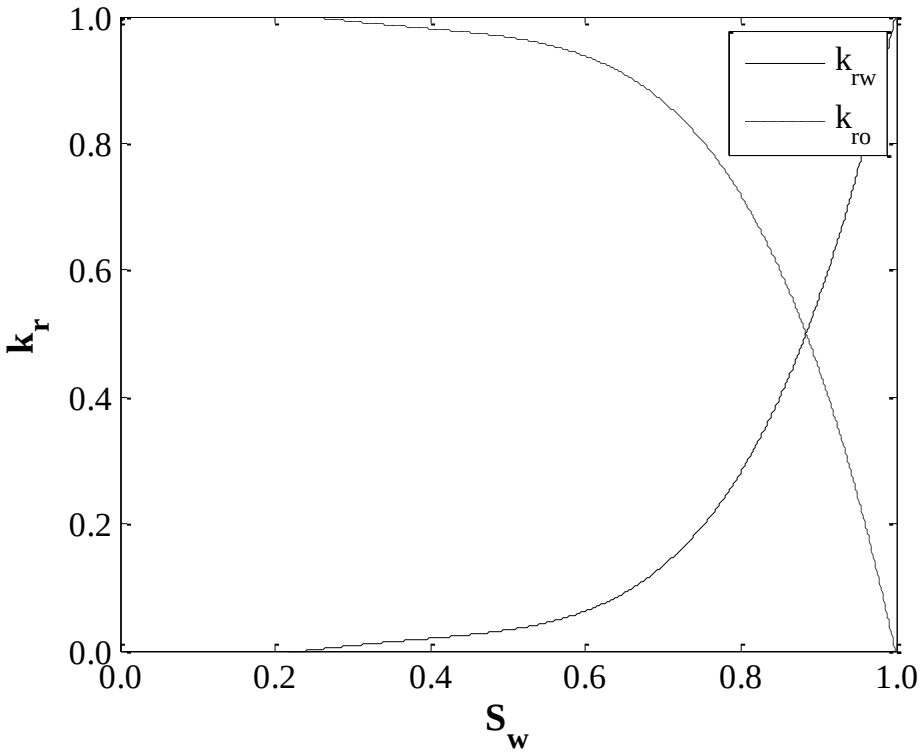

Figure 4.7: Normalized relative permeability curves

Step 3: the connate water saturations and residual oil saturations are chosen for the water-wet condition, intermediate-wet condition and oil-wet condition, as shown in Table 4.2. Then, the normalized relative permeability curves are squeezed to fit different wetting conditions shown in Figure 4.8, Figure 4.9 and Figure 4.10.

Table 4.2: Connate water and residual oil saturations for different wetting conditions

	water-wet	intermediate-wet	oil-wet
S_{wc}	0.3	0.2	0.1
S_{or}	0.2	0.3	0.4

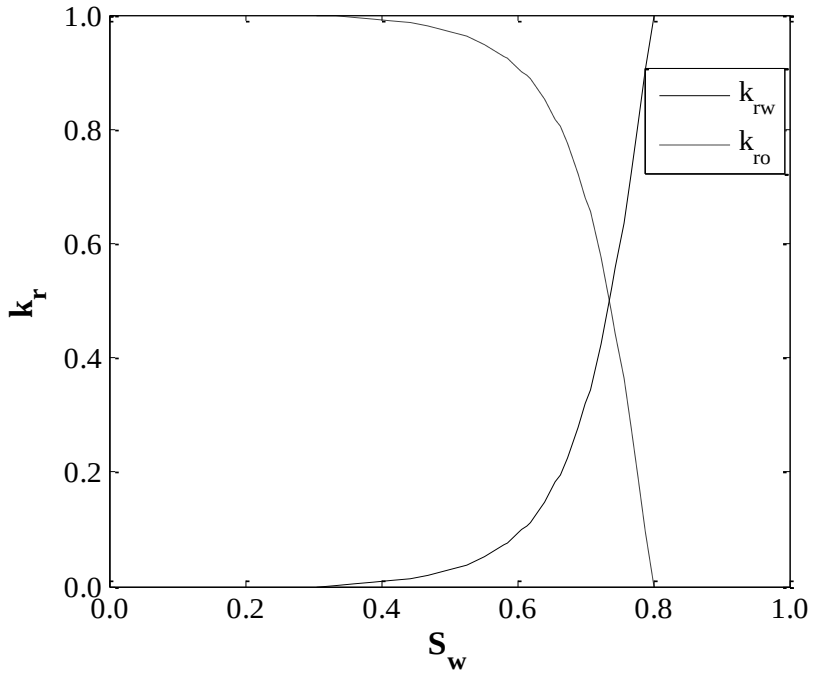

Figure 4.8: Squeezed relative permeability curves for water-wet condition

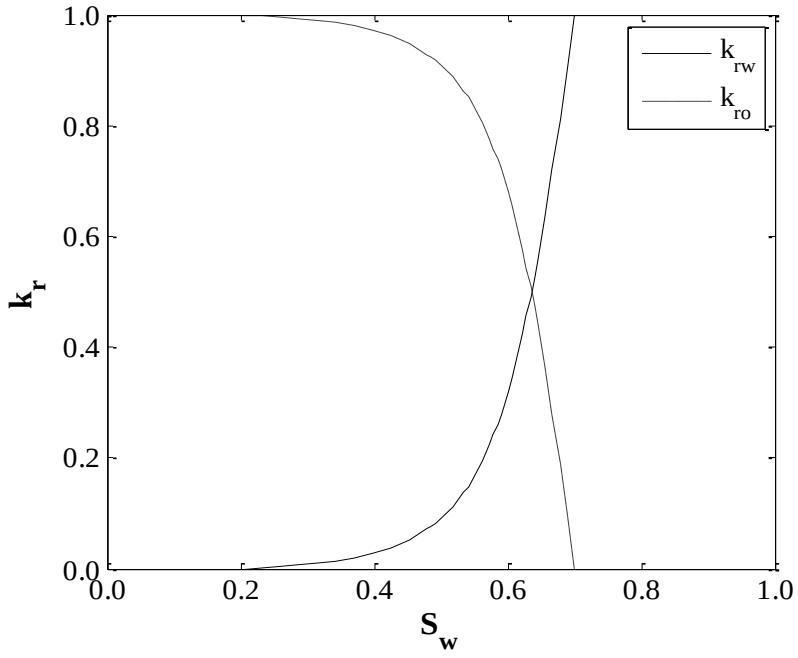

Figure 4.9: Squeezed relative permeability curves for intermediate-wet condition

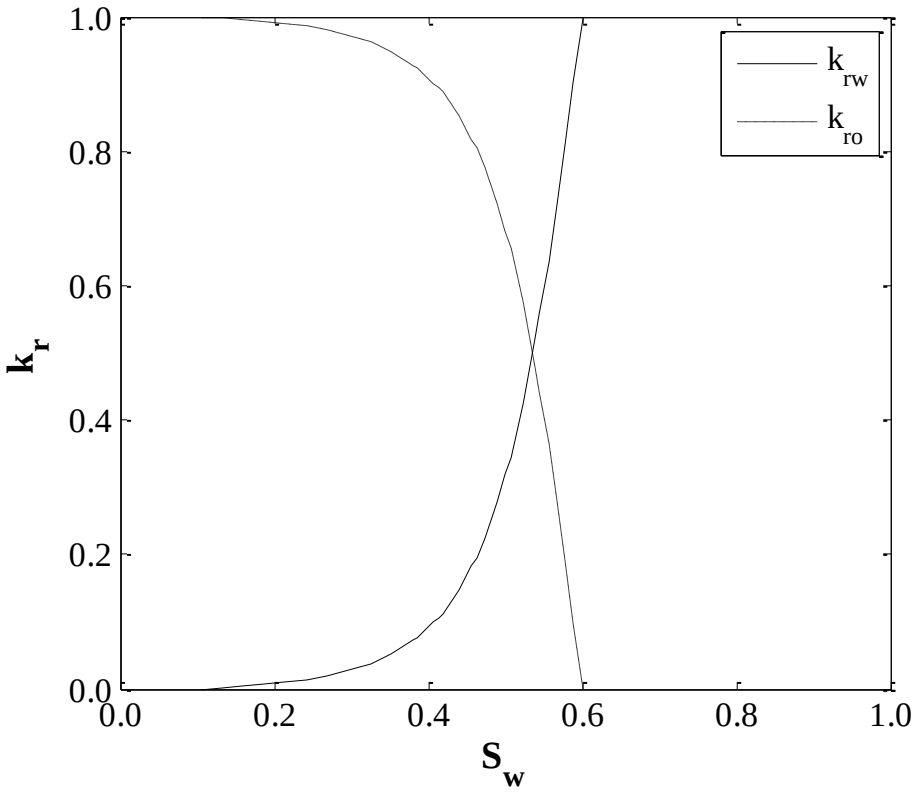

Figure 4.10: Squeezed relative permeability curves for oil-wet condition

Step 4: use cotangent function to imitate the imbibition capillary pressure curves for different wetting conditions:

$$P_c = cotf + m\,, \tag{4.4}$$

where,

$$f = \frac{S_w - S_{wc}}{S_{or} - S_{wc}}\pi\,, \tag{4.5}$$

and m is a constant and is chosen to be $m = 4$, $m = 1$ and $m = -1$ for water-wet, intermediate-wet and oil-wet respectively, in this case study. The same connate water

saturations and residual oil saturations (Table 4.2) are used for the simulation of capillary pressure curves. The curves are shown in Figure 4.11.

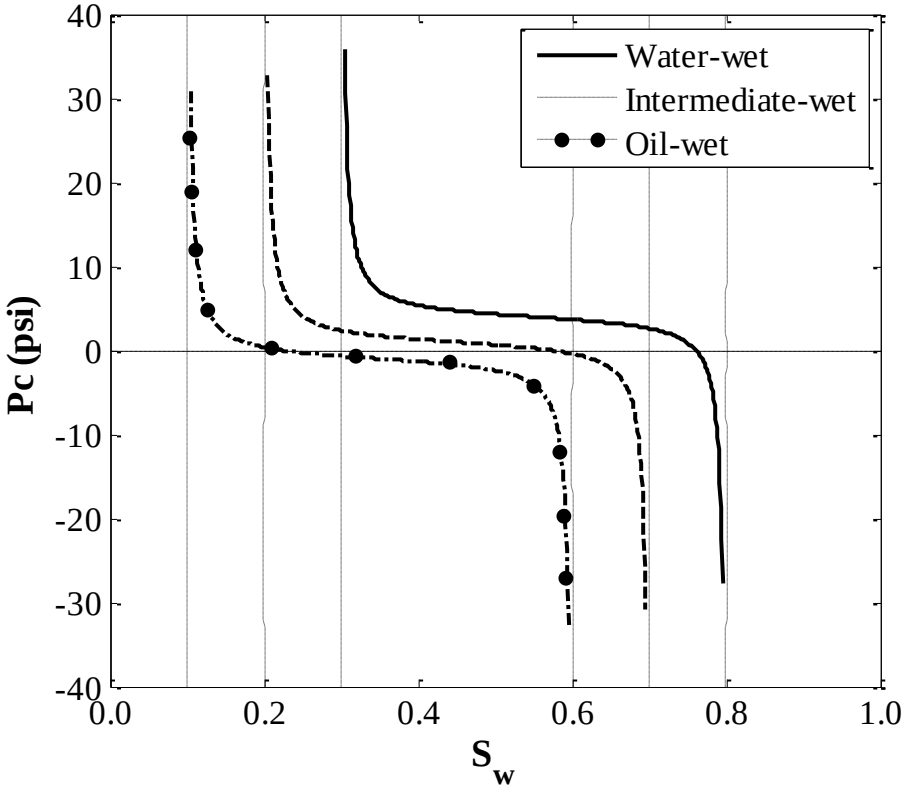

Figure 4.11: Imbibition capillary pressure curve for water-wet, intermediate-wet and oil-wet conditions

Step 5: calculate the USBM (US Bureau of Mines) index for different wetting conditions and use the index to get the input relative permeability curves from the squeezed relative permeability curves in Step 3.

The USBM index is given as:

$$I_{USBM} = log\frac{A_1}{A_2}, \tag{4.6}$$

where A_1 is the area between the positive part of the capillary pressure curve and the zero capillary pressure line and A_2 is the area between the negative part of the capillary pressure curve and the zero capillary pressure line. The USBM index calculated from the above three figures are:

$I_{USBM1} = 0.9$, for water-wet condition,

$I_{USBM2} = 0.3$, for intermediate-wet condition,

$I_{USBM3} = -0.9$, for oil-wet condition.

In order to get the final input relative permeability curves to fit the criteria in Table 4.3, the following formulas are used:

$$k_{rw,input} = [1 - 0.4 \times (1 + I_{USBM})]k_{rw}, \tag{4.7}$$

$$k_{ro,input} = 0.4 \times (1 + I_{USBM})k_{ro}, \tag{4.8}$$

where $k_{rw,input}$ and $k_{ro,input}$ are the final input relative permeabilities, k_{rw} and k_{ro} are the relative permeability values from Step 3.

Then, the final input relative permeability curves can be plotted, as shown in Figure 4.12, Figure 4.13 and Figure 4.14. These relative permeability curves should be input in pairs with their corresponding imbibition capillary pressure curves (Figure 4.11).

Table 4.3: Criteria for relative permeability curves

	water-wet	oil-wet
S_w@intersection point	> 50%	< 50%
$K_{rw}@S_{or}$	< 0.3	> 0.5
S_{wc}	> 25%	< 15%

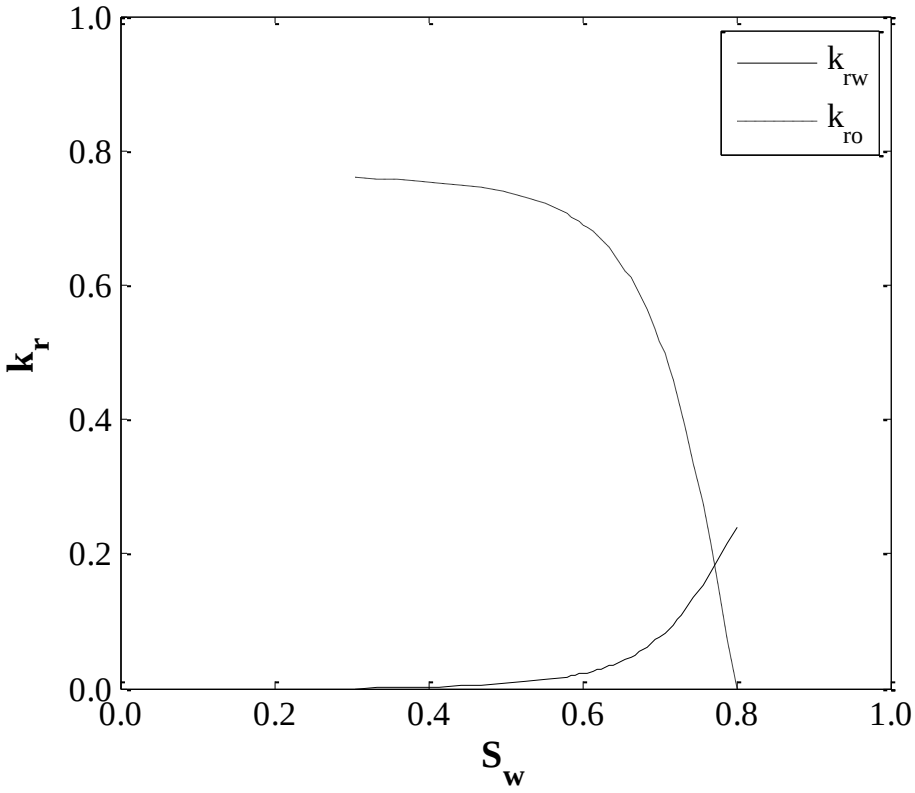

Figure 4.12: Input relative permeability curves for water-wet condition

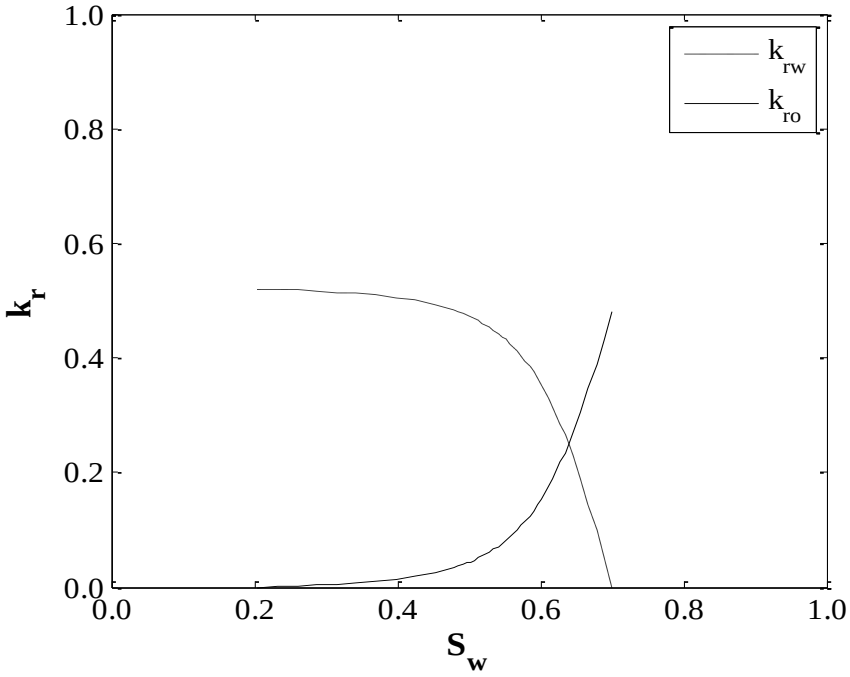

Figure 4.13: Input relative permeability curves for intermediate-wet condition

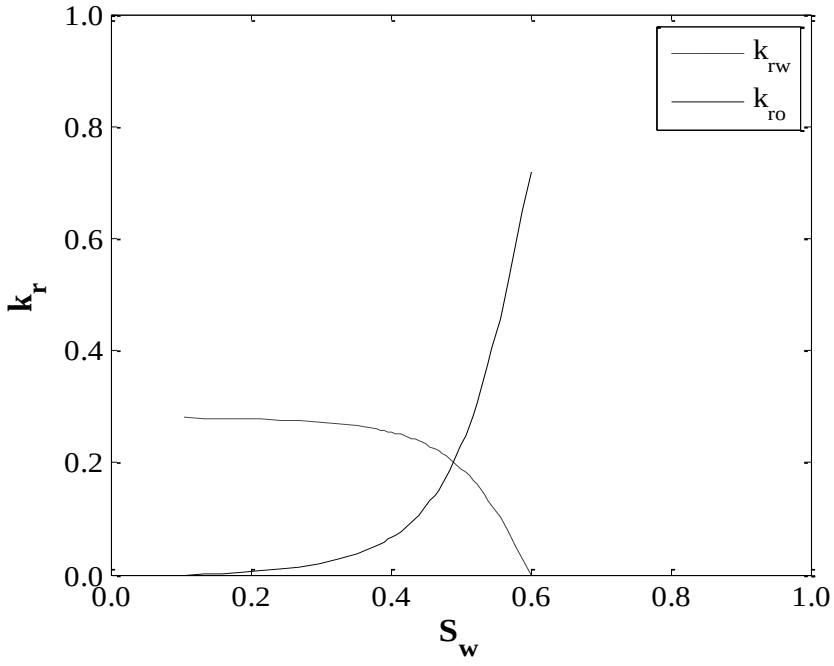

Figure 4.14: Input relative permeability curves for oil-wet condition

4.2.3 Results and Discussions

The above input parameters are applied in the tracer model in chapter 3. Twenty-seven runs were conducted as designed previously. The breakthrough time of each case is listed in Table 4.4.

Table 4.4: Breakthrough time for each run

Run#	K	Adsorption Type	Wetting Condition	T_b
1	0.1	Zero Adsorption	Water-wet	0.80
2	0.1	Zero Adsorption	Intermediate-wet	0.69
3	0.1	Zero Adsorption	Oil-wet	0.60
4	0.1	Langmuir Adsorption	Water-wet	0.88
5	0.1	Langmuir Adsorption	Intermediate-wet	0.75
6	0.1	Langmuir Adsorption	Oil-wet	0.65
7	0.1	Linear Adsorption	Water-wet	0.95
8	0.1	Linear Adsorption	Intermediate-wet	0.88
9	0.1	Linear Adsorption	Oil-wet	0.78
10	0.5	Zero Adsorption	Water-wet	0.85
11	0.5	Zero Adsorption	Intermediate-wet	0.78
12	0.5	Zero Adsorption	Oil-wet	0.73
13	0.5	Langmuir Adsorption	Water-wet	0.93
14	0.5	Langmuir Adsorption	Intermediate-wet	0.86
15	0.5	Langmuir Adsorption	Oil-wet	0.81
16	0.5	Linear Adsorption	Water-wet	0.98
17	0.5	Linear Adsorption	Intermediate-wet	0.97
18	0.5	Linear Adsorption	Oil-wet	0.93
19	0.9	Zero Adsorption	Water-wet	0.90
20	0.9	Zero Adsorption	Intermediate-wet	0.87
21	0.9	Zero Adsorption	Oil-wet	0.86
22	0.9	Langmuir Adsorption	Water-wet	0.98
23	0.9	Langmuir Adsorption	Intermediate-wet	0.96
24	0.9	Langmuir Adsorption	Oil-wet	0.95
25	0.9	Linear Adsorption	Water-wet	1.00
26	0.9	Linear Adsorption	Intermediate-wet	0.99
27	0.9	Linear Adsorption	Oil-wet	0.98

Next, the effects of partitioning coefficient, adsorption type and wetting condition on tracer breakthrough time were analyzed. Figures 4.15, 4.16 and 4.17 show the change of tracer breakthrough time under different wetting conditions for a certain adsorption type (zero adsorption, linear adsorption and Langmuir adsorption).

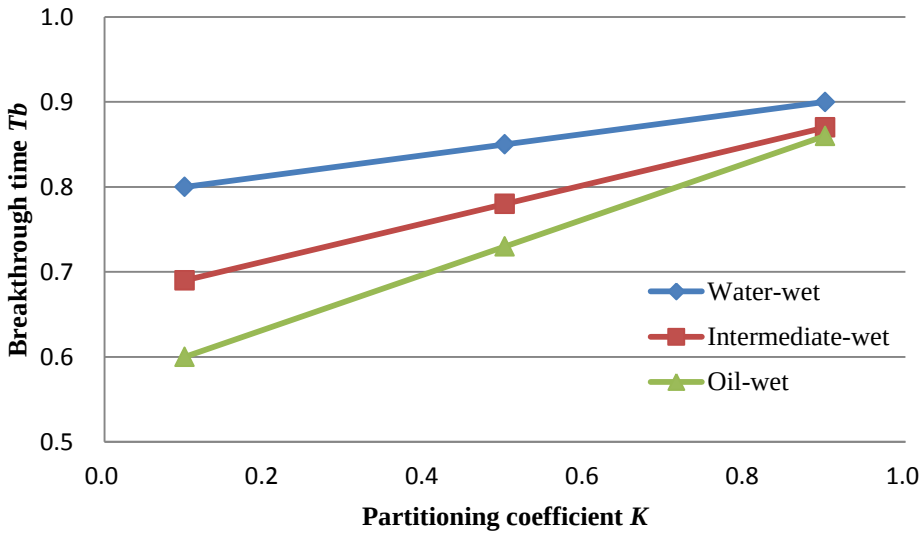

Figure 4.15: Breakthrough time as a function of partitioning coefficient and wetting condition for zero adsorption

Figure 4.15 shows that for zero adsorption case, the breakthrough time of water-wet, intermediate-wet and oil-wet conditions increases as the partitioning coefficient increases. The breakthrough time of water-wet is the highest, intermediate-wet is in between and oil-wet is the lowest. This observation can be used to imply reservoir wetting condition.

Figure 4.16 and Figure 4.17 show that the linear adsorption case and the Langmuir adsorption case have the similar trend as the zero adsorption case, i.e., the

breakthrough time of water-wet, intermediate-wet and oil-wet conditions increases when the partitioning coefficient increases. Similarly, the breakthrough time of water-wet is the highest, intermediate-wet is in between and oil-wet is the lowest; however, the difference in breakthrough time is not as severe as the zero adsorption case.

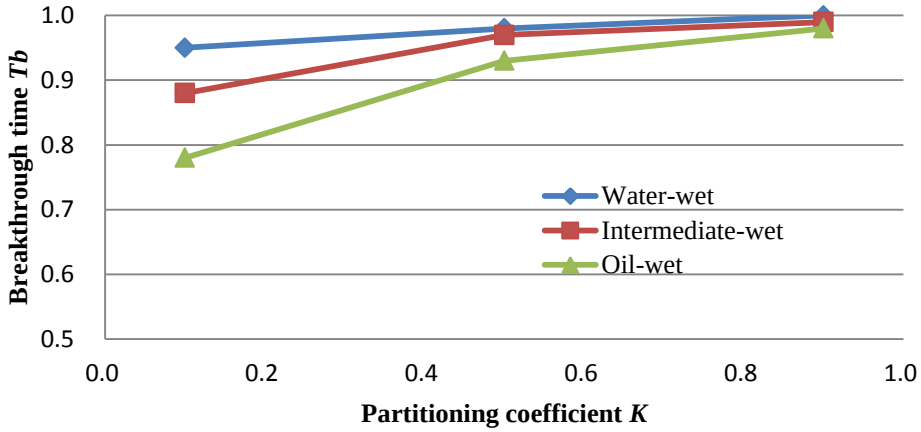

Figure 4.16: Breakthrough time as a function of partitioning coefficient and wetting condition for linear adsorption

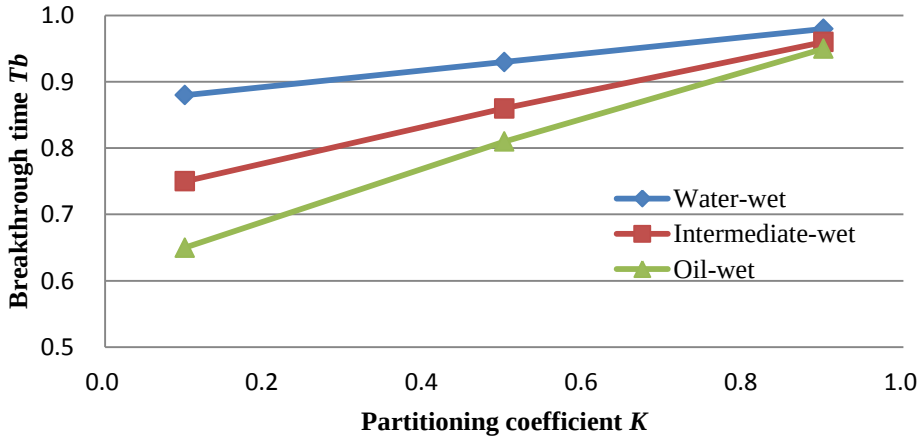

Figure 4.17: Breakthrough time as a function of partitioning coefficient and wetting condition for Langmuir adsorption

For all the three cases, the breakthrough time of the tracer slug in oil-wet condition is

the shortest, and in water-wet condition is the longest. The observation of this phenomenon provides a method to indicate reservoir wetting through tracer tests. The figures also show that as the partitioning coefficient increases, the breakthrough time increases. When the partitioning coefficient is small, the difference in breakthrough time is severe for different wetting conditions. As the partitioning coefficient increases, the difference in breakthrough time is small.

Figures 4.18, 4.19 and 4.20 are plotted to show the effect of adsorption type under a certain wetting condition, i.e. water-wet, intermediate-wet or oil-wet.

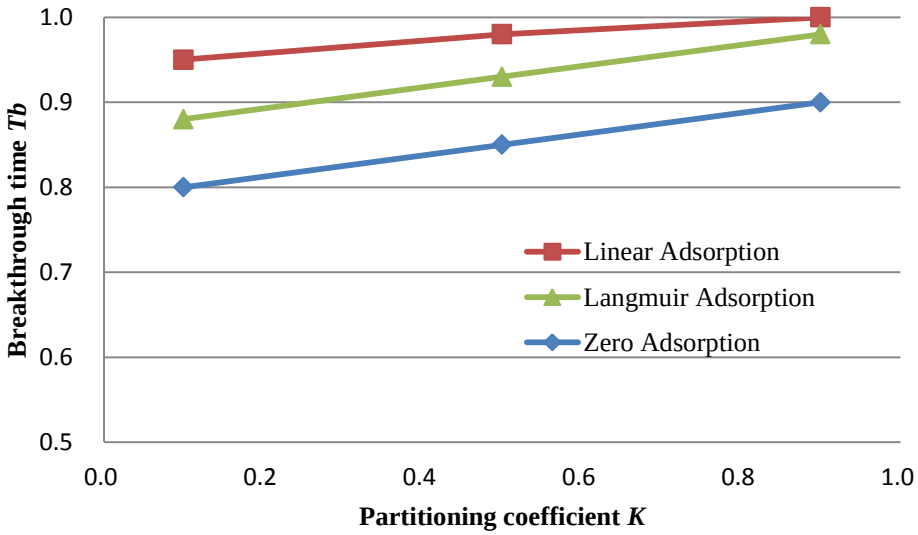

Figure 4.18: Breakthrough time as a function of partitioning coefficient and adsorption type for water-wet condition

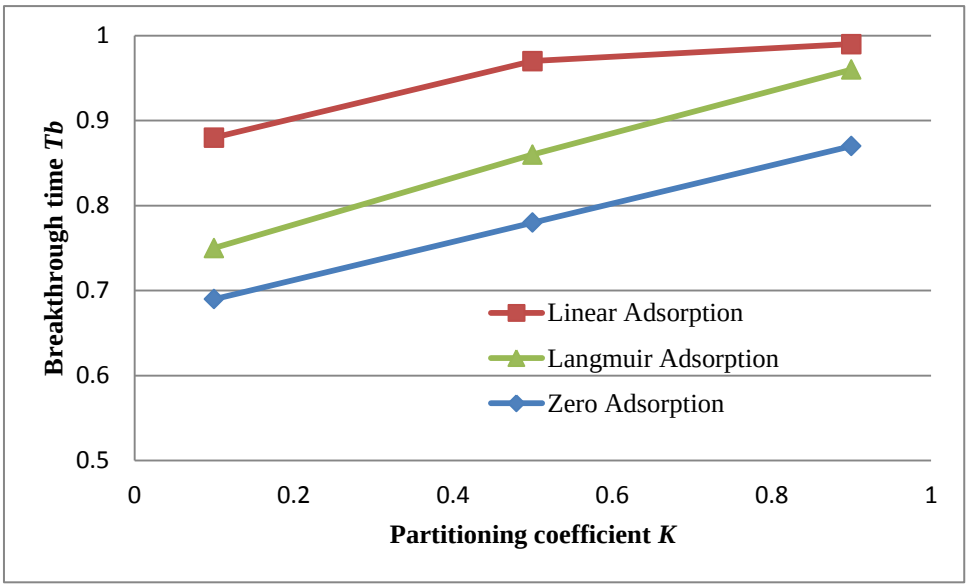

Figure 4.19: Breakthrough time as a function of partitioning coefficient and adsorption type for intermediate-wet condition

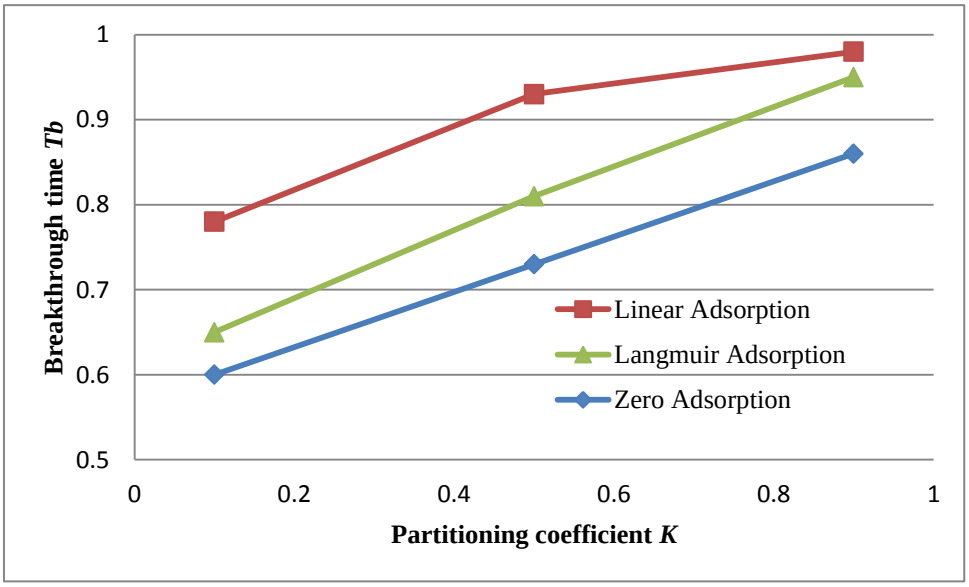

Figure 4.20: Breakthrough time as a function of partitioning coefficient and adsorption type for oil-wet condition

As can be seen from the above figures, for all the three wetting conditions, linear adsorption gives the longest breakthrough time and zero adsorption gives the shortest

breakthrough time, and Langmuir adsorption is in between. The Langmuir and linear adsorption models predict similar breakthrough times when partitioning coefficient is large; however, with a small partitioning coefficient, adsorption model has an effect. Thus, an accurate adsorption model is important for tracer breakthrough time prediction.

In conclusion, this case study indicates that adsorption type, partitioning coefficient and reservoir wetting condition do have effects on tracer flow. Investigating the effect of partitioning coefficient gives guidance for tracer test design; investigating the effect of adsorption type gives instruction for tracer test modeling; investigating the effect of wetting condition shows that tracer test could be applied to determine reservoir wetting.

Chapter 5 Conclusions and Recommendations

5.1 Conclusions

This research covers the numerical modeling of one-dimensional single-phase tracer flow and two-phase partitioning tracer flow that includes convection, Langmuir adsorption, partitioning between phases, hydrodynamic dispersion and radioactive decay. The final complete model implemented in Matlab is an improvement of previously-used models as it includes radioactive decay and uses Langmuir adsorption instead of linear adsorption. From the discussion and comparison of different tracer models, we conclude that:

1. The tracer profile from convection dispersion equation acts as a diffusive wave, i.e., the mixing zone tracer slug expends, which is caused by dispersion. The larger the dispersion coefficient, the larger mixing zone of the tracer slug.
2. The effects of adsorption and partitioning between phases decrease the tracer slug propagation. Thus, the breakthrough time is delayed by adsorption and partitioning between phases.
3. Radioactive tracers get large tracer concentration losses caused by the radioactive effect and the smaller the half-life, the larger the concentration loss.
4. The complete model with convection, Langmuir adsorption, partitioning between phases, hydrodynamic dispersion and radioactive decay can predict the tracer slug propagation and the tracer breakthrough time accurately.

Finally, for the case study, different adsorption models, different partitioning coefficients and different reservoir wetting conditions were chosen and the conclusions are:

1. The tracer slug in an oil-wet porous media breaks through earlier than the intermediate-wet condition and the latest break through is for the water-wet condition. This can be used to measure reservoir wetting conditions.
2. When the partitioning coefficient increases, the breakthrough time increases.
3. A small partitioning coefficient results in a relatively large difference in breakthrough time for different wetting conditions. The difference in breakthrough time is inconsequential when the partitioning coefficient is close to 1.
4. A linear adsorption model gives the longest breakthrough time, a zero adsorption model gives the shortest breakthrough time, and a Langmuir adsorption model is in between. When partitioning coefficients are large, Langmuir and linear adsorption models behave similarly. When partitioning coefficients are small, there are marked differences in adsorption models. Thus, an accurate adsorption model is important for tracer breakthrough time prediction.

5.2 Recommendations

Recommendations for future work include:

1. The model could be extended to two-dimensional or even three-dimensional three-phase flow using stream line models combined with the one-dimensional models.

2. A further experimental tracer study is recommended to compare with numerical tracer models.
3. The effect of adsorption on tracer flow should be studied in more detail. In this thesis, we only show that differences can be observed when using different adsorption models. However, for tracers with very low adsorption capacity, the difference could be small, while for easily adsorbed tracers, it would be important to choose an accurate adsorption model. The differences are also affected by the value of partitioning coefficients. Thus, further work could be done in finding the critical conditions for using different adsorption models.

Bibliography

Amott, E. 1959. Observations Relating to the Wettability of Porous Rock, *Transactions*. AIME **216**, 107-116.

Bear, J. 1972. Dynamics of Fluids in Porous Media. *Soil Science*.

Bird, R. B., Stewart W. and Lightfoot, E. 1960. *Transport Phenomena*. New York, NY: Wiley.

BjØrnstad, T. 1992. Tracer Types. In *Recent Advances in Improved Oil Recovery Methods for North Sea Sandstone Reservoirs*, eds. Skjæveland, S.M. and Kleppe, J., pp. 157-161. SPOR Monograph.

Brigham, W. E. and Smith, D. H. 1965. Prediction of Tracer Behavior in Five-spot Flow. In *Conference on Production Research and Engineering*. Society of Petroleum Engineers.

Buckley, S. E. and Leverett, M. C. 1942. Mechanism of Fluid Displacement in Sands, *Transactions*. AIME **146** (01), 107-116.

Carpenter, P. G., Morgan, T. D. and Parsons, E. D. 1952. Use of Boron Compounds as Water Flood Tracers. *Prod. Mon*, **16** (12), 12-19.

Cooke Jr, C. E.1971. Method of Determining Fluid Saturation in Reservoirs. No. US 3590923.

Corey, A. T. 1954. The Interrelation between Gas and Oil Relative Permeabilities. *Producers monthly*, **19** (1), 38-41.

Darcy, H. 1856. Les Fontaines Publiques de la Wille de Dijon. Paris.

Deans, H and Carlisle, C. 2006. The Single-Well Chemical Tracer Test—A Method For Measuring Reservoir Fluid Saturations In Situ. In *Petroleum Engineering Handbook V(A)*, eds. Lake, L. W., pp. 615-649.

Deans, H. A. and Shallenberger, L. K. 1974. Single-Well Chemical Tracer Method to Measure Connate Water Saturation. In *SPE Improved Oil Recovery Symposium*. Society of Petroleum Engineers.

Donaldson, E. C., Thomas, R.D. and Lorenz, P.B. 1969. Wettability Determination and Its Effect on Recovery Efficiency. *Bureau of Mines*.

Dugstad, φ. 2006. Well-To-Well Tracer Tests. In *Petroleum Engineering Handbook V(A)*, eds. Lake, L. W., pp. 651-681.

Fick, A. 1855. On Liquid Diffusion. *Journal of Membrane Science*, **100** (1), 33-38.

Guan, L., Du, Y., Johnson, S. G. and Choudhary, M. K. 2005. Advances of Interwell Tracer Analysis in the Petroleum Industry. *Journal of Canadian Petroleum Technology*, **44** (05).

Gupta, A. D., Pope, G. A., Sepehrnoori, K., and Thrasher, R. L. 1986. A Symmetric, Positive Definite Formulation of a Three-Dimensional Micellar/Polymer Simulator. *SPE Reservoir Engineering*, **1** (06), 622-632.

Hagoort, J. 1982. The Response of Interwell Tracer Tests in Watered-Out Reservoirs. In *SPE Annual Technical Conference and Exhibition*. Society of Petroleum Engineers.

Johansen T. and Winther R. 1988. The Solution of Riemann Problems for Hyperbolic Systems of Conservation Laws Modeling Polymer Flooding, *SIAM Journal of Mathematical Analysis*, 19.

Johansen, T., Antonsen, B., Sagen, J. and Hidle, S. 1989. A Theory of Multicomponent Chromatography for Tracers in Two Phase Flow. In *Proceedings from "The Fifth European Symposium on Improved Oil Recovery", Budapest*.

Johansen, T., Wang Y., Orr Jr F. M. and Dindoruk B. 2005. Four- Component Gas/Oil Displacements in One Dimension: Part I: Global Triangular Structure, *Transport in Porous Media*, 61, 59-76

Johansen, T. 2008. *Principles of Reservoir Engineering*. Memorial University of Newfoundland.

Kewen, L. and Horne, R. 2006. Comparison of methods to calculate relative permeability from capillary pressure in consolidated water-wet porous media. *Water resources research*, **42** (6).

Lake, L.W. 1989. *Enhanced Oil Recovery*. Englewood Cliffs, New Jersey: Prentice Hall.

Langmuir, I. 1916. The Constitution and Fundamental Properties of Solids and Liquids. Part 1. Solids. *Journal of the American Chemical Society*, **38** (11), 2221-2295.

Lax, P. D. 1957, *Hyperbolic systems of conservation laws. II*, Comm. Pure Appl.

Math. 10.

Melo, M. A., Holleben, C. R. and Almeida, A. R. 2001. Using Tracers to Characterize Petroleum Reservoirs: Application to Carmospolis Field, Brazil. Paper SPE 69474 presented at Latin American and Caribbean Petroleum Engineering Conference held in Buenos Aires, Argentina, 25-28 March.

Purcell, W. R. 1949. Capillary Pressures-Their Measurement Using Mercury and the Calculation of Permeability. *Journal of Petroleum Technology*, **1** (02), 39-48.

Shook, G. M., Ansley, S. L., Wylie, A. and Wyliea, A. 2004. Tracers and Tracer Testing: Design, Implementation, and Interpretation Methods.

Sturm, P. W. and Johnson, W. E. 1951. Field Experiments with Chemical Tracers in Flooding Waters.

Tomich, J. F., Dalton Jr, R. L., Deans, H. A., and Shallenberger, L. K. 1973. Single-Well Tracer Method to Measure Residual Oil Saturation. *Journal of Petroleum Technology*, **25** (02), 211-218.

Application of Radiotracer Techniques for Interwell Studies, 2012. International Atomic Energy Agency, Vienna, IAEA Radiation Technology Series. http://www-pub.iaea.org/books/IAEABooks/8658/Application-of-Radiotracer-Techniques-for-Interwell-Studies.